

University of Nevada, Reno

Reductive Dehalogenation by Aqueous Biochars

A dissertation submitted in partial fulfillment of the requirements for the degree of

Doctor of Philosophy in Civil and Environmental Engineering

by

Srinidhi Lokesh

Dr. Yu Yang /Dissertation Advisor

May 2023

Copyright by Srinidhi Lokesh, 2023

All Rights Reserved



THE GRADUATE SCHOOL

We recommend that the dissertation
prepared under our supervision by

entitled

be accepted in partial fulfillment of the
requirements for the degree of

Advisor

Committee Member

Committee Member

Committee Member

Graduate School Representative

Markus Kemmelmeier, Ph.D., Dean
Graduate School

Reductive Dehalogenation by Aqueous Biochars

ABSTRACT

Biochars (BCs), carbon-rich products obtained from biomass pyrolysis, have been used as cost-effective materials for environmental remediation and wastewater treatment processes. Although BCs were primarily used as passive sorbents, recent studies have uncovered their reactivity toward the degradation of toxic compounds. In the reactions with pollutants, sorption by bulk BC particles can inhibit their availability and slow down the degradation. Alternatively, BC mobilized to the aqueous phase, termed aqueous BCs (a-BCs), can potentially promote the degradation of target pollutants without inhibiting their availability, for which relevant data is rare. Therefore, our study targets the reactivity of a-BCs toward the reductive degradation of organohalogen. This Ph.D. project aims to: 1) study the degradation of organohalogen (with triclosan (TCS) as a model compound) by reduced a-BCs; 2) investigate the impact of the chemical nature of quinones (QNs) as presumed reactive components in a-BCs, on their reactivity for organohalogen degradation; 3) analyze the reactive chemical components of a-BCs by coupling high-resolution mass spectroscopy (HRMS) with characteristic reactions of a-BCs. The completed work has demonstrated the reductive dehalogenation of TCS by microbially-reduced a-BCs and their different reactivities dependent on parent materials and production processes. Experimental studies with model QNs and related thermodynamic/kinetic analysis have uncovered the critical roles of semiquinones (SQs) in reductive degradation reactions. HRMS and UV spectra analysis confirmed the rapid reactions between model quinones and cysteine, and the tagging efficiency was not affected by other co-occurring compounds. Orbitrap MS analysis coupled with chemical tagging through Michael addition reactions with cysteine identified possible QN-based compounds in a-BCs and their formula. This study laid the foundation for the potential applications of

the demonstrated reactions in the engineering treatment processes. Chemical tagging of a-BC using Michael addition reactions with cysteine was efficient and effective for identifying QNs.

DEDICATION

I want to dedicate my dissertation to my mother, Anitha, who would have been very proud of my Ph.D. journey and would be smiling down on me. I would also like to dedicate my dissertation to my father, Dr. K.V. Lokesh, who dreamt of me graduating with a Ph.D. long before the journey started and has been my inspiration throughout. I would also like to dedicate this dissertation to my sister, Priyanka, my biggest cheerleader.

ACKNOWLEDGEMENT

First and foremost, I express my gratitude to my advisor, Dr. Yu Yang, for providing guidance, support, and invaluable insights during my research endeavor. Dr. Yang's expertise, patience, and unwavering dedication to academic excellence played a crucial role in shaping the direction and quality of this thesis. He motivated me to delve deeper into the subject, consistently demonstrating faith in my abilities. Moreover, Dr. Yang encouraged me to pursue my interests while ensuring access to top-notch facilities, as he often remarked, "Your only limitation is your mind." I genuinely appreciate his mentorship and am privileged to have Dr. Yang as a teacher and a partner in my Ph.D. journey.

I am also indebted to the members of my thesis committee, Dr. Eric Marchand, Dr. David Hanigan, Dr. Charles Coronella, and Dr. Paul Verburg, for their valuable feedback, constructive criticism, and scholarly advice. Their expertise and rigorous examination of my work significantly strengthened the final outcome, and I am grateful for their time and dedication.

I would also like to thank all my collaborators, Dr. Rene Boiteau, Dr. Ching-Hua Huang, Dr. Sebastian Behrens, and the many graduate students and postdocs from their labs.

I would also like to express my heartfelt gratitude to my colleagues and research peers, both past and present, for their friendship, support, and stimulating discussions.

Specifically, I would like to thank Yasha Jathan, Abrar Shahriar, Anil Timilsina, Utsav Thapa, and Haley Grable. Their camaraderie and shared passion for knowledge made this academic journey memorable and rewarding. I would also like to thank our amazing laboratory manager Dr. Veronica Alumbaugh, who has always put the needs of the students first.

I am immensely grateful to express my heartfelt appreciation to all my friends in Reno, whose unwavering support has made this journey an incredibly enjoyable experience.

With deep reverence and overwhelming gratitude, I would like to remember my beloved mother, Anitha, whose presence and love continue to guide and inspire me every day.

Though she is no longer physically by my side, her unwavering support and belief in my abilities have been a constant strength throughout my Ph.D. journey. Her spirit is interwoven within the very fabric of this work, and it is with heartfelt appreciation that I honor her in these pages. I can almost envision her beaming with pride and joy as I reach this significant milestone. In addition, I extend my heartfelt dedication to my father, Dr.

K.V. Lokesh, whose unwavering faith in my potential and dreams of my Ph.D. graduation has been a driving force behind my pursuit of knowledge. His guidance, wisdom, and unwavering support have shaped me into the scholar I am today. I am forever indebted to him for instilling in me the ambition to reach new heights and being a constant source of inspiration throughout this challenging journey. Lastly, I thank my sister, Priyanka, my rock and biggest cheerleader. Her unwavering encouragement, belief in my abilities, and love have been an anchor in my life. She has been there to uplift and motivate me during moments of doubt and exhaustion. Her solid presence and support have given me the strength to overcome obstacles and persevere. I am forever grateful for her unwavering belief in me.

May the dedication to these extraordinary individuals serve as a testament to their immeasurable impact on my academic journey. Their unwavering love, guidance, and support have shaped me into the person and scholar I am today. As I embark on a new journey, I carry their spirits within me, knowing their influence will continue shaping my future endeavors.

Table of Contents

<i>Chapter 1: Introduction & Background</i>	1
1.1 Biochar	1
1.2 Aqueous Biochar	4
1.3 Reactive Components for Electron Shuttling	4
<i>Chapter 2: Research Objectives & Overview</i>	11
<i>Chapter 3: Anaerobic Dehalogenation by Reduced Aqueous Biochars</i>	13
3.1 Introduction	14
3.2 Methods and Materials	16
3.3 Results and Discussion	22
3.4 Environmental Implications	44
<i>Chapter 4: Critical Role of Semiquinones in the Reductive Dehalogenation</i>	46
4.1 Introduction	47
4.2 Methods and Materials	49
4.3 Results and Discussions	58
4.4 Environmental Implications	74
<i>Chapter 5: Analysis of Reactive Components of Aqueous Biochars</i>	76
5.1 Introduction	77
5.2 Materials and Methods	79

5.3 Results and Discussions	82
<i>Chapter 6: Conclusion</i>	93

List of tables:

Table 3-1: Parent materials and physicochemical properties of BCs and activated carbon used in this study.....	17
Table 3-2: Samples and controls setup with their target.....	20
Table 3-3: Setup for numerical fittings for the kinetics.....	41
Table 4-1: Model hydroquinone compounds used in this study and their basic physicochemical properties.....	51
Table 4-2: Key reactions and rate constants at pH 5 considered for the kinetic fitting ^a ..	55
Table 4-3: Key reactions considered for thermodynamic calculation.....	57

List of Figures:

Figure 1-1: Various ways BC can react with pollutants (Lu et al., 2020).	2
Figure 1-2: Graphical scheme for the reactions between quinones and Fe (Jiang et al., 2015).	6
Figure 3-1: Time-dependent concentrations of electrons accepted by a-BC during its reduction by <i>Shewanella putrefaciens</i> CN32, measured through the consequent reaction with ferric nitrilotriacetate (Fe(III)-NTA). Error bars represent standard deviations obtained from the triplicate experiment, with most of them unobservable due to the small size. a-CBC400, a-UBCS, a-UBCL, a-SW, and a-AC represent the aqueous BC samples prepared using b-CBC400, b-UBCS, b-UBCL, b-SW, and b-AC, respectively.	23
Figure 3-2: Degradation kinetics of triclosan (TCS) in the presence of different reduced a-BCs: a-CBC200(A), a-CBC400(B), a-UBCL(C), a-UBCS(D), a-SW(E), and a-AC(F) at different starting carbon concentration. Aerobic control, anaerobic control, and bacteria control were also shown. Full concentration indicates samples started directly with a-BC prepared through the leaching of bulk BC with 284.6, 27.3, 9.5, 6.9, 2.8, and 1.2 mg C/L for CBC200, CBC400, UBCS, UBCL, SW a-BC, and aqueous AC. Samples with diluted a-BC (1/2 of the original concentration and 1/3 of the original concentration) were also presented. Error bars indicate the standard error obtained from triplicate experiments, with most of them smaller than the symbol.	27
Figure 3-3: The correlation between the pseudo first-order rate constant for the degradation of triclosan (TCS) with the total organic carbon (TOC) concentration of aqueous BCs (a-BCs).	31

- Figure 3-4:** Relationship between the pseudo first-order rate constant (h^{-1}) for the degradation of TCS and a-BC-bound electron-donating capacity ($\text{mmol e}^{-1}/\text{L}$)..... 32
- Figure 3-5:** Kinetics for the generation of Cl^{-} together with the total chlorine recovery and the residual fraction of TCS. Results for the TCS reacted with a-CBC400 and a-SW, pre-reduced for 24, 12, and 6 h were shown. Error bars represent results from triplicate experiments. a-CBC400 and a-SW represents the aqueous BC samples prepared using bulk CBC400 and bulk SW, respectively. 33
- Figure 3-6:** By-products analysis of TCS degradation as analyzed by LC-TOFMS: **A)** Chromatograph of TCS (5-chloro-2-(2,4-dichlorophenoxy) phenol) standard solution; **B)** Chromatograph of 2-(2,4-dichlorophenoxy) phenol) standard solution; **C)** Chromatograph of 2(2-chlorophenoxy) phenol) standard solution; **D)** Chromatograph of TCS (5-chloro-2-(2,4- dichlorophenoxy) phenol) in the sacrificial sample after 192 hours of reaction with reduced a-CBC400; **E)** Chromatograph of 2-(2,4- dichlorophenoxy) phenol in the sacrificial sample after 192 hours of reaction with reduced a-CBC; **F)** Chromatograph of 2-(2-chlorophenoxy) phenol) in the sacrificial sample after 192 hours of reaction with reduced a-CBC400. 35
- Figure 3-7:** Kinetics for the generation of Cl^{-} and by-products of (5-chloro-2-(4-chlorophenoxy) phenol (CCPP) (with one chlorine removal from TCS) ($\text{TCS}-\text{Cl}^{-}$) and 5-chloro-2-(phenoxy)phenol) (CPP) (with two chlorine removal from TCS) ($\text{TCS}-2\text{Cl}^{-}$) together with the total chlorine recovery and the residual fraction of TCS for samples of a-CBC400. Error bars represent results from triplicate experiments. 36
- Figure 3-8:** By-products analysis of TCS degradation as analyzed by LC-TOFMS: **(A)** Mass spectra of Triclosan (5-chloro-2-(2,4- dichlorophenoxy) phenol); **(B)** Mass spectra

of 2-(2,4-dichlorophenoxy) phenol; (C) Mass spectra of 2-(4-chlorophenoxy) phenol in the sacrificial sample after 192 hours of reaction with reduced α -CBC400.....	37
Figure 3-9: Possible degradation by-products examined in LC-TOFMS analysis but not detected.	38
Figure 3-10: Reaction theme proposed for the dehalogenation of TCS by α -BC. The dissociation equilibrium for phenol groups was also noted, although not included in our calculation.	40
Figure 3-11: Least squares-based numerical fitting for the kinetics of TCS degradation and generation of Cl^- for the reactions with α -CBC400 pre-reduced for 24 h (A)(D), 12 h (B)(E), and 6 h (C)(F). Circles represent measured value when the blue lines stand for the fitting results. α -CBC400 represents the aqueous BC sample prepared using CBC400. .	43
Figure 4-1: Redox reactions of 1,4-benzoquinone and associated protonation/deprotonation.	48
Figure 4-2: TCS calibration curve in the presence and absence of $3\mu\text{M}$ Q and H_2Q	52
Figure 4-3: A) Q and H_2Q calibration curve; B) HPLC-UV absorbance spectra for Q and H_2Q	53
Figure 4-4: Kinetics for triclosan (TCS) degradation in the reactions between hydrobenzoquinone (H_2Q) ($3\mu\text{M}$) and TCS ($3\mu\text{M}$) in the absence (A) and presence (B) of FeCl_3 ($3\mu\text{M}$). All reactions were conducted at pH 3, 5, and 7; and in anoxic (with dissolved $\text{O}_2 < 10\mu\text{M}$) (filled symbols) and oxic condition (dissolved $\text{O}_2 = 200\mu\text{M}$) (open symbols). Error bars represent the standard deviation collected from triplicate measurements. Some error bars were too small to visualize.	59

Figure 4-5: (A) Time-dependent concentrations of triclosan (TCS) in the controlled experiments at pH 5 with a) Fe(II) ($3 \mu\text{M FeCl}_2$); b) Fe(III) ($3 \mu\text{M FeCl}_3$); c) benzoquinone (Q) ($3 \mu\text{M}$) under anoxic conditions. To verify the possibility of the degradation of TCS by the radicals generated through the oxidation of Fe(II), data for TCS in the presence of Fe(II) under oxic condition was also shown. (B) Time-dependent concentrations of hydrobenzoquinone (HBQ) in reactions with TCS under oxic and anoxic conditions..... 60

Figure 4-6: (A) Kinetics for the degradation of triclosan (TCS) reacted with hydrobenzoquinone (H_2Q) and FeCl_3 in the absence of O_2 at pH 5, together with the simulation. Four initial concentrations of $\text{H}_2\text{Q}/\text{FeCl}_3/\text{TCS}$ were used, including 20/20/0.3, 20/20/0.2, 20/20/0.15, and 200/20/0.15 μM , marked in the figure legends. Dots represent the measured results, while the lines represent the simulation. (B) Measured time-dependent concentrations of Fe(II), benzoquinone (Q), and H_2Q in the system with an initial concentration of 20/20/0.3 $\mu\text{M H}_2\text{Q}/\text{FeCl}_3/\text{TCS}$ with the simulation. Error bars represent the standard deviation collected from triplicate measurements. Some error bars were too small to visualize..... 62

Figure 4-7: By-products analysis of TCS degradation as analyzed by LC-TOFMS: (A) Mass spectra of Triclosan at day) of reaction; (B) Mass spectra of TCS degradation products after 2 days of reaction; (C) Mass spectra of TCS degradation by-products after 4 days of reaction. 64

Figure 4-8: Electron paramagnetic resonance (EPR) signals detected for reactions between Fe(III) ($3 \mu\text{M}$) and H_2Q ($300 \mu\text{M}$). Control experiments with only Fe(III) or H_2Q were conducted to account for background signals. 66

- Figure 4-9:** Time-dependent concentration of semibenzoquinone (SQ⁻) in the reactions between hydrobenzoquinone (H₂Q) (3 μM) and FeCl₃ (3 μM) in the presence of different concentration of dissolved O₂ (0, 1 μM, saturated dissolved O₂ (200 μM)). 67
- Figure 4-10:** pH-dependent *Eh* for the redox pairs involved in the system. 69
- Figure 4-11:** pH-dependent equilibrium concentrations of SQ⁻ in the system with an initial concentration of 20/20 μM FeCl₃/ H₂Q, considering the complexation of Fe³⁺/Fe²⁺ with OH⁻ and the solubility restriction for Fe(OH)₃ and Fe(OH)₂. 70
- Figure 4-12:** Comparison between the thermodynamic equilibrium and steady-state concentration (based on the kinetic simulation) of SQ, HQ, Q, and Fe(II) and thermodynamic equilibrium concentration for the system with 20/20 μM H₂Q/FeCl₃ under anoxic condition. 71
- Figure 4-13:** Time-dependent TCS concentration in anoxic reactions with substituted hydroquinones (HQs) (dimethyl hydroquinone (DMH), trimethyl hydroquinone (TMH), 1,2-dihydroxynaphthlene (DHN)) with initial concentrations of 20/20/0.3 μM HQ/FeCl₃/TCS (A) and (B) calculated equilibrium semiquinone (SQ) concentrations in the system with different HQs in the system of 20/20/0.3 μM HQ/FeCl₃. The result for HBQ was shown as a comparison. 73
- Figure 4-14:** Reactions between mitoxantrone (red) and epigallocatechin (blue) and TCS in the presence (circles) and absence (squares) of FeCl₃ under anoxic (filled symbols) and oxic conditions (open symbols). 74
- Figure 5-1:** Mass spectrometry analysis by Orbitrap mass spectrometry of a-SW. 78
- Figure 5-2:** UV-spectra and time of flight mass spectrometry (TOF-MS) analysis of quinone and cysteine (CY) reactions. (A1) and (B1): UV and MS spectra of 50 μM CY,

(A2) and (B2): UV and MS spectra of 50 μM 1,4-benzoquinone (BQ) and 50 μM CY reaction, (A3) and (B3): UV and MS spectra of 50 μM 2-methyl-1,4-benzoquinone (MBQ) and 50 μM CY reaction, (A4) and (B4): UV and MS spectra of 50 μM 2-chloro-1,4-benzoquinone (CBQ) and 50 μM CY reaction, (A5) and (B5): UV and MS spectra of 50 μM 1,4-naphthoquinone (NQ) and 50 μM CY reaction, (A6) and (B6): UV and MS spectra of 50 μM 1,4-anthraquinone (AQ) and 50 μM CY reaction, (A7) and (B7): UV and MS spectra of 50 μM 9,10-anthraquinone-2-carboxylic acid (AQA) and 50 μM CY reaction.
 84

Figure 5-3: Calibration curve for benzoquinone based on the TOF-MS intensity for the selected peaks ($m/z = 230.048$) resulting from the Michael addition reactions between benzoquinone and cysteine. 86

Figure 5-4: UV-spectra and TOF-MS analysis for tagging selectivity. (A-1) and (B-1): UV and MS spectra of 50 μM cinnamic acid (CnA) and 50 μM CY reaction, (A-2) and (B-2): UV and MS spectra of 50 μM coumaric acid (CoA) and 50 μM CY reaction, (A-3) and (B-3): UV and MS spectra of 50 μM caffeic acid (CaA) and 50 μM CY reaction. (C-1) and (D-1): UV and MS spectra of 50 μM BQ and 50 μM CY (1:1) reaction in the presence of 50 μM CnA, 50 μM CoA, and 50 μM CaA. (C-2) and (D-2): UV and MS spectra of 25 μM BQ and 50 μM CY (0.5:1) reaction in the presence of 50 μM CnA, 50 μM CoA, and 50 μM CaA. (C-3) and (D-3): UV and MS spectra of 10 μM BQ and 50 μM CY (0.1:1) reaction in the presence of 50 μM CnA, 50 μM CoA, and 50 μM CaA..... 87

Figure 5-5: Time of flight mass spectrometry (TOF-MS) analysis of (A) Swiss biochar extract (SW) and 10 μM Cysteine (CY) reaction, (B) SW, 10 μM 1,4-benzoquinone (BQ),

and 10 μM CY reaction, **(C)** SW, 10 μM 1,4-naphthoquinone (NQ), and 10 μM CY reaction..... 89

Figure 5-6: Orbitrap mass spectrometry (MS) analysis of solid phase extracted (SPE) concentrated Swiss biochar extracts reacted with cysteine. Mass difference on X-axis is the difference between the m/z value of the candidate compound after the reaction and the m/z value of the candidate compound before the reaction. The scale on the Y-axis is the log transformed ratio of the candidate compound's intensity before the reaction to the candidate compound's intensity after the reaction. The gray circle represents the candidates with a mass difference of cysteine, and the red circle highlights the unique candidates formed after the reaction. Panels **A** and **B** are the results of positive mode, and **C** and **D** are the results of negative mode. 91

Chapter 1: Introduction & Background

1.1 Biochar

Biochar (BC) has attracted much interest for its application in natural and engineered systems (Agegnehu et al., 2017; Hasan, 2018; Sanroman et al., 2017; Windeatt et al., 2014; Yu et al., 2019). BC is the material produced by the thermal decomposition of biomass with a limited supply of oxygen, typically at temperatures less than 700°C (Lehmann & Joseph, 2009, 2015). BC can be used for various benefits, including carbon sequestration, moisture retention, inhabiting microbial communities, etc. It has been well documented that BC can sorb pollutants similar to activated carbon (AC), with BC being more cost-effective. Recent studies have shown the positive roles that BCs play in mediating electrons for the microbial dehalogenation processes, which has been attributed to the quinone groups (Kluepfel et al., 2014; Lefevre et al., 2018; Tong et al., 2014; Yu et al., 2015). Previous studies have reported that the content of quinones (QNs) in BC (redox-capable moieties) is relatively higher than in natural organic matter (NOM), enabling BC to promote dehalogenation reactions more effectively (Zhang et al., 2020).

BC has been used as an adsorbent for heavy metals such as arsenic, chromium, cadmium, lead, mercury, and organic pollutants such as polycyclic aromatic hydrocarbons and herbicides, insecticides, and antibiotics in solution. BC is a promising sorbent for metals such as arsenic and chromium, with a sorption capacity ranging from 3.44–429 mg/kg (Chen et al., 2012; Wang et al., 2015). BC can also sorb organic compounds with similar performance as AC. For example, polychlorinated biphenyls were sorbed by BC with a sorption capacity of up to 415 µg/g compared to 420 µg/g for AC (Wang et al., 2013). As

an important note, ACs cost \$1100–\$1700/ton compared to \$350–\$1200/ton for BC (Thompson et al., 2016). Considering its advantages and socio-economic benefits, the application of BC as a replacement or alternative for AC has attracted much interest. However, there are issues with the disposal of BCs that have sorbed pollutants, as the residual non-degraded toxic compounds could potentially re-enter the environment (Lefevre et al., 2018).

Partially triggered by the issues with the disposal of BCs with sorbed pollutants, recent studies have shown that BCs can promote a range of reactions to degrade pollutants. So far, the BC-promoted reactions include surface, redox, and adduct reactions, as shown in

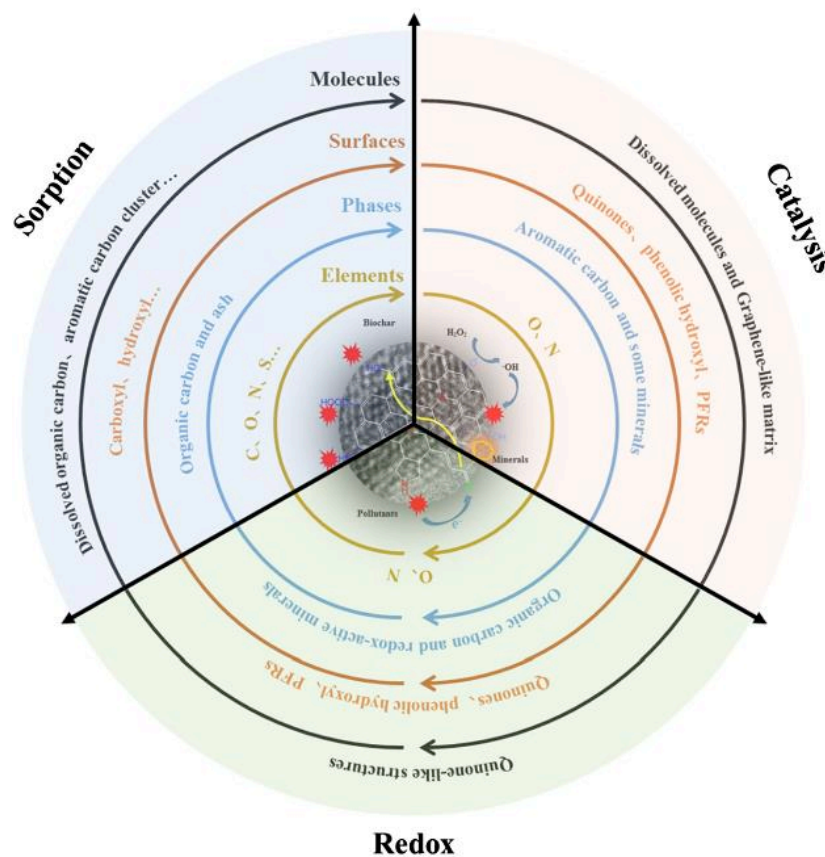


Figure 1-1: Various ways BC can react with pollutants (Lu et al., 2020).

BC has been used as a catalyst to transform vegetable/animal oils to biodiesel via esterification and transesterification, used to produce hydroxyl radicals, sulfate radicals, or chlorine-free radicals for application in oxidation processes (Dai et al., 2019; Lu et al., 2020). As an important mediator for redox reactions, BC can conduct electrons or facilitate electron transport. For example, the addition of BC to co-cultures of *G. metallireducens* and *G. sulfurreducens* with ethanol as the electron donor stimulated the syntrophic metabolism of ethanol (Chen et al., 2014). Xu et al. (2013) measured the conductivity of BC to be up to $0.65 \text{ S}\cdot\text{mm}^{-1}$ and demonstrated that the conduction of electrons through BC facilitated the transformation of RDX by sulfides.

Alternatively, BC particles can promote reduction reactions by shuttling electrons. Kappler et al. (2014) showed that BC could facilitate the microbial reduction of ferrihydrite, and Xu et al. (2016) demonstrated the capability of BC for promoting the reduction of hematite, which is more crystalline and challenging to reduce. In addition to Fe minerals, BCs have been shown to promote the reductive degradation of organic pollutants through the electron shuttling process. Oh et al., (2013) found that BCs could shuttle electrons between reductant dithiothreitol and organic contaminants, e.g., nitro herbicides and explosives, and thus promote the reductive reactions of pendimethalin, trifluralin, 2,4-dinitrotoluene, and hexahydro-1,3,5-trinitro-1,3,5-triazine. Other studies have reported an increase in the biodegradability of a wide range of organic pollutants in the presence of BC and AC, which includes pentachlorophenol (Tong et al., 2014; Yu et al., 2015), azo dyes (Van der Zee et al., 2003), phenanthrene (Leglize et al., 2008), 2,6-Dichlorophenol (Agarry et al., 2013), polychlorinated biphenyls (Kjellerup et al., 2014), and TBBP (Lefevre et al., 2018). These

BC-mediated reactions are promising for degrading pollutants. However, as many studies have reported, BCs can sorb contaminants, inhibit their bioavailability, and consequently hinder the reactions responsible for their degradation.

1.2 Aqueous Biochar

Lately, aqueous phase biochar (a-BC) (BC < 450 nm) has attracted substantial interest, as it can promote reactions of pollutants similar to bulk BC particles but not inhibit their availability due to the small size. Xu et al. (2016) showed that BC in the aqueous phase contributed to the accelerated reactions of hematite. To date, minimal work has been dedicated to comprehensively examining the a-BC-mediated reactions of pollutants. So far, most of the work for the role of a-BCs in the reactions of pollutants has been done in conjugation with bulk BC particles, which poses a challenge to distinguish the different processes, including the sorption/desorption of pollutants, electron shuttling by both bulk BC particles and a-BC, and electron conductance through BC particles. Hence, a study explicitly using a-BC would be crucial for unambiguously demonstrating the reactions between a-BC and organohalogen.

1.3 Reactive Components for Electron Shuttling

For BC-mediated reductive reactions, quinone (QN) structures have been assigned as the important component for the electron shuttling process, although direct evidence is limited. Many studies have demonstrated the critical role QNs play in shuttling electrons in NOM. Various studies have shown that BC contains a higher aromatic carbon content and likely a larger number of QN structures than NOM, enabling BC to promote the transformation of pollutants more efficiently than NOM. Lovley et al. (1996) showcased that NOM promoted the microbial reduction of Fe, with anthraquinone-2,6-disulfonate (AQDS) as

an analog compound. The following study by Scott et al., (1998) linked the electron-accepting capacity of the humic substances to the amount of QNs quantitatively, based on the electron paramagnetic resonance (EPR) measurement of semiquinone (SQ) radicals. More recently, Roden et al. (2010) showed that solid-phase humic substance could also shuttle the electrons and used the EPR signals as evidence for the role of QNs in facilitating Fe reduction.

Recent studies have been dedicated to studying the thermodynamics and kinetics of the reactions between different kinds of QNs and Fe. A study by Jiang et al. (2015) has shown that in acidic conditions, benzohydroquinone (H_2Q) can be oxidized by Fe(III) to form the benzosemiquinone (SQ) radical, which in turn can oxidize Fe(II) to Fe(III). Fe(II) oxidation to Fe(III) by SQ is more rapid when the SQ radical is in its deprotonated form. This result highlights the importance of SQ radical speciation in the redox cycling of the QN system. Further, this study investigated these redox reactions under oxygenated conditions and reported the oxidation of SQ by O_2 at circumneutral pH conditions but not below pH 5. Oxygen cannot oxidize H_2Q due to spin restriction (Garg et al., 2013; Jiang et al., 2015). For larger QN molecules, which are likely present in a-BCs, the reactions would presumably be slower due to larger conjugated aromatic structures, which could stabilize the free radical more than the hydrobenzoquinone system. The scheme for the reaction between Fe(III)/Fe(II) and the QN system is shown in **Figure 1-2**.

For the dehalogenation process, Zhang & Katayama (2012) showed that solid humic substances could promote microbial dehalogenation of pentachlorophenol using anthraquinone-2,6 disulfonate (AQDS) as an analog to QNs contained in humic substances.

However, these studies regarding the reactive components in NOM or BCs have certain drawbacks: 1) most of the studies are qualitative rather than quantitative for measurement of QNs and their roles in the redox reactions; 2) AQDS was used as a relatively arbitrary model compound to represent the reactive functional groups in NOM and BCs. Even with the model compounds, there are rare data regarding how the QNs react with organohalogen or other organic pollutants; 3) the direct measurement of QN in the complex mixture of NOM or BC is challenging. Up to date, the most reliable observation of the SQ radical by EPR analysis could not rigorously represent the total amount of QNs in the natural environment, when in fact, the SQ typically only represented a minor fraction due to the thermodynamics for reactions of Q, SQ, and H₂Q. Finally, no information is available about how the chemical properties of QNs can affect their reactivities toward the dehalogenation process.

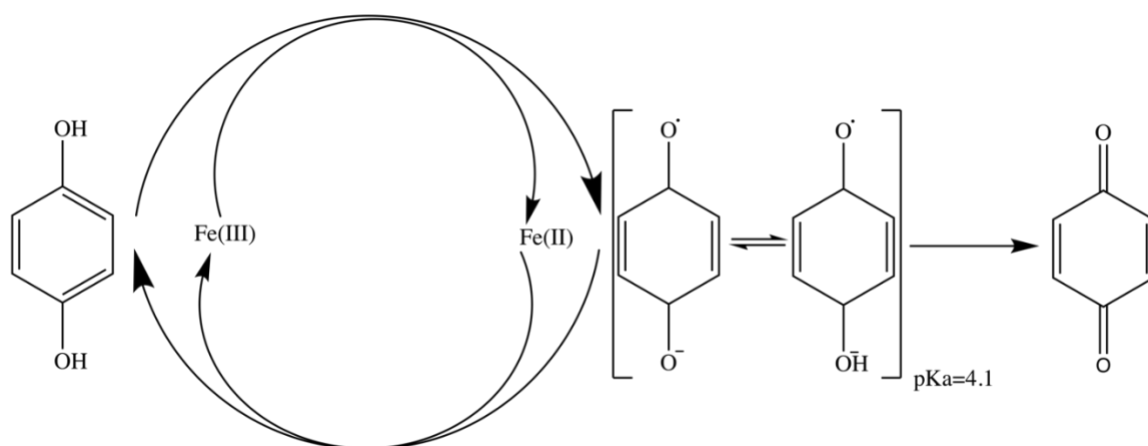


Figure 1-2: Graphical scheme for the reactions between quinones and Fe (Jiang et al., 2015).

The development of high-resolution mass spectroscopy (HRMS) analysis has opened new avenues for studying the reactive components of complex NOM or BCs. Accurate

determination of molecular mass coupled with various data analyses such as van Krevelen plots, Kendrick mass defect analysis, and isotopologue pattern analysis can be used to screen for potential target compounds of interest (Sleighter & Hatcher, 2007). The presence of possible compounds can be confirmed by additional MSⁿ fragment analysis upon the available authentic standards.

For instance, Boiteau et al. (2016) have demonstrated the structures for microbial siderophores complexing with Fe through the application of Fourier-transform ion cyclotron resonance mass spectrometry (FT-ICR-MS) coupling with liquid chromatography with inductively coupled plasma mass spectrometry (LC-ICP-MS). Recently, through sequential fractionation and HRMS analysis, Tian et al. (2021) were able to unambiguously identify a highly toxic quinone transformation product of N-(1,3-dimethylbutyl)-N'-phenyl-p-phenylenediamine (6PPD)-6PPD-quinone—a widely used tire antioxidant, as the primary cause for the death of coho salmon in U.S Pacific northwest regions. A similar method can be used to identify the reactive components of a-BC, which has not been done yet.

1.3.1 Quinone Redox Reactivity

Recent research has highlighted the ability of biochar to facilitate redox reactions that affect nutrient and metal/metalloid speciation, in addition to its traditional role as an inert adsorbent (Saquing et al., 2016; Tan et al., 2019). The conductor and battery-type mechanisms of electron transfer through biochar are mediated by redox-active moieties, including aromatic rings, oxygen, and nitrogen-containing functional groups, non-covalently bound redox-active metals, and persistent free radicals. The importance of oxygenated functional groups and quinoid chemical moieties on biochar in facilitating

electron transfer and contaminant remediation has been studied extensively (Sun et al., 2017).

Oxygenated functional groups, including phenolic, carbonyl, and other quinones, contribute to biochar's electron exchange capacity (EEC). Low H/C and high O/C elemental ratios of biochar have also been correlated with enhanced conductor mechanism of electron transfer through biochar, where a higher O/C ratio indicates a greater presence of oxygen-containing functional groups (Chacon et al., 2020; Yuan et al., 2017). These oxygenated functional groups create electron gradients and flux through the biochar, thereby enhancing electron transfer. It should be noted that surface functional groups also contribute to the sorption characteristics of biochar, which can affect the mediation of biochar-contaminant interactions. Quinoid functional groups have been implicated in biochar's stimulation of reductive dehalogenations. For example, Li et al. (2019) found positive correlations between the quinoid content of biochar, its measured EEC, and the enhancement of electron transfer from the dissimilatory iron-reducing bacteria *Shewanella putrefaciens* CN32 to nano zero-valent iron (NZVI), thus accelerating reductive dechlorination of PCP. Quinoid chemical moieties have also been shown to be important active sites on pyrogenic carbon materials used in the reductive degradation of nitro and azo compounds.

Quinones are naturally occurring organic compounds that are ubiquitous in the environment. They are commonly found in natural organic matter (NOM) and biochar's organic matrix. Quinones play important roles in the redox chemistry of NOM and biochar, and they have been the subject of extensive research in recent years (Yuan et al., 2017; Zhang & Katayama, 2012). Quinones in NOM are formed through the oxidative

transformation of organic matter by natural processes, such as sunlight, microbial activity, and chemical oxidation (Zhang et al., 2019). Quinones are highly reactive compounds that can undergo reversible redox reactions with a wide range of electron donors and acceptors. These reactions play important roles in the biogeochemical cycling of elements, such as carbon, nitrogen, and sulfur.

Quinones in NOM have been shown to act as electron shuttles, facilitating the transfer of electrons between different redox-active species in the environment (Kappler et al., 2014; Kluepfel et al., 2014). For example, quinones can accept electrons from organic acids and amino acids, which are common components of NOM, and transfer these electrons to other redox-active species, such as iron and manganese oxides. This electron transfer process can significantly impact the biogeochemical cycling of elements in aquatic and soil systems.

In biochar, quinones are formed through the pyrolysis of organic matter. Quinones in biochar have been shown to act as electron acceptors, facilitating the transfer of electrons from microorganisms to biochar. This process, known as electron shuttling, can significantly impact soil microbial communities and the biogeochemical cycling of nutrients, such as nitrogen and phosphorus. Quinones in biochar have also been shown to have important implications for the remediation of contaminated soils and water. Quinones can react with a wide range of organic and inorganic contaminants, such as polycyclic aromatic hydrocarbons (PAHs) and heavy metals, leading to their immobilization or degradation. This has led to the development of quinone-modified biochar as a promising tool for the remediation of contaminated environments.

In summary, quinones are important compounds in natural organic matter and biochar. They play important roles in the redox chemistry of these systems and have significant implications for the biogeochemical cycling of elements, the formation of disinfection by-products in drinking water, and the remediation of contaminated soils and water. Further research on the properties and behavior of quinones in these systems is needed to fully understand their impact on environmental processes and develop effective management strategies.

Chapter 2: Research Objectives & Overview

Objective 1: *Study the degradation of organohalogen (with triclosan as a model compound) by aqueous biochars*

Rationale: Although bulk BC particles have been shown for their reactivities of degrading organohalogens, no existing studies have analyzed the reactions between organohalogens and a-BC, which can potentially promote the reaction of organohalogens but not affect their availability.

Summary of research activities: Triclosan (TCS) was used as a model organohalogen due to its wide detection in US water bodies as a top pollutant and demonstrated persistence under certain environmental conditions, although it was banned for use in over-the-counter antiseptic products. A range of BCs with different parent materials (hardwood and soft biomass), production temperatures, and physicochemical properties (different particle sizes) were used as representative BCs. a-BCs were produced by mixing BCs with deionized (DI) water, shaking the slurries for seven days, and then filtering the samples (< 0.45 μm).

We studied the reactions between TCS and microbially-reduced a-BCs. We analyzed the electron-accepting capacities of a-BCs and their impact on their reactivity toward degrading TCS. We measured the kinetics for the production of TCS degradation by-products and obtained the rate constants for critical steps by mathematical simulations.

Objective 2: *Investigate the impact of the chemical nature of quinones on their reactivity for organohalogen degradation*

Rationale: QNs have been assumed as the reactive components in BCs and other similar NOM toward redox reactions. Rare direct evidence exists regarding the reactions between

organohalogen and QN compounds, and little information is available on the impact of chemical properties (molecular weight and oxidation-reduction potentials) of QNs on their reactions with organohalogens. As phenol groups, SQ and H₂Q speciation can be affected by pH, and consequently, their reactions with organohalogens can also be regulated by pH, which has not been studied before.

Summary of research activities: Available model QN compounds (including benzoquinone (Q)/hydrobenzoquinone (H₂Q)) were used to directly demonstrate the reactions between organohalogen (TCS) and QNs. We studied: 1) the degradation of TCS by model HQs at different aqueous chemical conditions (pH, different redox conditions); 2) fit the reaction kinetics to obtain the reaction rate constants for the critical reactions; 3) analyzed the impact of chemical properties (molecular weight, oxidation-reduction potential) of model HQs on the thermodynamics and kinetics of their reactions with TCS.

Objective 3: *Analyze the reactive chemical compositions of aqueous biochars*

Rationale: Due to the heterogeneity and complexity of a-BC, it is challenging to determine the chemical nature of their reactive components, which impairs the complete understanding of their reactions with organohalogens and appropriate applications.

Summary of research activities: Multiple strategies were used to tackle the challenges of identifying reactive components of a-BC: 1) method was developed to chemically tag BQs with cysteine using Michael addition. 2) using the developed method, a-BCs were chemically tagged and analyzed by LC-UV and HRMS to identify the tagged quinone-containing molecules.

Chapter 3: Anaerobic Dehalogenation by Reduced Aqueous Biochars

Status:

Lokesh S, Juhee K, Zhou YW, Wu DP, Pan B, Wang XL, Behrens S, Huang CH, Yang Y. 2020. Anaerobic dehalogenation by reduced aqueous biochars. *Environmental Science & Technology*. 54, 15142–15150

Abstract

*Dehalogenation is one of the most important reactions for eliminating trace organic pollutants in natural and engineering systems. This study investigated the dehalogenation of a model organohalogen compound, triclosan (TCS), by aqueous biochars (a-BCs) (<450 nm). We found that TCS can be anaerobically degraded by reduced a-BCs with a pseudo first-order degradation rate constant of 0.0011–0.011 h⁻¹. The 288 h degradation fraction of TCS correlated significantly with the amount of a-BC-bound electrons (0.055 ± 0.00024 to 0.11 ± 0.0016 mol e⁻/mol C) available for donation after 24 h of pre-reduction by *Shewanella putrefaciens* CN32. Within the reduction period, the recovery of chlorine based on residual TCS and generated Cl⁻ ranged from 73.6 to 85.2%, implying that a major fraction of TCS was fully dechlorinated, together with mass spectroscopic analysis of possible degradation by-products. Least-squares numerical fitting, accounting for the reactions of hydroquinones/semiquinones in a-BCs with TCS and by-products, can simulate the reaction kinetics well (R² > 0.76) and suggest the first-step dechlorination as the rate-limiting step among the possible pathways. These results showcased that the reduced a-BCs can reductively degrade organohalogenes with potential applications for wastewater treatment and groundwater remediation. While TCS was used as a model*

compound in this study, a-BC-based degradation can likely be applied to a range of redox-sensitive trace organic compounds.

3.1 Introduction

Organohalogen compounds, utilized in a variety of industrial applications, cause persistent harmful effects on ecosystems and human health (Bhatt et al., 2007; Letcher et al., 2009; Pessah et al., 2019; Redon et al., 2011; Vriens et al., 2019). Their widespread use in solvents, degreasing agents, biocides, and many other products requires large volumes to be synthesized (Adrian & Löffler, 2016; Bellar et al., 1974; Häggblom & Bossert, 2004). Once used, organohalogen compounds are ultimately released into the environment, raising concerns about the toxicity of these compounds and their environmental effects (Khan et al., 2013; Kodavanti & Loganathan, 2016; Richardson, 2003; Richardson & Ternes, 2018; Vreugdenhil et al., 2002). Most organohalogen compounds are persistent and hard to degrade; with half-lives of up to 34 years, they pose challenges for engineering treatment and remediation (Atashgahi et al., 2018; Exner & Färber, 2006; Field & Sierra-Alvarez, 2008; Kookana et al., 2011; J. Liu & Mejia Avendaño, 2013; Singer et al., 2002; Sinkkonen & Paasivirta, 2000; Ying et al., 2007). Dehalogenation is the most critical step in the degradation of organohalogen compounds. Uncovering useful dehalogenation reactions and developing efficient engineering treatment processes for the degradation of organohalogens are needed for wastewater treatment and remediation of polluted soils and groundwater (Berggren et al., 2013; Häggblom & Bossert, 2004; Mohn & Tiedje, 1992; Weatherill et al., 2018; Wiegel & Wu, 2000; Zhao et al., 2018). As a potential cost-effective material for environmental treatment and remediation, BCs have attracted considerable interest in their application in environmental engineering systems. The chemical properties

of BCs can enable them to degrade organic compounds, including organohalogens, potentially reductively. A few recent studies have shown that bulk BC particles can promote the dehalogenation of organohalogens, e.g., tetra-bromobisphenol A and pentachlorophenol mediating the electron transfer (Lefevre et al., 2018; Yu et al., 2015). However, sorption by bulk BC particles may reduce the bioavailability of the compounds and inhibit their susceptibility to biodegradation, and sorbed organohalogens can cause long-term concerns due to their persistence (Cornelissen et al., 2005; Koelmans et al., 2006; Marchal et al., 2013; Yang et al., 2009). Instead, if bulk BCs are mobilized to the aqueous phase ("a-BCs"), a-BCs potentially could mainly accelerate the degradation of organohalogens but not affect their bioavailability. In addition, the reactions between a-BCs and organohalogens can be controlled by the degree of reduction of a-BCs. The fully reduced a-BCs may degrade organohalogens more rapidly or thoroughly as more electrons are available for donation to the organohalogens. Up to date, although more and more interest has been given to characterizations and applications of BCs in the aqueous phase, such as those nano-sized, no reported studies have comprehensively examined the reactions between a-BCs and organohalogens and unambiguously determined the critical processes (Liu et al., 2018; Song et al., 2019). This study aimed to investigate the reaction between reduced a-BC and organohalogens using triclosan (TCS) as a model compound. TCS is among the most common contaminants in surface waters and wastewaters in the United States due to its widespread usage and remains a problem for water quality in many regions even after the ban on its primary usage (Weatherly & Gosse, 2017). There are three chlorine atoms in one TCS molecule, which makes TCS a suitable model compound for studies regarding the dehalogenation process. The primary objectives of this study were to

(1) investigate the reactions of TCS with various types of a-BC generated from different parent materials, including bulk-activated carbon (AC) as a reference for comparison, (2) study the controlling factors for the degradation of TCS by a-BC, including the available electrons for donation, and (3) analyze the by-products and pathways for the degradation of TCS by a-BC.

3.2 Methods and Materials

3.2.1 Materials

Triclosan ($\geq 98\%$ purity) was purchased from Sigma-Aldrich (St. Louis, MO, USA). The stock solution of 100 mg/L TCS was made in methanol ($\geq 99.9\%$, Sigma-Aldrich). Bulk corn biochar was produced by pyrolysis of corn straw at 200°C (CBC200) and 400°C (CBC400). Bulk Swiss biochar (SW) was bought from Swiss Biochar Sàrl, Switzerland. Slashed materials from pinyon pine-juniper wood were pyrolyzed in steel kilns to prepare the UBCX BCs. The biochar prepared was then sieved through US sieves #28 (600 μm), #35 (425 μm), #48 (300 μm), and #100 (150 μm). The fractions retained by sieve #28 (>600 μm) and #100 (150–300 μm) were used for the experiments and named UBCL and UBCS, respectively (Yanala, 2019). Granular activated carbon (FILTRASORB 400) was purchased from Calgon Carbon (Moon Township, PA, USA) (**Table 3-1**). All the other chemicals used in this study were of analytical grade. The strain *Shewanella putrefaciens* (*S.putrefaciens*) CN32 was kindly donated by Dr. Scott Fendorf of Stanford University.

Table 3-1: Parent materials and physicochemical properties of BCs and activated carbon used in this study.

	Parent material	Preparation Temperature	C (w/w)	O (w/w)	N (w/w)	SA ^a (m ² g ⁻¹)	Particle Size (mm)	a-BC in BC (%)	Small compounds in a-BC
CBC200 ^b	Cornstalk	200°C	47.8%	46.2%	0.7%			2.85%	20.6%
CBC400 ^c	Cornstalk	400°C	59.2%	22.4%	1.2%			0.27%	53.8%
UBCS ^d	Pinyon Pine– Juniper wood	500–700°C	73.0%	16.7%	0.64%	50	0.15– 0.3	0.09%	61.4%
UBCL ^e	Pinyon Pine– Juniper wood	500–700°C	73.0%	16.7%	0.64%	50	>0.6	0.07%	71.3%
SW ^f	Pinewood	700°C	73.2%	5.7%	0.64	231.8	0.25– 0.5	0.03%	86.9%
AC ^g	Bituminous coal	Thermal Activation	84.6%	10.7%	2.35%	1174	0.55– 0.75	0.01%	ND*

^a SA: surface area; ^b CBC 200: corn stalk-derived bulk biochar by pyrolysis at 200 °C; ^c CBC 400: corn stalk-derived bulk biochar by pyrolysis at 400 °C; ^d UBCS: Pinyon Pine–Juniper wood-derived bulk biochar with particle size of 0.3–0.15 mm; ^e UBCL: Pinyon Pine–Juniper wood-derived bulk biochar with particle size of >0.6 mm; ^f b–SW: Swiss bulk biochar derived from pine wood; ^g AC: Bulk activated carbon; a–BC: aqueous biochars derived from the corresponding parent bulk biochar; *ND: not detected

3.2.2 Preparation and characterization of a–BCs

To make the working solutions of a–BCs, bulk biochars (BCs) were suspended in milliQ water (18.3 MΩ·cm) with a ratio of 100 mg BC:10 mL milliQ water. The mixture was shaken horizontally at 150 rpm for seven days. Then, the mixture was filtered through a

0.45 μm glass fiber filter to get a-BCs (<450 nm). The total organic carbon contents in the a-BCs were measured with a Shimadzu TOC-VCSH (Kyoto, KYT, Japan). Size fraction analysis of a-BCs was carried out by centrifuging samples at 3000 g for 15 min with an Amicon centrifugal filter unit (cutoff molecular size of 3 kDa) (Sigma-Aldrich, St. Louis, MO), and the total organic carbon content in fractions smaller than 3 kDa was measured. For investigating the chemical compositions and their roles in the degradation of TCS, partial BC samples were analyzed with a fusion Orbitrap mass spectrometer (ThermoFisher Scientific, USA).

3.2.3 Microbial reduction of a-BC and Electron Transfer

Aqueous BC was reduced by *S. putrefaciens* CN32 (10^8 cells/mL), dissimilatory metal-reducing bacteria that can reduce a range of natural organic carbon and BCs, at pH 7 (3 mM bicarbonate buffer) with H_2 in the headspace as the terminal electron donor, and electron transfer to a-BC was monitored by the following reactions between reduced a-BC and Fe(III)-NTA (Roden et al., 2010; Xu et al., 2016). Similar to our recent work, the strain CN32 was grown for 24 h under aerobic conditions in 25 g/L Luria Bertani (LB) soy broth. Then, cells were harvested by centrifugation (4500 g, 20 min at 4°C) and washed twice with a 3 mM NaHCO_3 buffer (pH 7). The washed cells were re-suspended in an O_2 -free NaHCO_3 buffer (pH 7) and then reacted with a-BC. After different periods of reduction (up to 72 h), the strain CN32 cells were removed by filtration with 0.2 μm sterilized membranes. The filtrate (1 mL) was reacted with 0.1 mL of 10 mM Fe(III)-nitriloacetate (NTA) for 1 min. The resulting Fe(II) was measured as an indicator for the electrons accepted by a-BC using the ferrozine assay following previous studies (Xu et al., 2016). In brief, buffered ferrozine (0.1 mL) was added to the sample solution (1 mL) for

the measurement of Fe(II)–ferrozine with absorbance at 562 nm. The number of electrons accepted by a–BC was calculated based on the Fe(II) concentration. All the experiments were conducted in triplicate.

3.2.4 Degradation of TCS by Reduced a–BCs

For the investigation of TCS degradation, a–BCs in 3 mM NaHCO₃ buffer (pH 7) were pre-reduced by strain CN32 for 24 h, as described above. The concentrations of a–BCs used were determined to be 284.6, 27.3, 9.5, 6.9, 2.8, and 1.2 mg C/L for CBC200, CBC400, UBCS, UBCL, SW a–BC, and aqueous AC, respectively (**Table 3-1**). After the reduction, the samples were filtered with 0.2 µm membrane filters to sterilize the reduced aqueous BCs. The filtered samples were then spiked with 1 mg/L TCS. The filtration with 0.2 µm filters reduced the concentration of aqueous BCs only moderately (by 16%) for CBC200, which is determined to be minimally reactive and not the focus for most of the reaction analysis, and minimally for other samples (<6%). Samples of pre-reduced a–BC spiked with TCS were enclosed in glass vials with thick butyl rubber septa with a headspace of mixed H₂/N₂ (3.5%/96.5%) in an anaerobic glove chamber (COY, Grass Lake, MI) and then incubated in the dark on a rotary shaker (150 rpm) at 25°C. After different reaction intervals within 288 h, triplicate samples were sacrificed for the analysis of TCS. Three different controls were used (**Table 3-2**). (1) aerobic control: TCS was reacted with unreduced a–BC under aerobic conditions with ambient air in the headspace during the reaction; (2) anaerobic control: TCS was incubated with unreduced a–BC under the same anaerobic conditions as in the experiment; and (3) bacteria control: TCS was incubated with only the filtrate of the bacterial cell solution used to reduce a–BC under the same anaerobic protocol as in the experiment.

Table 3-2: Samples and controls setup with their target.

Sample/Control	Set up	Target
Sample	TCS+ reduced a-BC+ bacteria filtrate+ H ₂ /N ₂ in headspace	Dehalogenation reaction
Aerobic control	TCS+ unreduced a-BC + ambient atmosphere	Effect of condition
Anaerobic control	TCS+ unreduced a-BC + H ₂ /N ₂ in headspace	Contribution of reduction by H ₂
Bacteria control	TCS+ bacteria filtrate+ H ₂ /N ₂ in headspace	Contribution of reduction by bacteria filtrate

Additional experiments were also conducted to examine the impact of the a-BC concentration (as half and one-third of the original working solution of a-BCs) on the degradation of TCS. For the most reactive a-BC samples (CBC400 and SW), the impact of different pre-reduction periods were analyzed by reacting a-BCs pre-reduced in different periods (6 and 12 h) with TCS.

3.2.5 Analysis of TCS

For the analysis of TCS, the samples were passed through 0.2 µm glass fiber filters. Filtered samples were analyzed using high-performance liquid chromatography (HPLC, Agilent Technologies 1260, Folsom, CA, USA) equipped with a C18 column (5 µm, 4.6×150 mm). TCS was analyzed by detecting the UV absorbance at 284 nm. The mobile phase was 78:22 (v/v) of methanol and MilliQ water with a flow rate of 1 mL/min. The standard curve was established for TCS with concentrations ranging from 100 to 1000 µg/L.

3.2.6 Analysis of Chloride

To determine the quantity of chloride ions (Cl^-) generated during the degradation of TCS, Cl^- was measured using the mercuric thiocyanate method (EPA Method 8113) with a DR 6000 laboratory spectrophotometer (Hamilton, 1966; Zall et al., 1956). Samples (10 mL) were mixed with mercuric thiocyanate solution (0.8 mL) and Fe(III) solution (0.4 mL) and remained static for 2 min after vigorous mixing. The generated orange ferricthiocyanate complex, an index for the amount of Cl^- , was measured by analysis of UV absorption at 455 nm with a detection limit of 0.045 mg/L.

3.2.7 By-product Analysis

Standard compounds of 5-chloro-2-(4-chlorophenoxy)phenol (CCPP) (with one-chlorine removal from TCS) and 5-chloro-2-(phenoxy)phenol (CPP) (with two-chlorine removal from TCS) were donated by Dr. Kristopher McNeill and Dr. Jennifer Apell of the Swiss Federal Institute of Technology. The sample was collected during the sacrifice of samples for the identification of TCS at various time points of analysis and was used for LC/MS analysis. The samples were analyzed by an Agilent 1260 Infinity HPLC with a 6230 accurate mass time-of-flight mass spectrometry (LC-TOFMS) system equipped with a Poroshell 120 EC-C18 column (2.1×150 mm, 2.7 μm) at 10 μL of the injection volume. The eluent consisted of two mobile phases at a 0.4 mL/min flow rate with gradient elution: (A) 5 mM ammonium acetate and (B) acetonitrile. The gradient was as follows: B started at 50% for the first minute, increasing to 55% in 4 min, increasing to 100% in 10 min, and decreasing to 50% in 11 min. Negative electrospray ionization (ESI) at fragmentation voltages of 140, 180, 220, and 250 V with a mass scan range of 50–1000 m/z was conducted. The drying gas was controlled at 9 mL/min at 200°C. The nebulizer

pressure was set at 40 psi, and the capillary was maintained at 4000 V. Data acquisition and data processing were conducted with mass accuracy (exact mass ± 10 ppm), retention time ($t_R \pm 0.5$ min), isotope patterns (deviation of $< 5\%$), and formula finding.

3.2.8 Numerical Fitting and Statistical Analysis

IBM SPSS Statistics (version 26, IBM Corp., Armonk, NY, USA) was used for performing statistical analyses using the Student's t-test, Pearson test, or Spearman test in which $p > 0.1$ was considered insignificant. Model fitting was done with MATLAB 2019 (The Math Works, Inc.). To fit the kinetics for the presumed reactions involved in the degradation of TCS, the toolbox of "fcn2optimexpr" was used for the least-squares fitting.

3.3 Results and Discussion

3.3.1 Physicochemical Properties of Bulk and Aqueous Biochars

Bulk BCs with a carbon content of 47.8–73.2% (**Table 3-1**), used in this study, represent different types of parent materials, including hardwood like pinewood or pinyon pine–juniper wood and soft biomass material (corn stalk). We also compared corn stalk–derived BCs generated at two different temperatures (200°C and 400°C). Pinyon pine–juniper wood-derived BCs with two different particle sizes ($> 600 \mu\text{m}$ and $150\text{--}300 \mu\text{m}$) were also used to explore the impact of bulk BC particle size on the release of a-BC and its reactivity. Bulk-activated carbon produced through thermal activation has been used as a comparison. The release of a-BC accounted for 0.01–2.85% of bulk BC-bound C with values highest for CBC200 and lowest for AC; it is higher for the bulk BCs generated with a lower temperature than with a higher temperature ($\text{CBC200} > \text{CBC400}$) and higher for the bulk BCs derived from soft biological materials (corn stalk) than from hardwood (Rajapaksha et al., 2019; Yang et al., 2019). The difference between BCs with different particle sizes in

the release of a-BC was moderate. Stock suspensions of a-BC contained 284.6, 27.3, 9.5, 6.9, 2.8, and 1.2 mg C/L for a-CBC200, a-CBC400, a-UBCS, a-UBCL, and a-SW, respectively. Size fraction analysis of the a-BCs showed that 20.6%, 53.8%, 61.4%, 56.4%, and 86.9% of a-BC-bound carbon was below 3 kDa as freely dissolved small compounds for CBC200, CBC400, UBCS, UBCL, and SW a-BCs, respectively.

3.3.2 Electron Transfer for a-BC

Electrons accepted by a-BCs during the microbial reduction sharply increased within the first 6–12 h of the reaction and achieved the highest level within 24 h (**Figure 3-1**).

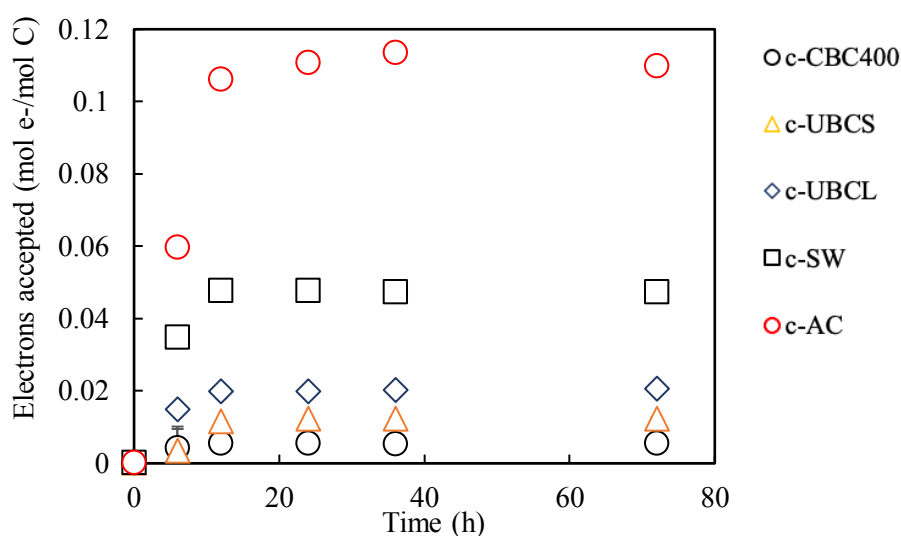


Figure 3-1: Time-dependent concentrations of electrons accepted by a-BC during its reduction by *Shewanella putrefaciens* CN32, measured through the consequent reaction with ferric nitrilotriacetate (Fe(III)-NTA). Error bars represent standard deviations obtained from the triplicate experiment, with most of them unobservable due to the small

size. a-CBC400, a-UBCS, a-UBCL, a-SW, and a-AC represent the aqueous BC samples prepared using b-CBC400, b-UBCS, b-UBCL, b-SW, and b-AC, respectively.

Electrons accepted by CBC200 a-BC were not detected as it was below $0.0018 \text{ mol e}^-/\text{mol C}$ based on the experimental detection limit. For other a-BCs at 24 h, the electrons accepted by a-BCs were determined to be 0.11, 0.047, 0.020, 0.011, and $0.0054 \text{ mol e}^-/\text{mol C}$ for aqueous BC of AC, SW, UBCL, UBCS, and CBC400, respectively. The amount of electrons accepted per molar carbon was, in general, higher than that measured for bulk BCs, as high as approximately $0.012 \text{ mol e}^-/\text{mol C}$, indicating the favorable leaching for the components enriched in electron-accepting domains, presumably quinoid groups (Heymann et al., 2011; Keiluweit et al., 2010; Kluepfel et al., 2014). SW and UBCL a-BCs had relatively higher electron acceptance capacity, indicating the higher density of electron-accepting moieties. The electron-accepting capacity was higher for hardwood-derived a-BCs, e.g., SW, UBCL, and UBCS a-BCs, than that from the soft biomass material of corn stalk, consistent with previous results (Jiang et al., 2017; Tomczyk et al., 2020). For corn-derived a-BC, the electron acceptance capacity was higher for samples generated at a higher temperature (400°C) than that of those produced at 200°C . It could be due to the higher formation of hydroxyl groups and aromatic structures, including quinoid groups, during pyrolysis at higher temperatures (Kluepfel et al., 2014; Lehmann, 2007; Pariyar et al., 2020). For bulk AC, Van der Zee et al. (2003) determined the electron acceptance amount of bulk AC with acetate as the terminal electron donor was approximately $0.004 \text{ mol e}^-/\text{mol C}$, much lower than the value we determined for the a-AC released. As the reduction potential (E^0_{H} vs. standard hydrogen electrode) for Fe(III)-

NTA/Fe(II) was -587 mV, comparable to the reduction potential of most organohalogenes of -500 to 1000 mV (-500 mV for TCS/dechlorinated products) (Curtis & Reinhard, 1994; Keum & Li, 2005; Martinez et al., 2012; Y. Wang et al., 2009), the electrons available for donation measured by reduction of Fe(III)–NTA would be relevant for the reaction with organohalogenes, such as the model compound TCS in this study.

3.3.3 Kinetics of Triclosan Degradation

Triclosan was degraded anaerobically by the pre-reduced a–BCs with the 288 h degradation fraction ranging from $26.9 \pm 1.8\%$ to $93.0 \pm 0.6\%$ (**Figure 3-2**). As the electron transfer experiment documented that the a–BC-bound donatable electrons achieved the highest value within 24 h, the 24 h-reduced a–BCs were used in this experiment. For the anaerobic control with unreduced a–BCs, the 288 h degradation fraction of TCS was $1.65 \pm 1.09\%$ (a–AC) to $27.0 \pm 8.58\%$ (a–CBC400). For CBC400 a–BC, the moderate degradation of TCS may indicate the reduction of TCS by the persistent semiquinone groups. When ambient air was used in the headspace for aerobic control, TCS degradation was much less than anaerobic samples, with the 288 h degradation fraction of $7.58 \pm 1.18\%$ to $18.9 \pm 0.71\%$ when O_2 served as a much stronger electron acceptor. The microbial control with the bacteria filtrate under the anaerobic conditions showed less than 20% of TCS to be degraded by the microbial-derived compounds (e.g., extracellular polymeric substances) in the filtrate within 288 h (Chan et al., 2002). Chan et al. (2002) showed that the reduction potential E^0_H of the EPS released by *Desulfovibrionaceae* and *Desulfobacteriaceae* was -540 mV (standard hydrogen electrode), which was potentially able to degrade TCS reductively. Compared to controls, the degradation of TCS by the reduced a–BCs under the anaerobic condition was substantially higher, documenting the strong anaerobic

reactions between reduced a-BCs and TCS. The 288 h anaerobic degradation fraction of TCS was $26.9 \pm 1.80\%$, $87.8 \pm 0.4\%$, $39.4 \pm 0.4\%$, $92.0 \pm 0.2\%$, $93.0 \pm 0.6\%$, and $91.2 \pm 0.2\%$ for reduced CBC200, CBC400, UBCS, UBCL, SW, and AC a-BC, respectively.

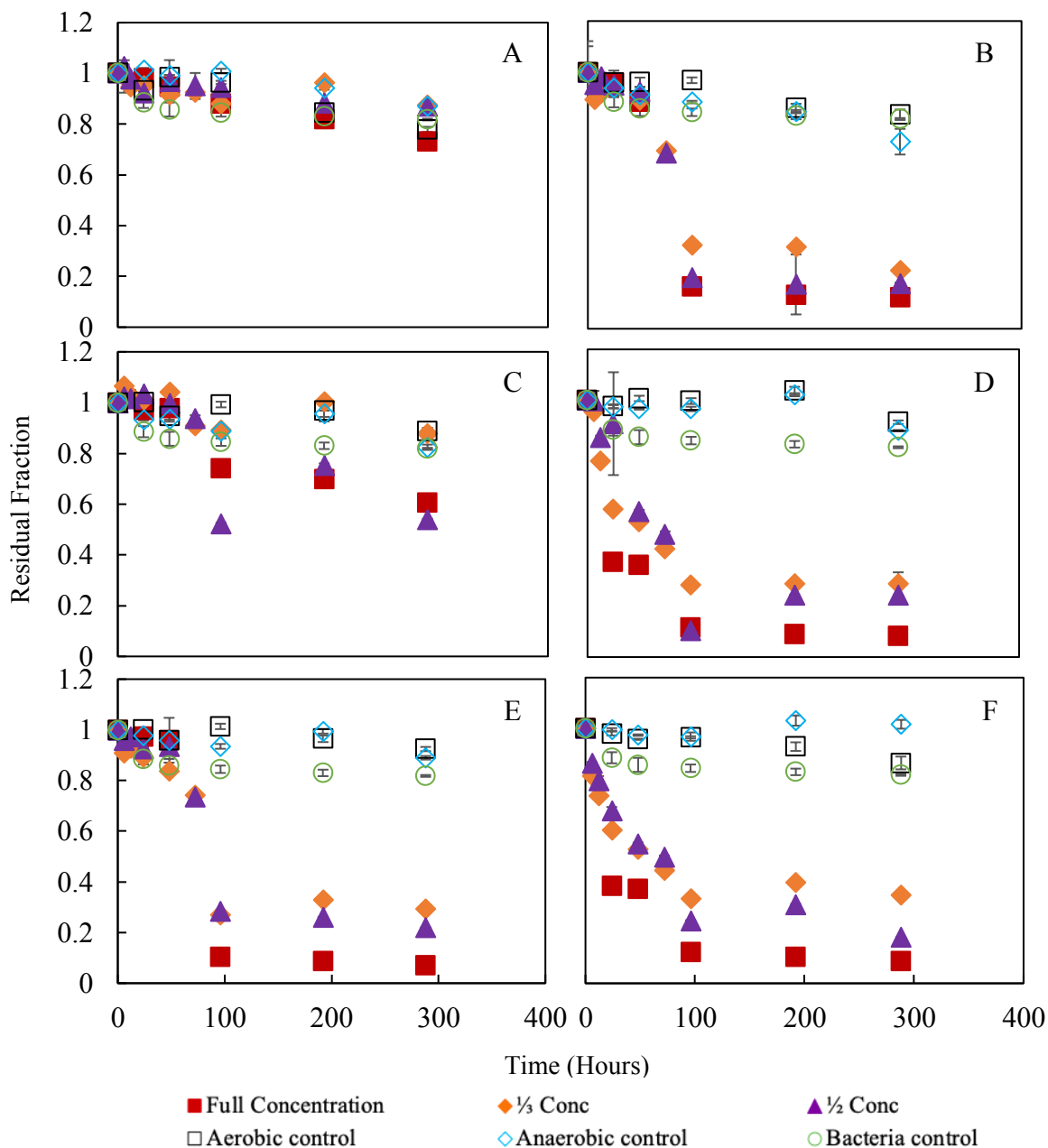


Figure 3-2: Degradation kinetics of triclosan (TCS) in the presence of different reduced a-BCs: a-CBC200(A), a-CBC400(B), a-UBCL(C), a-UBCS(D), a-SW(E), and a-AC(F) at different starting carbon concentration. Aerobic control, anaerobic control, and bacteria control were also shown. Full concentration indicates samples started directly with a-BC

prepared through the leaching of bulk BC with 284.6, 27.3, 9.5, 6.9, 2.8, and 1.2 mg C/L for CBC200, CBC400, UBCS, UBCL, SW a-BC, and aqueous AC. Samples with diluted a-BC (1/2 of the original concentration and 1/3 of the original concentration) were also presented. Error bars indicate the standard error obtained from triplicate experiments, with most of them smaller than the symbol.

Degradation of TCS by CBC200 a-BC was lowest with $26.9 \pm 1.80\%$ within 288 h, very close to controls (12.9–22.1%). Therefore, the following discussion regarding the reaction kinetics is focused on other BCs except for CBC200 a-BC. Based on the pseudo first-order fittings ($r^2=0.75-0.99$, $p<0.05$), the rate constant for TCS degradation ranged from 0.00108 h^{-1} to 0.0105 h^{-1} , corresponding to a half-life of 65.8–644 h. Anaerobic degradation of TCS by CBC400 and SW a-BC was relatively slow within the first 24 h. Then, substantial degradation occurred after 24 h, making the kinetics deviate from an apparent first-order kinetic pattern. Such derivation from the first-order pattern indicates more complicated reactions, to be discussed in the sections below. In addition, this study measured the degradation of the total TCS in the solution phase (freely dissolved TCS and TCS associated with a-BC) as the presence of a-BC did not affect the measurement of TCS; the effects of association with a-BC on the availability and reactivity of TCS are expected to be minor and beyond the scope of this work. The reaction was relatively slower than the abiotic reductive or oxidative reaction of organohalogen with metals. Rate constants for the dehalogenation of polybrominated diphenylethers (PBDE) and polychlorinated biphenyl (PCBs) by nano zero-valent iron (nZVI) ranged from 0.0001 to 0.1 h^{-1} (Bokare & Choi, 2010; Zhuang et al., 2010). Bokare & Choi, (2010) determined that the rate

constant for the reaction between TCS and nZVI was around 0.04 h^{-1} , which could be further accelerated by doping palladium. Trainer et al. (2020) found that rate constants for the oxidation of phenol compounds by manganese oxide ($\delta\text{-MnO}_2$) ranged from 0.001 to 149 h^{-1} with a value of 7.6 h^{-1} for TCS. The relatively lower reaction rate constants for TCS in this study are primarily because the concentration of a-BC and associated electrons were much lower than the metals. If normalized by the electrons bound with the nZVI, the rate constant for the dehalogenation of PCBs and PBDEs was approximately or below $1 \text{ h}^{-1}/(\text{mol e}^-/\text{L})$, while the corresponding values in this study ranged from 110 to $560 \text{ h}^{-1}/(\text{mol e}^-/\text{L})$. This indicates the efficient electron transfer between TCS and a-BC. There are limited studies regarding the microbial dehalogenation mediated by BC for which the half-lives were similar to this study, with a value above 120 h for pentachlorophenol and approximately 480 h for tetrabromobisphenol A (Lefevre et al., 2018; Yu et al., 2015). A few studies investigated carbonaceous nanomaterial-mediated reductive dehalogenation (Fu et al., 2014; Toral-Sánchez et al., 2018). Fu et al. (2014) showed that the rate constant for reductive degradation of hexachloroethane by sulfide increased from 0.001 to $0.002\text{--}0.0045 \text{ h}^{-1}$ in the presence of 10 mg/L carbon nanotube or graphene oxide. Although difficult to directly compare, the increase in the rate constant was of the same order of magnitude as the degradation rate constant for TCS in the presence of aqueous BC used in this study. Such comparison placed the reactions of TCS with a-BC in a potential abiotic method to degrade organohalogenes. In addition, the reactions of a-BC have an advantage of having low costs ($\$2.48/\text{kg}$ for BC compared to $\$69/\text{kg}$ for nZVI) and no by-products in particle phase, compared to the reactions with nZVI (Arun Gavaskar et al., 2005; Stefan Jirka & Thayer Tomlinson, 2014). These results and analyses indicate significant potential

for the application of a-BC in the engineering treatment of wastewater and remediation of groundwater. To evaluate the effects of the amount of a-BC on TCS degradation, TCS was also reacted with different concentrations of a-BC (**Figure 3-2**). When the a-BC concentration was decreased, the reactions were slowed down differently. CBC200 a-BC with reduced concentrations showed no significant differences compared to controls (*t-test, $p > 0.1$*); for UBCL with a concentration of one-third of the stock suspension, the TCS kinetics was also similar to the controls. For other BCs, when the a-BC concentration was reduced to 50% and 33% of the concentration in stock suspensions, the degradation slowed down and the 288 h degradation fraction decreased. When TCS was reacted with CBC400 a-BC of 13.8 mg C/L (1/2 concentration) and 9.2 mg C/L (1/3 concentration), the 288 h degradation fraction was 82.4% and 77.2%, respectively, compared to the value of 87.8% of the reaction with CBC400 a-BC of 27.58 mg C/L. Based on the kinetics, degradation of over 85% of TCS (at an initial concentration of 1.0 mg/L) within the reaction period of 288 h required CBC400, UBCL, SW a-BC, and a-AC at a concentration of 27.6, 7.32, 2.83, and 1.16 mg C/L, respectively. Bearing analysis uncertainty, the fitted pseudo first-order reaction rate constants were correlated with the total organic carbon (TOC) concentration of CBC400, CBCS, CBCL, SW a-BC, and a-AC (*Spearman test for data with 3 points, $p < 0.01$*) (**Figure 3-3**). When all a-BCs were analyzed together, no significant correlation existed (*Pearson or Spearman test, $p > 0.20$*).

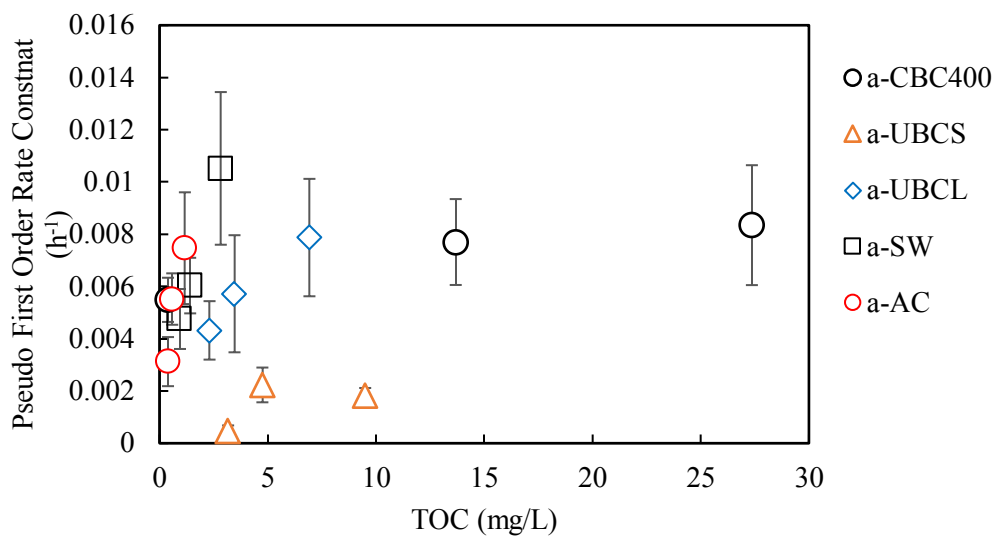


Figure 3-3: The correlation between the pseudo first-order rate constant for the degradation of triclosan (TCS) with the total organic carbon (TOC) concentration of aqueous BCs (a-BCs).

These results determined that the concentration of a-BCs can be used to predict the reaction rate of TCS when considering a single type of a-BC. If different types of a-BCs were evaluated, other properties need to be taken into account for the reaction rate prediction. For that perspective, there was a significant correlation between the pseudo first-order reaction rate constant and a-BC-bound electrons available for donating (*Pearson correlation coefficient, $r^2 = 0.64$, $p = 0.01$*) (**Figure 3-4**). In addition, the 288 h degradation fraction of TCS was also correlated with the a-BC-bound electrons (*Pearson correlation coefficient, $r^2 = 0.82$, $p = 0.04$*). For a-BC from different sources, a-BC-bound electrons available for donation could be used to predict the reaction rate constant. In terms of the “reactions” between TCS and a-BC-bound electrons, the pseudo second-order rate constant was determined to be $759 \text{ h}^{-1}/(\text{mol e}^-/\text{L})$ based on the regression between the

pseudo first-order reaction rate constant and the concentration of a-BC-bound electrons ($p < 0.05$) (**Figure 3-4**).

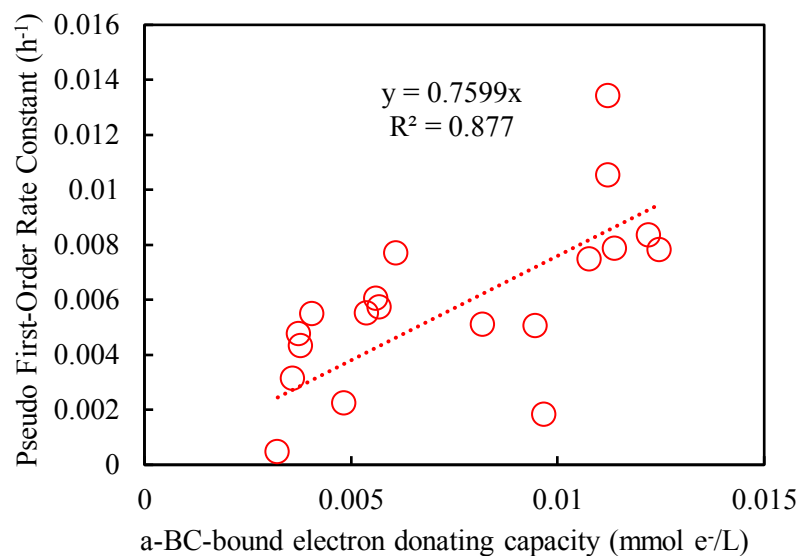


Figure 3-4: Relationship between the pseudo first-order rate constant (h^{-1}) for the degradation of TCS and a-BC-bound electron-donating capacity ($\text{mmol e}^{-1}/\text{L}$).

For the samples with CBC400 (soft material-based) and SW (hard wood-based) a-BC where TCS degradation was relatively high among a-BC samples used in this study, the impact of the reduction period for a-BC on the TCS degradation was also assessed (**Figure 3-5**). When the a-BC-bound electrons were slightly different for a-BC reduced for 12 and 24 h, the pseudo first-order reaction rate constant was also close for the two sets of samples. As a comparison, the a-BC-bound electrons were substantially lower for the 6 h reduced a-BC, and the pseudo first-order reaction rate constant was proportionally lower. To achieve the highest potential for degrading TCS, a-BC needs to be reduced for at least 12 h.

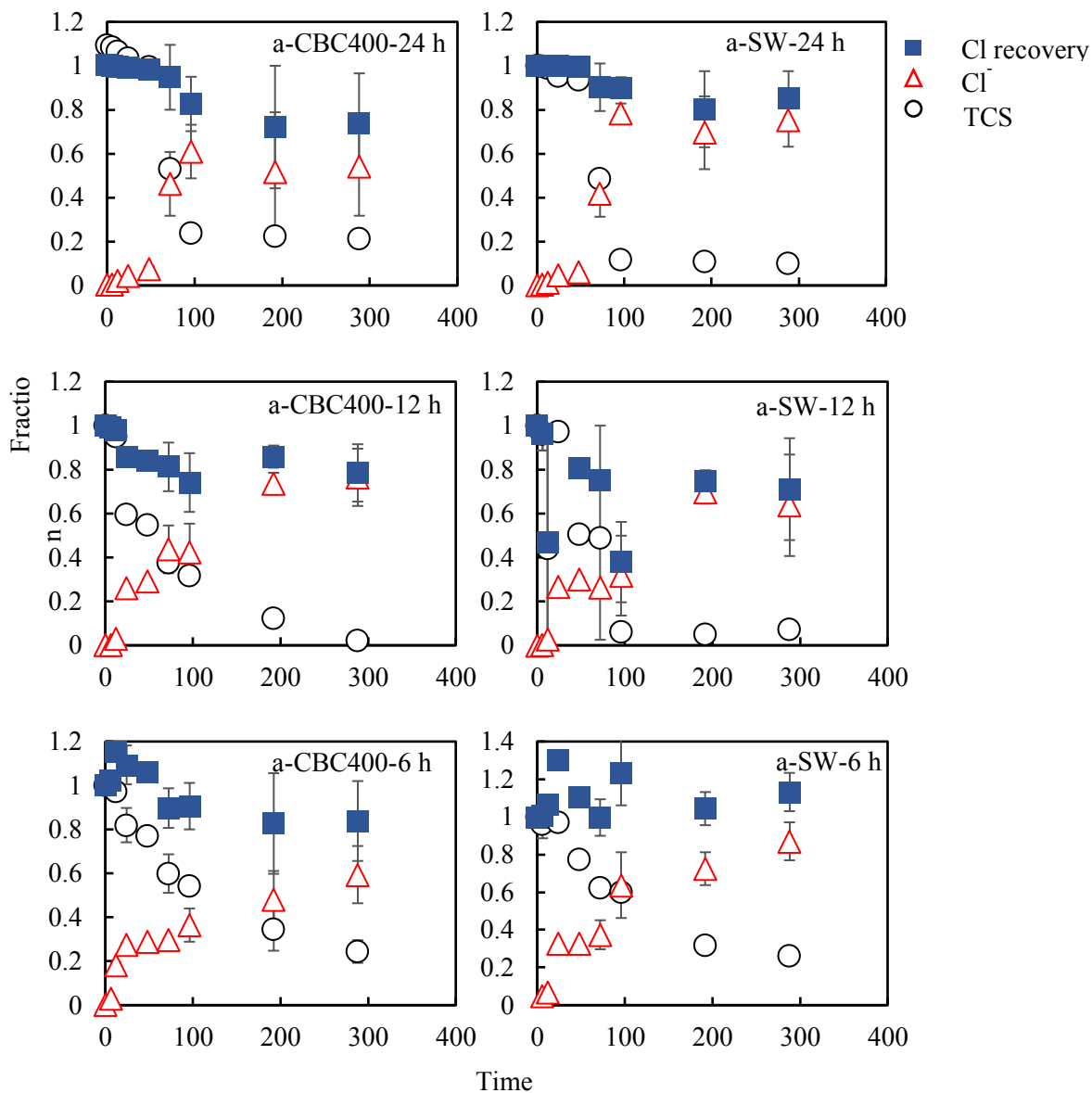


Figure 3-5: Kinetics for the generation of Cl⁻ together with the total chlorine recovery and the residual fraction of TCS. Results for the TCS reacted with a-CBC400 and a-SW, pre-reduced for 24, 12, and 6 h were shown. Error bars represent results from triplicate experiments. a-CBC400 and a-SW represents the aqueous BC samples prepared using bulk CBC400 and bulk SW, respectively.

3.3.4 By-product Analysis

In parallel to the TCS degradation, Cl^- was detected as a degradation by-product. Upon the degradation of TCS, Cl^- emerged with the fraction of $\text{Cl}^-/\text{total chlorine}$ (TOTCl^-) increasing sharply after 48 h and reaching $54.2 \pm 22.4\%$ and $75.3 \pm 2.2\%$ at 288 h for samples of CBC400 and SW a-BC, respectively. The total recovery of chlorine by Cl^- and residual TCS gradually decreased and ranged from 73.5 to 82.6% and 85.1 to 90.0% for CBC400 and SW samples during the period of 96–288 h. This relatively high recovery of chlorine by Cl^- and residual TCS suggests that most of the TCS was fully dechlorinated, with the remaining of TCS degraded to incompletely dechlorinated by-products. Furthermore, for the samples of a-CBC400 with the a-BC concentration in stock suspension, other dechlorination by-products were analyzed based on the LC-TOFMS analysis. Two major by-products were detected: a dechlorinated phenoxyphenol (m/z of 252.9829, $\text{C}_{12}\text{H}_8\text{Cl}_2\text{O}_2$) and a monochlorinated phenoxyphenol (m/z of 219.0222, $\text{C}_{12}\text{H}_9\text{ClO}_2$). These two products were identified by comparing the accurate masses, retention times, and mass spectra with those of the synthesized standards (5-chloro-2-(4-chlorophenoxy) phenol (CCPP) and 5-chloro-2-(phenoxy)phenol) (CPP) (**Figure 3-6–Figure 3-9**).

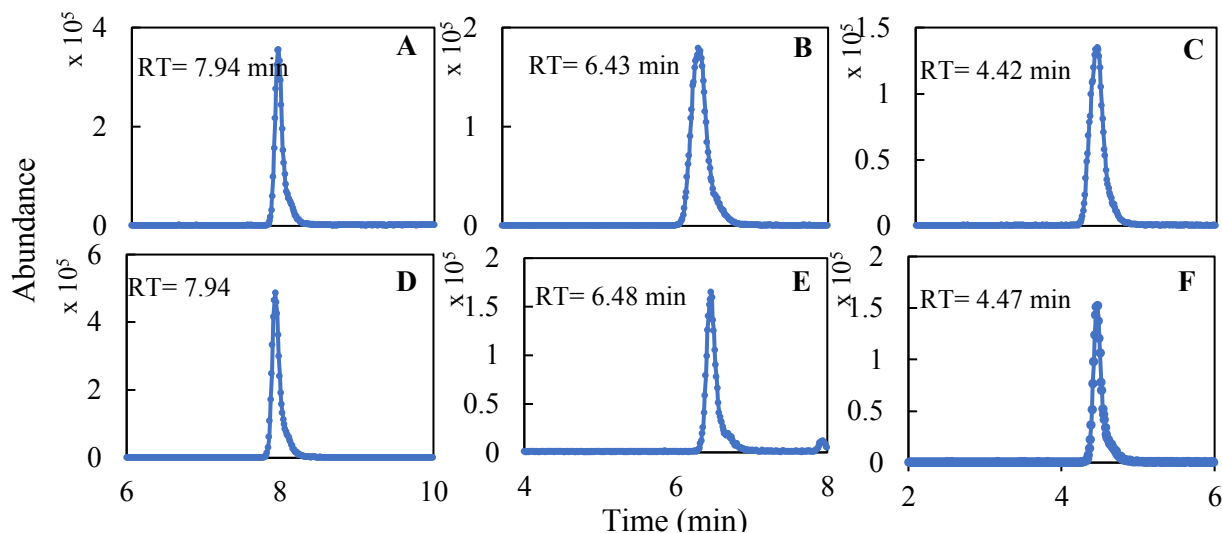


Figure 3-6: By-products analysis of TCS degradation as analyzed by LC-TOFMS: **A)** Chromatograph of TCS (5-chloro-2-(2,4-dichlorophenoxy) phenol) standard solution; **B)** Chromatograph of 2-(2,4-dichlorophenoxy) phenol) standard solution; **C)** Chromatograph of 2-(2-chlorophenoxy) phenol) standard solution; **D)** Chromatograph of TCS (5-chloro-2-(2,4-dichlorophenoxy) phenol) in the sacrificial sample after 192 hours of reaction with reduced α -CBC400; **E)** Chromatograph of 2-(2,4-dichlorophenoxy) phenol in the sacrificial sample after 192 hours of reaction with reduced α -CBC; **F)** Chromatograph of 2-(2-chlorophenoxy) phenol) in the sacrificial sample after 192 hours of reaction with reduced α -CBC400.

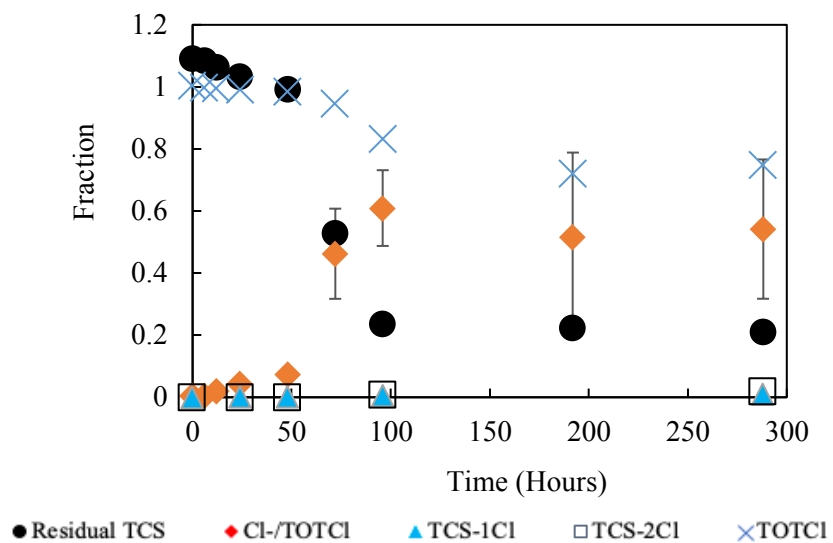
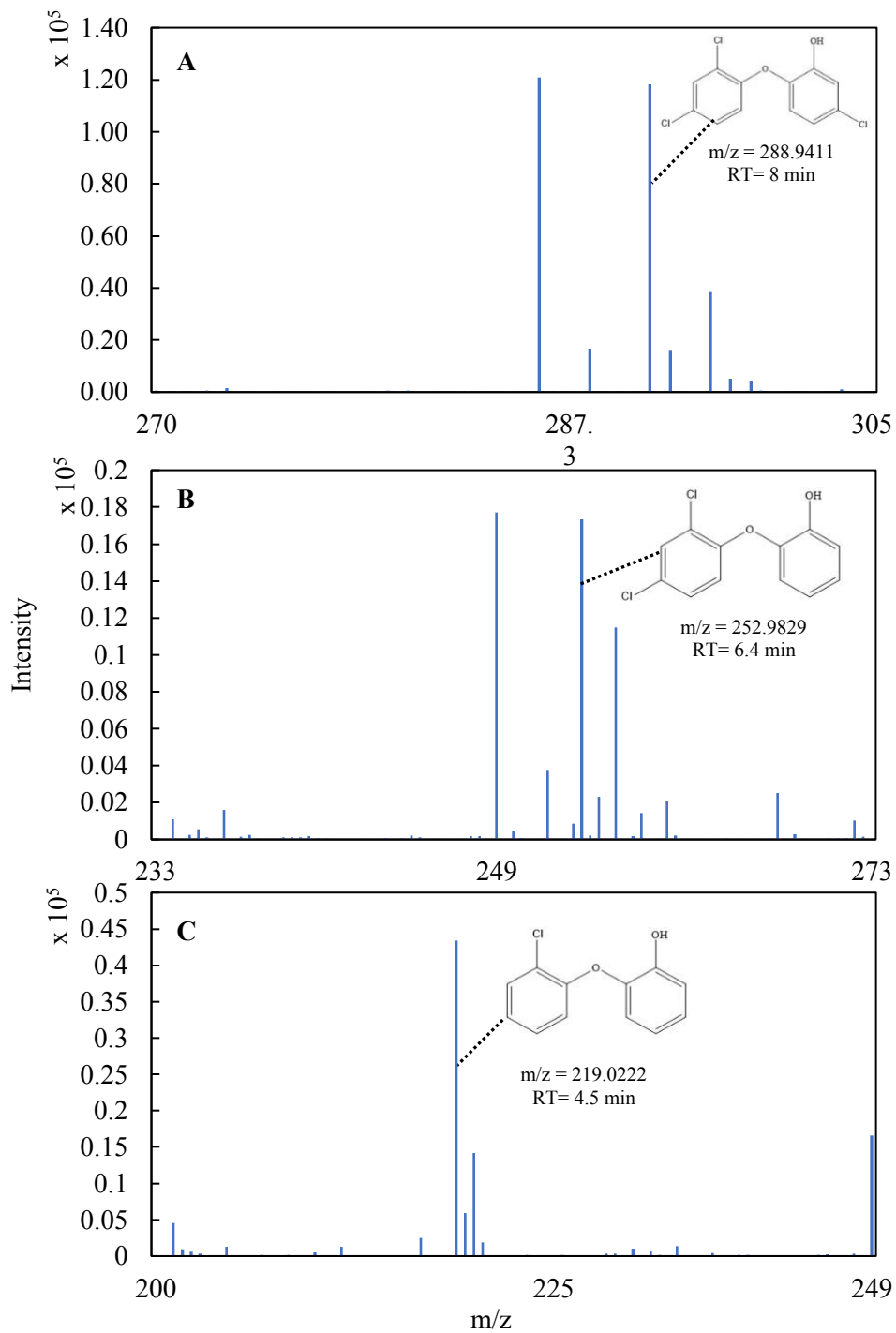


Figure 3-7: Kinetics for the generation of Cl^- and by-products of (5-chloro-2-(4-chlorophenoxy) phenol (CCPP) (with one chlorine removal from TCS) (TCS- Cl^-) and 5-chloro-2-(phenoxy)phenol (CPP) (with two chlorine removal from TCS) (TCS- 2Cl^-) together with the total chlorine recovery and the residual fraction of TCS for samples of a-CBC400. Error bars represent results from triplicate experiments.



of 2-(2,4-dichlorophenoxy) phenol; (C) Mass spectra of 2-(4-chlorophenoxy) phenol in the sacrificial sample after 192 hours of reaction with reduced α -CBC400.

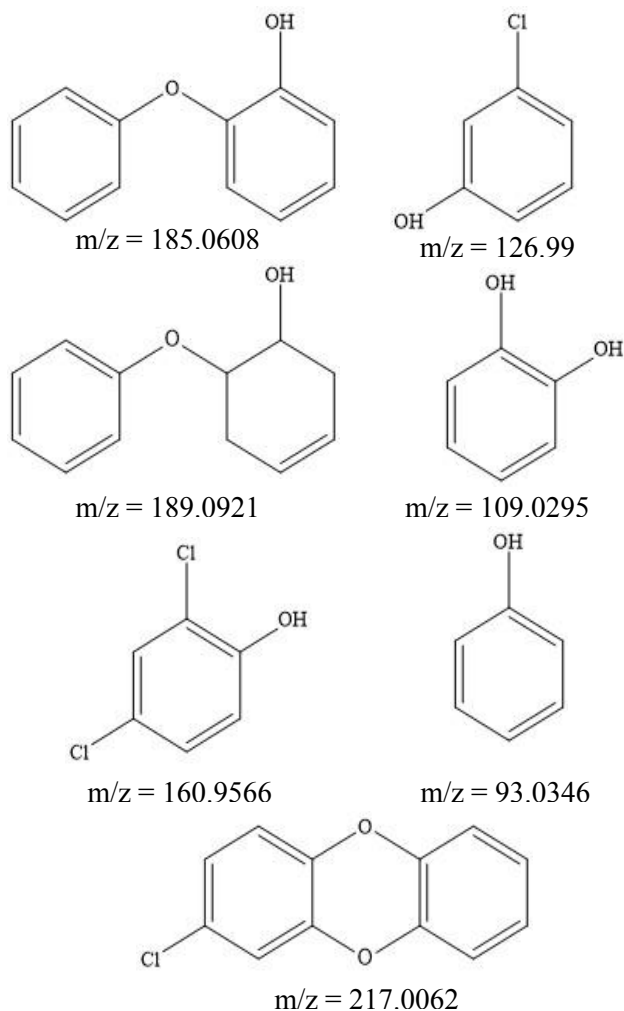


Figure 3-9: Possible degradation by-products examined in LC-TOFMS analysis but not detected.

Note that the C-Cl bonds on the dichlorophenoxy ring of TCS are more susceptible to cleavage than the C-Cl bond on the phenol ring, according to the previous study (Kliegman et al., 2013), which is also supported by the observation of the common fragment ion (m/z of 141.9827, $C_6H_3ClO_2$) from these two products that represent the phenol moiety of TCS

without dechlorination. Quantification of the CCPP and CPP products based on the standards indicated that their concentrations were low (<0.5 mg/L). Although only with two standards, we also screened other fragments and molecular peaks from possible dechlorination reactions, including the fully dechlorinated product (2-(phenoxy)phenol(PP)), and none of them were detected (**Figure 3-9**). The ortho-positioned electron-drawing ether group may make the Cl⁻ easier to knock off. The detection of these two by-products confirmed the dechlorination reaction. However, there may be other reaction pathways and by-products that can contribute as much as 25% of chlorine in the system and warrant further investigations.

3.3.5 Reaction Pathways and Kinetic Fitting

For the numerical fittings of reaction kinetics, we proposed reactions between TCS and presumable a-BC-based electron donors, i.e., QN groups, including SQs and H₂Qs (**Figure 3-10** and **Table 3-3**).

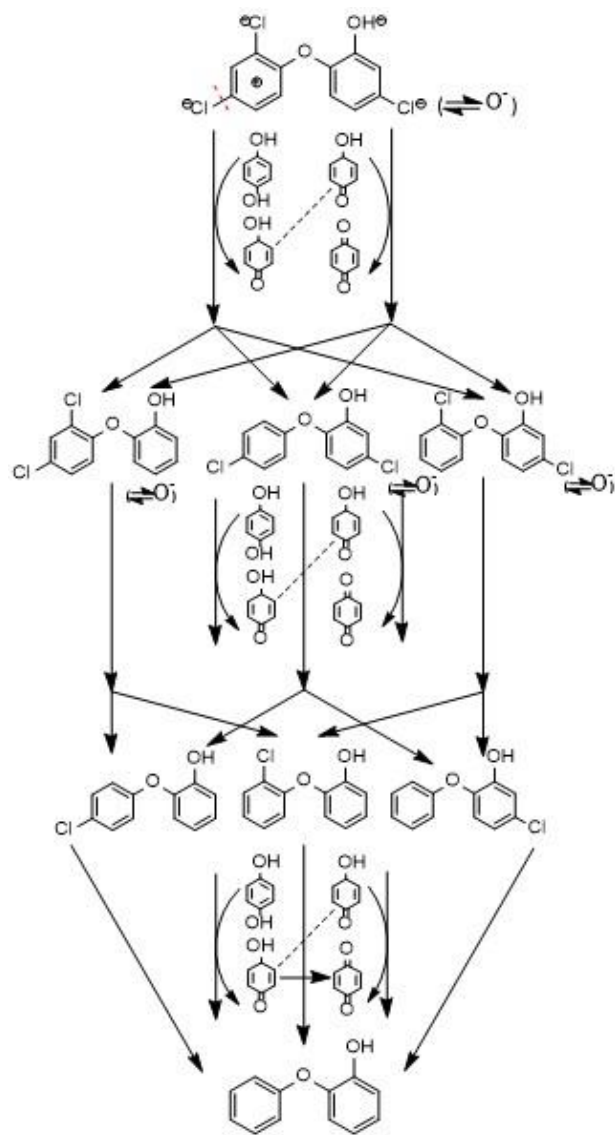


Figure 3-10: Reaction theme proposed for the dehalogenation of TCS by α -BC. The dissociation equilibrium for phenol groups was also noted, although not included in our calculation.

Table 3-3: Setup for numerical fittings for the kinetics.

Reactions	Rate constant	Variant	
$TCS + 2HQ$ $\rightarrow P + 2SQ + Cl^-$	k_1	TCS	triclosan
$P + 2HQ$ $\rightarrow P' + 2SQ + Cl^-$	k_2	P	2-Cl ⁻ by-products
$P' + 2HQ$ $\rightarrow P'' + 2SQ + Cl^-$	k_3	P'	1-Cl ⁻ by-products
$TCS + 2SQ$ $\rightarrow P + 2Q + Cl^-$	k_4	Cl^-	Cl ⁻ ion
$P + 2SQ$ $\rightarrow P' + 2Q + Cl^-$	k_5	Q	quinone
$P' + 2SQ$ $\rightarrow P'' + 2Q + Cl^-$	k_6	SQ	semiquinone
		HQ	hydroquinone
Equations			
$\frac{dTCS}{dt} = -k_1[TCS][HQ] - k_4[TCS][SQ]$			
$\frac{dP}{dt} = -k_2[P][HQ] - k_5[P][SQ] + k_1[TCS][HQ] + k_4[TCS][SQ]$			
$\frac{dP'}{dt} = -k_3[P'][HQ] - k_6[P'][SQ] + k_2[P][HQ] + k_5[P][SQ]$			
$\frac{dP''}{dt} = k_3[P'][HQ] + k_6[P'][SQ]$			
$\frac{dCl^-}{dt} = k_1[TCS][HQ] + k_2[P][HQ] + k_3[P'][HQ] + k_4[TCS][SQ] + k_5[P][SQ] + k_6[P'][SQ]$			
$\frac{dSQ}{dt} = 2(-k_4[TCS][SQ] - k_5[P][SQ] - k_6[P'][SQ] + k_1[TCS][HQ] + k_2[P][HQ] + k_3[P'][HQ])$			

$$\frac{dHQ}{dt} = 2(-k_1[TCS][HQ] - k_2[P][HQ] - k_3[P'] [HQ])$$

$$\frac{dQ}{dt} = 2(k_4[TCS][SQ] + k_5[P][SQ] + k_6[P'] [SQ])$$

For further investigation of chemical compositions in a-BCs involved in the reduction, mass spectrometry analysis of CBC400 and SW a-BC has detected over 500 peaks. The highest peak intensities were with m/z of 315.087 and 357.151 for CBC400 and SW a-BC, respectively, with multiple possible quinone-based structures (Chapter 5). In addition, EPR signals for the semiquinone radicals ($g = 2.00315$) have been captured for CBC400 bulk samples when this is minor for the CBC200 bulk BCs, which is consistent with the higher electron-accepting capacity of CBC400 a-BC. These analyses indicate that the reductive degradation of TCS by reduced a-BC is likely derived from the quinone groups, the chemical nature of which requires further investigations. Dechlorination was hypothesized to occur stepwise. Six rate constants for reactions between TCS as well as its degradation by-products and hydroquinone/semiquinone, were fitted using the least-squares method based on the kinetics for TCS degradation and generation of Cl^- .

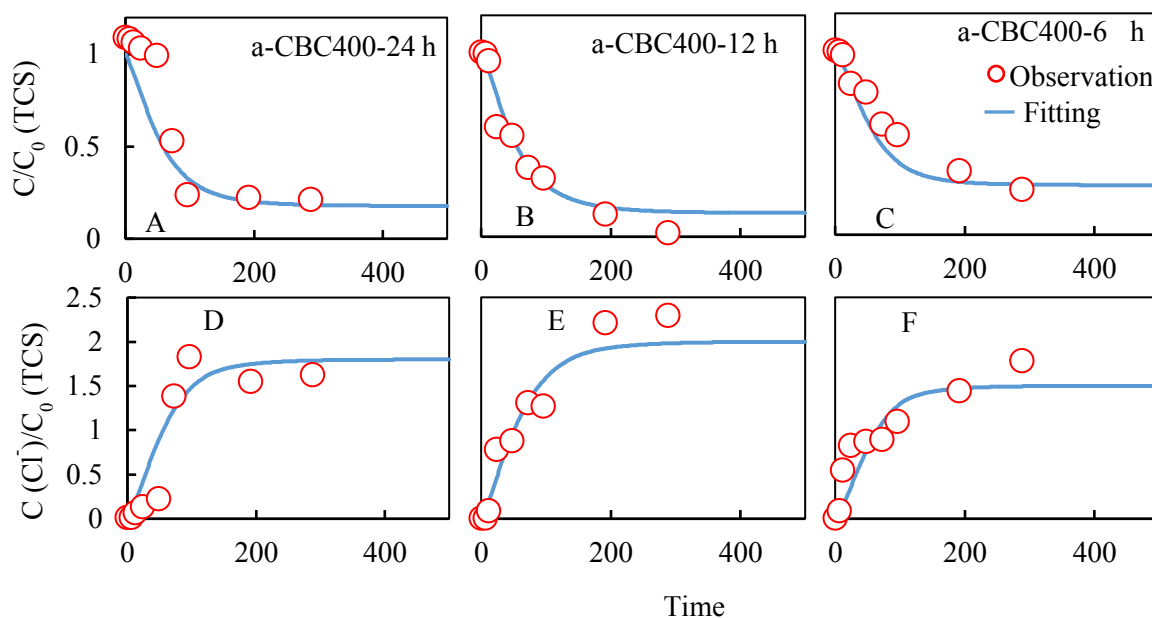


Figure 3-11: Least squares-based numerical fitting for the kinetics of TCS degradation and generation of Cl^- for the reactions with a-CBC400 pre-reduced for 24 h (A)(D), 12 h (B)(E), and 6 h (C)(F). Circles represent measured value when the blue lines stand for the fitting results. a-CBC400 represents the aqueous BC sample prepared using CBC400.

Based on the fitting ($r^2 > 0.76$, **Figure 3-11**), the reaction rate constants ranged from 4.48×10^{-5} to $1.65 \times 10^{-2} \text{ h}^{-1}$ for the reactions between a-BC and TCS. Consistent with the high recovery of chlorine as Cl^- and residual TCS, the second-step and third-step dechlorination were faster than the first step. For a-CBC400, consideration of kinetics for additional by-products can alter the fitting results, but the trend stays in that the first step dechlorination was much slower than the following reactions. In the literature, there are inconsistent reports regarding the relationship between the reaction rate for the different steps of dechlorination (Arnold & Roberts, 2000; Kim et al., 2008; Lowry & Johnson, 2004; Scherer et al., 1998; Wang & Zhang, 1997). Scherer et al. (1998) developed the linear

free-energy relationships (LFER) for predicting the dechlorination rate for chlorinated aliphatics and found that the rate constant decreased dramatically from tri-halogenated aliphatics to dehalogenated aliphatics to mono-halogenated aliphatics. Dechlorination of polychlorinated biphenyls was determined to increase with the number of chlorine in the molecules (Kim et al., 2008; Lowry & Johnson, 2004). The contrast trend for the reaction rate constant with the chlorination number has also been reported (Arnold & Roberts, 2000; Butler & Hayes, 1999). In this study, we found that the first-step dechlorination was much slower than the removal of remaining chlorine, for which the complete understanding warrants more investigation. The electron attraction of chlorine and its impact on the accessibility of remaining aromatic rings can be an essential regulating factor for the degradation rate.

3.4 Environmental Implications

This study has demonstrated a novel dehalogenation reaction between a model organohalogen compound (TCS) by a-BC with an apparent first-order rate constant of 0.0011–0.011 h⁻¹. As a comparison, the reduced aqueous activated carbon can also degrade TCS with a first-order rate constant of 0.0075 h⁻¹. Although the reaction was slower than other abiotic reductive dehalogenation reactions, such as by nZVI, the electron transfer between a-BCs and the organohalogen compound is efficient. The advantages of a-BC being environmentally friendly and cost-effective and that these reactions do not produce any by-products as precipitates make these reactions promising for their potential applications in engineering treatment, including removal of organohalogen from wastewater effluent and remediation of contaminated groundwater. The concentration of a-BC can impact the reaction rate roughly linearly, and it has been demonstrated that a-

BC can be mobilized substantially with sonication or other methods. It can enable and further promote the large-scale application of a-BCs in degrading important organohalogen compounds. With the anaerobic dehalogenation by pre-reduced a-BCs demonstrated unambiguously in this study, the direct addition of a-BCs to enhance microbial degradation as electron shuttles would also be feasible. Although there has been substantial interest in the reactions of BC materials and their applications in agricultural and engineering systems, to the best of our knowledge, there is rarely a report about the reductive dehalogenation by a-BC. Bulk BC can sorb the compounds, which can consequently slow down their reactions. Differently, association with a-BC may not alter the availability and reactions of compounds due to the size of a-BC; reduced a-BC can act as a strong electron donor to reductively degrade organohalogen. While, in this study, a common dissimilatory reductive bacteria (*Shewanella*) was used to produce reduced a-BC, other reactions, including the abiotic reactions, can also be used to generate reduced a-BC. Last but not least, TCS was used as a model organohalogen compound in this study. It has been phased out for significant use nationally in the United States. Still, it remains a concern for the quality of water bodies due to its persistence under certain geochemical conditions. The pathways for reactions between TCS and a-BC can shed light on the possible reactions between a-BC and other persistent organohalogens. Our experimental observations and numerical fitting determined that the first step of dechlorination was the rate-limiting step for the multi-step dehalogenation reactions. Reactions between a-BC and other organohalogen compounds, as well as pathways and the chemical nature of reactive components, require further studies.

Chapter 4: Critical Role of Semiquinones in the Reductive Dehalogenation

Status: (Under revision; to be resubmitted by May 21st, 2023)

Lokesh S, Lard M, Cook R, Yang Y. 2023. Critical role of semiquinones in the reductive dehalogenation.

Abstract

Quinones (QNs) and products of their redox reactions (i.e., hydroquinones (HQs) and semiquinones (SQs)) were suggested as important players in the reductive degradation of organohalogen mediated by natural and pyrogenic organic matter, but direct evidence is limited. This study investigated the reductive dehalogenation of a model organohalogen (triclosan (TCS)) by 1,4-benzohydroquinone (H₂Q) or corresponding 1,4-benzosemiquinone (SQ^{•-}). Degradation of TCS did not occur within the experimental period (up to 288 h) in the presence of H₂Q only but happened in the presence of H₂Q and FeCl₃ under the anoxic condition at pH 5 and 7 (above the pK_a of SQ^{•-}, 4.1). The degradation of TCS was shut down in the presence of saturated dissolved oxygen. Kinetic simulation and thermodynamic calculation indicated that SQ^{•-} was responsible for the reductive degradation of TCS, with the fitted rate constant for the reaction between SQ^{•-} and TCS to be 317 M⁻² h⁻¹. The critical role of SQs in reductive dehalogenation can be ubiquitous in natural and engineering systems based on the reported reduction potentials of QNs/SQs and SQs/HQs and supported by experiments with additional model hydroquinones (HQs). SQs can be produced by the reactions between HQs and Fe(III), although thermodynamically, Fe(III) can further oxidize SQs to QNs, which is much slower than the oxidation of HQs to SQs and kinetically restricted. This study has uncovered the previously unreported critical role of SQs in reductive dehalogenation reactions.

4.1 Introduction

Enhancement of dehalogenation is important for natural attenuation, remediation, and engineering treatment of wastewater. Natural organic matter (NOM) or pyrogenic compartments (including black carbon, activated carbon, and biochar (BC)) can promote dehalogenation by accelerating electron transport (Lefevre et al., 2018; Lokesh et al., 2020; Yu et al., 2015). Previous studies have attributed the redox reactivity of NOM and BC to their quinone (QN) components (aromatic domain with conjugated dione structure), but there is limited direct evidence. Perlinger et al. (1996) showed that the hydroquinone form of juglone, namely mercaptojuglone, was able to reduce pentachloroethane in the presence of sulfide with a first-order rate constant of $9 \times 10^{-3} \text{ h}^{-1}$. Scott et al. (1998) quantitatively demonstrated a relationship between the amounts of semiquinone (SQ) radicals in humic substances (HS) generated through the reduction by *Geobacter metallireducens* and their electron-accepting capacities. Xu et al., (2016) showed that BC could increase the microbial reduction of hematite through QN-involved reactions, supported by the electron paramagnetic resonance (EPR) signals for SQs in BCs.

Due to the difficulty in quantifying QNs in NOM or BC beyond EPR analysis of SQ—thermodynamically a minor fraction of all QNs under normal conditions—their redox reactivities have been demonstrated using model QN compounds as analogs. Anthraquinone-2,6-disulfonate was widely used as an analog to QNs in NOM to demonstrate their reactions with various electron acceptors, such as ferric minerals (Jiang & Kappler, 2008; Liu et al., 2007; Orsetti et al., 2013). Jiang et al., 2015 have studied the reactions between 1,4-benzohydroquinone (H₂Q) and Fe(III) in the solution phase and determined that H₂Q can be reversibly oxidized by Fe(III) with a reaction rate constant

determined by the simulation of kinetics. Based on studies using a range of model QNs, O'Loughlin, (2008) demonstrated a relationship between the reaction rate constant for QN-mediated microbial reduction of lepidocrocite and the reduction potentials of QNs. However, rare studies have been devoted to directly demonstrating the reactions between organohalogen and QNs.

This study examined the reactions between triclosan (TCS) as a model organohalogen and H₂Q (**Figure 4-1**). Rate constants for critical reactions were determined by mathematical fitting of the kinetics, assuming first order for all reactants. The thermodynamic calculation was used to determine the equilibrium concentrations of SQs and compared to the kinetic simulation. Finally, additional model HQs were reacted with TCS to validate SQs' ubiquitous role in the reductive dehalogenation.

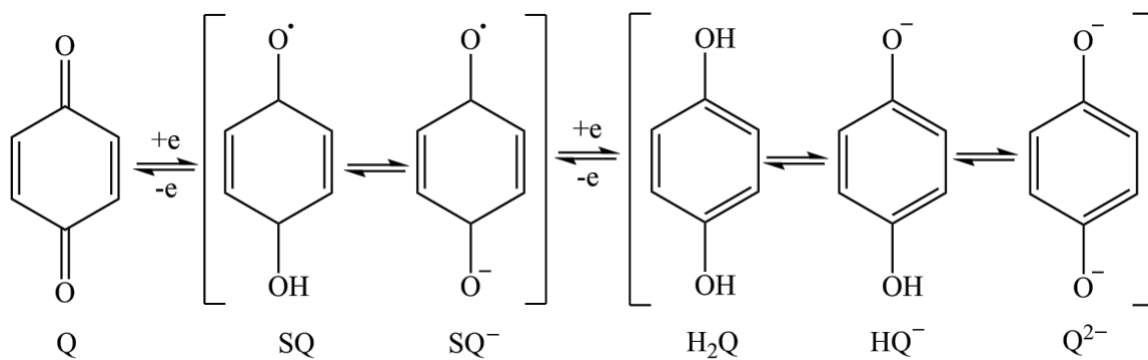


Figure 4-1: Redox reactions of 1,4-benzoquinone and associated protonation/deprotonation.

4.2 Methods and Materials

4.2.1 Materials

The standard compound of TCS (purity $\geq 98\%$) was purchased from Sigma-Aldrich (St. Louis, MO, USA). 1,4-benzoquinone (purity $\geq 98\%$) (Q) was purchased from Alfa Aesar (Haverhill, MA, USA). Model hydroquinones, including benzoquinone (H₂Q) (purity $\geq 99\%$), dimethyl hydroquinone (purity $\geq 99\%$), trimethyl hydroquinone (purity $\geq 99\%$), 1,2-dihydroxynaphthlene (purity $\geq 99\%$), Mitoxantrone (purity $\geq 97\%$), and epigallocatechin (purity $\geq 95\%$) were obtained from Sigma-Aldrich (St. Louis, MO, USA). FeCl₂ and FeCl₃ (purity $\geq 99\%$) were purchased from Sigma-Aldrich. All other chemical reagents used in this study were above analytical grade.

4.2.2 Redox Reactions

TCS was reacted with H₂Q in the presence and absence of oxygen at room temperature. For the reaction in the absence of O₂, the reaction solution was bubbled with compressed N₂ (purity of $> 98.5\%$, Praxair, Danbury, CT, USA) for 6 hours. Our tests showed that the dissolved O₂ concentration reduced to less than 1 μM after this process, measured by a dissolved oxygen probe (Seven2Go DO meter S4, Mettler Toledo, Columbus, OH, USA). Thereafter, the solution was transferred into an anoxic glove box ($\sim 100\%$ N₂) (Coy, Grass Lake, MI). Reactions in the presence of O₂ were conducted under ambient air, where the dissolved O₂ was measured to be constant at $\sim 200 \mu\text{M}$. To demonstrate the role of SQ⁻, the reaction was also conducted in the presence of FeCl₃, as previous studies have documented the oxidation of H₂Q by Fe(III) (O'Loughlin, 2008; Pracht et al., 2001; Stack et al., 2004). At various time points, solutions were sampled for analysis. Experiments were conducted with triplicates.

To get a reliable kinetic fitting for the reductive degradation of TCS without concerns for the generation of the by-product and their consumption for $\text{H}_2\text{Q}/\text{SQ}^-$ in kinetic simulation, additional experiments at pH 5 were conducted with low concentrations of TCS (0.15, 0.2, and 0.3 μM) in the presence of 20 μM of Fe(III) and H_2Q with and without O_2 . The impact of the initial concentration of H_2Q was also examined by reacting 200 μM of H_2Q with 20 μM FeCl_3 and 0.2 μM TCS. For these reactions, the residual concentration of TCS was analyzed at different intervals along with the concentration of H_2Q , Q, and Fe(III)/Fe(II). Following the same protocol, additional HQs (dimethyl hydroquinone (DMH), trimethyl hydroquinone (THM), and 1,2-dihydroxynaphthlene (DHN)) were reacted with TCS and Fe(III) with initial concentrations for HQ/TCS/Fe(III) of 3/3/3 μM and 3/3/0 μM , in the presence and absence of dissolved O_2 . To verify the reaction for more widely used HQs and naturally occurring HQs, Mitoxantrone—widely used in cancer treatment (Lin & Steinmetz, 2018; Mei et al., 2020; Wiseman & Spencer, 1997), and epigallocatechin; the most abundant catechin found in tea (Almatroodi et al., 2020; Khan et al., 2006; Nagle et al., 2006) were reacted with TCS and Fe(III), with initial concentrations for (HQ/TCS/Fe(III)) of 3/3/3 and 3/3/0, in the presence and absence of dissolved O_2 .

Table 4-1: Model hydroquinone compounds used in this study and their basic physicochemical properties

Compound	MW	$E_H^0 (W)$ (QN/ \cdot SQ $^-$) (mV vs. SHE)	$E_H^0 (W)$ (SQ/ \cdot SQ $^-$) (mV vs. SHE)
Hydrobenzoquinone	110	78 (Swallow, 1982), 99 (Ilan et al., 1976)	448 (Swallow, 1982), 459 (Wardman, 1989), 473 (Ilan et al., 1976)
Mitoxantrone	445	-527 (Svingen & Powis, 1981)	
Epigallocatechin	458		430 (Jovanovic et al., 1995)

4.2.3 Chemical Analysis

Using the same method in our recent work (Lokesh et al., 2020), TCS was analyzed by High-Performance Liquid Chromatography (HPLC) (Agilent Technologies 1260, Folsom, CA, USA) equipped with a C18 column (5 μ M, 4.6 x 150 mm). TCS was analyzed by detecting the UV absorbance at 287 nm, with a 78:22 (v/v) of methanol: milliQ water (18.2 M Ω ·cm) as the mobile phase and injection volume of 100 μ L. The flow rate was fixed at 1 mL/min. Based on the standard compound analysis, the retention time of TCS was 7.5 \pm 0.2 min. The standard curve was established for TCS with concentrations ranging from 0.1–5 μ M. Influences of H₂Q and Q on TCS measurement have been tested by analyzing TCS in the presence and absence of the same concentration of H₂Q, and Q. Results demonstrated that the presence of H₂Q or Q exerted no influence (**Figure 4-2**).

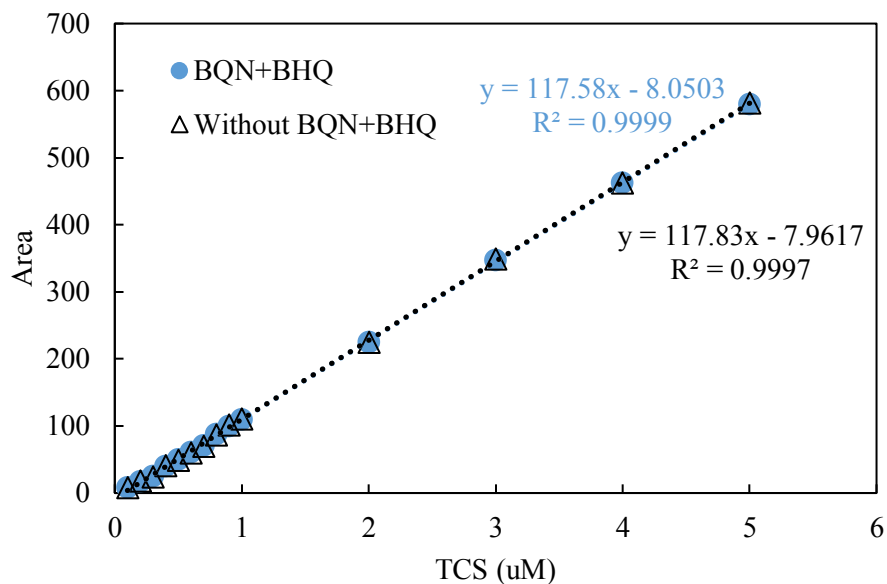


Figure 4-2: TCS calibration curve in the presence and absence of 3 μ M Q and H₂Q.

In addition, H₂Q and Q were also analyzed by HPLC-UV, with 0.1% phosphoric acid in water (A) and methanol (B), using a gradient of 0% B at 0 min and 100% B at 15 min as the mobile phase. Based on the standard compound analysis, the retention time of H₂Q and Q were 8.8 \pm 0.2 and 9.7 \pm 0.2 min, respectively. The flow rate was fixed at 1 mL/min, and the injection volume was 100 μ L. Based on the standard compound analysis, the retention time of H₂Q and Q were 8.8 \pm 0.2 and 9.7 \pm 0.2 min. The standard curve was established for H₂Q and Q with concentrations ranging from 1–30 μ M based on the UV absorbance at 250 nm (**Figure 4-3**). Fe(II) was analyzed with the ferrozine method detailed in previous publications (Xu et al., 2016). In brief, ferrozine (100 μ M) was added to the sample solution for the measurement of Fe(II)-ferrozine with absorbance at 562 nm.

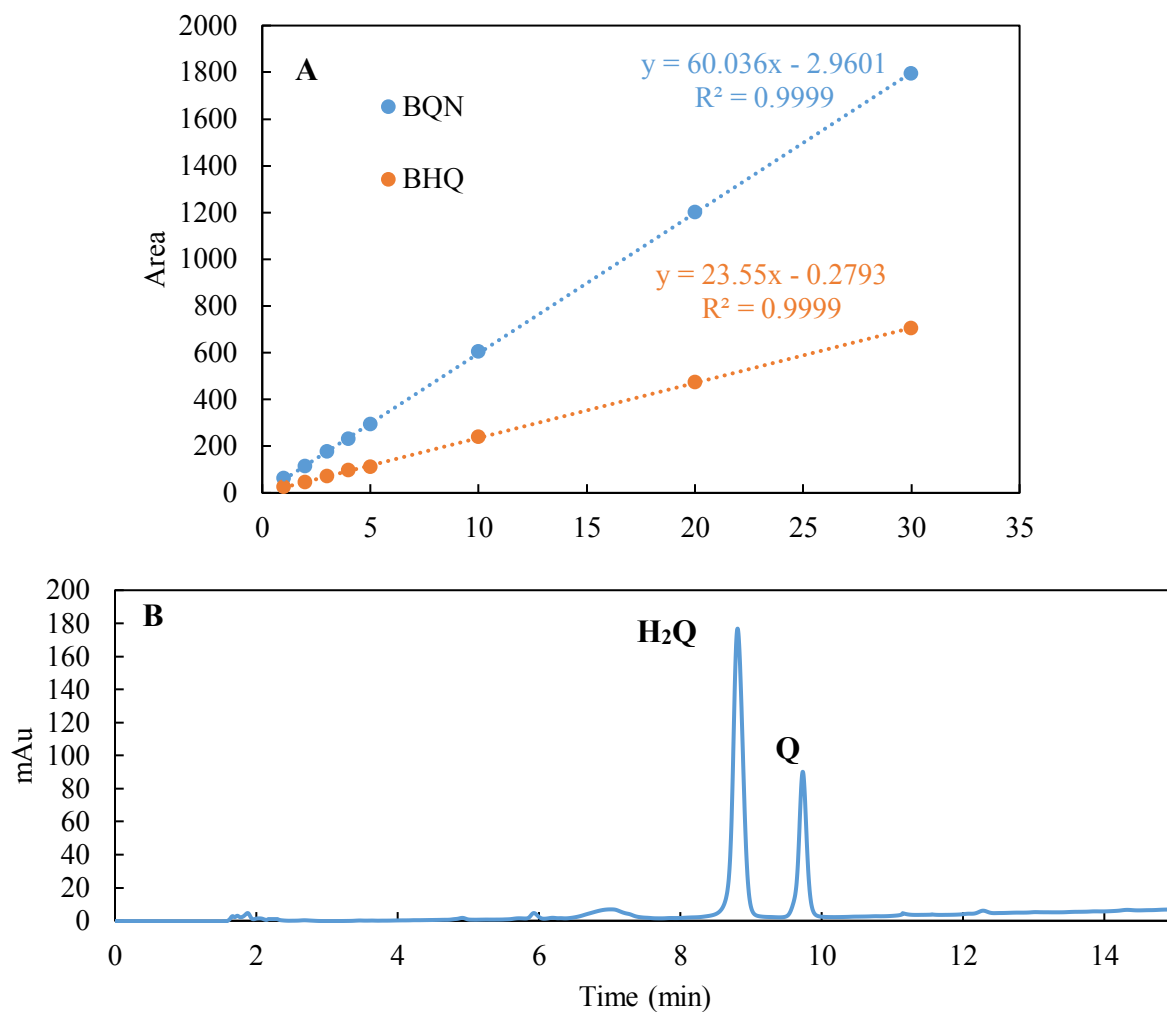


Figure 4-3: A) Q and H₂Q calibration curve; B) HPLC-UV absorbance spectra for Q and H₂Q.

4.2.4 By-product Analysis

The reaction samples were analyzed with direct injection electrospray ionization-time of flight mass spectrometry (ESI-TOF-MS) (G6230A, Agilent Technologies, Folsom, CA, USA). The mobile phase comprised MS-grade acetonitrile (80%) and water (20%). Both mobile phases contained 0.1% formic acid. The flow rate was fixed at 0.5 mL/min with an

injection volume of 20 μL . For the MS analysis, negative electrospray ionization (ESI) at a fragmentation voltage of 150 V with a mass scan range of 50–3000 m/z and a scan rate of 1 spectra/s was used. The drying gas temperature was set to 325°C at a flow rate of 5 L/min. The nebulizer pressure was set at 20 psi, and the capillary voltage was maintained at 3500 V. Data acquisition and data processing were conducted with mass accuracy of ± 10 ppm and isotope pattern deviation of less than 5%. MestReNova (14.2.0) (Santiago De Compostela, Spain) was used to process the TOF-MS data.

4.2.5 Electron Paramagnetic Resonance Analysis

EPR measurements were performed using a Bruker EMX-10/2.7 EPR spectrometer (X-band) with dual cavities under the following parameters: microwave frequency of 9.77 GHz, power of 2.01 mW, 5 scans, modulation amplitude of 4.00 G, modulation frequency of 100 kHz, center field of 3488.46 G, sweep width of 150 G and 6000 G, time constant of 1.280 ms, conversion time of 20.5 ms, sweep time of 41.93 s, resolution of 2048 points, and receiver gain of 1.0×10^4 . Measurements were done at room temperature, and quantitative analyses were conducted using Bruker's WINEPR program. Radical concentrations and the g -factor were estimated relative to the standard 2,2-diphenyl-1-picrylhydrazyl (DPPH), which was used to calibrate the field position.

4.2.6 Kinetic Simulation

The kinetics was fitted using Matlab 2020b (The Mathworks Inc.) with the self-developed coding. Fitting and analysis are detailed below (**Table 4-2**). The least-squares fitting was conducted with the toolbox of "fcn2optimexpr". Several types of kinetic simulation/fitting were conducted in this study: 1) for the system of H_2Q and FeCl_3 , based on the reported

rate constant for the reactions between H₂Q and Fe(III) (Jiang et al., 2015), the dynamics of Q/ H₂Q/SQ⁻, and Fe(III)/Fe(II) were calculated; 2) for the system of H₂Q, FeCl₃, and TCS, based on the reported rate constant for the reaction between H₂Q and Fe(III), the time-dependent concentration of TCS was simulated based on the least-squares fitting with the rate constant for the reaction between SQ⁻ and TCS fitted; 3) for the system of with initial 200/20/0.2 μM H₂Q, FeCl₃, and TCS, in addition to dynamics of TCS, the time-dependent concentrations of H₂Q/Q, Fe(III)/Fe(II) were also simulated.

Table 4-2: Key reactions and rate constants at pH 5 considered for the kinetic fitting^a.

No.	Reaction	Rate Constant (M ⁻¹ s ⁻¹ /M ⁻² S ⁻¹)	Reference
1	$Fe^{3+} + H_2Q \xrightleftharpoons[k_{-1}]{k_1} SQ^- + Fe^{2+} + H^+$	k1 1 x 10 ³	(Garg et al., 2015)
		k-1 9 x 10 ⁶	(Jiang et al., 2015)
2*	$SQ^- + Fe^{3+} \xrightleftharpoons[k_{-2}]{k_2} Q + Fe^{2+}$	k2 ≤ 1 x 10 ⁵	(Yamazaki & Ohnishi, 1966)
		k-2 ≤ 1 x 10 ³	(Yuan et al., 2013)
3	$2SQ^- + TCS + H^+ \xrightarrow{k_3} 2Q + Cl^- + P$	k3 317	this study
4*	$2SQ^- + 2H^+ \xrightleftharpoons[k_{-4}]{k_4} H_2Q + Q$	k4 ≤ 1 x 10 ¹⁰	(Yamazaki & Ohnishi, 1966; Yuan et al., 2013)
		k-4 ≤ 1 x 10 ⁷	
5	$SQ^- + O_2 + H^+ \xrightleftharpoons[k_{-5}]{k_5} Q + HO_2$	k5 1 x 10 ³	(Meisel, 1975; Yamazaki &

				Ohnishi, 1966)
		k-5	1.9 x 10 ⁷	(Meisel, 1975)
6	$HO_2 + HO_2 \xrightarrow{k6} H_2O_2 + O_2$	k6	2.5 x 10 ⁷	(Bielski et al., 1985)
7	$SQ^- + HO_2 + H^+ \xrightarrow{k7} H_2Q + O_2$	k7	5 x 10 ⁸	(Jiang et al., 2015)
8	$Fe^{3+} + HO_2 \xrightleftharpoons[k-8]{k8, k-8} Fe^{2+} + O_2 + H^+$	k8	2.5 x 10 ⁶	(Rush & Bielski, 1985)
		k-8	1.3	(Jiang et al., 2015)
9	$Fe^{2+} + HO_2 + H^+ \xrightarrow{k9} Fe^{3+} + H_2O_2$	k9	6.6 x 10 ⁶	(Rush & Bielski, 1985)

^a P denotes TCS degradation by-product; * As there is a lack of rigorously constricted values for the rate constants of these reactions, they were not accounted for in the mathematical fitting of this study.

4.2.7 Thermodynamic Calculation

The thermodynamic calculation was conducted through the resolution of equation groups (mass balance and electron balance) (by function 'fsolve') using Matlab 2020b (The Mathworks Inc.) with the self-developed coding. Based on the theme developed by Uchimiya & Stone (2009), the thermodynamic calculations were conducted based on the following equations and parameters collected from the literature (**Table 4-2 and Table 4-3**): 1) mass balance of Fe and quinone system: for Fe, the complexation with OH⁻ was considered with the stability constant collected from literature; for benzoquinone (BQ) system, quinone, semiquinone (SQH, and SQ⁻) (protonated and deprotonated), and hydroquinone (H₂Q, HQ⁻, Q²⁻) (protonated, partially deprotonated, and fully deprotonated);

2) electron balance: the electron level of Fe(II) and Fe(III) was assigned as 1 and 0, and the electron level of HQ, SQ, and QN was assigned as 2, 1 and 0; 3) equilibrium: equilibrium of dissociation/association, complexation, and redox reactions were counted. For Fe(II) and Fe(III), the system was assumed as unsaturated and calculated, and then the saturation index was calculated for the dissolution of Fe(OH)₂ and Fe(OH)₃; if the saturation index was above 1, the solubility product of Fe(OH)₂ and Fe(OH)₃ was counted for the calculation.

Table 4-3: Key reactions considered for thermodynamic calculation.

Mass balance equation of Fe

$$Fe(III)_T = [Fe^{3+}] + [Fe(OH)^{2+}] + [Fe(OH)_2^+] + [Fe(OH)_3(aq)] + [Fe(OH)_4^-] \quad (1)$$

$$Fe(II)_T = [Fe^{2+}] + [Fe(OH)^+] + [Fe(OH)_2(aq)] + [Fe(OH)_3^-] + [Fe(OH)_4^{2-}] \quad (2)$$

Mass balance equation of quinone system

$$BQ_T = [BQN] + [BSQ] + [BSQ^-] + [BHQ] + [BHQ^-] + [BHQ^{2-}] \quad (3)$$

Electron balance equations

$$e_T = [BSQ] + [BSQ^-] + 2 * ([BHQ] + [BHQ^-] + [BHQ^{2-}]) + Fe(II)_T \quad (4)$$

Nernst equations

$$E = E^0 + \frac{RT}{2F} \ln \left(\frac{[BQN][H^+]^2}{[BHQ]} \right) \quad (5)$$

$$E = E^0 + \frac{RT}{2F} \ln \left(\frac{[Fe^{3+}]}{[Fe^{2+}]} \right) \quad (6)$$

4.2.8 Statistical Analysis

Statistical analysis was conducted with IBM SPSS Statistics (version 26, IBM Corp., Armonk, NY, USA).

4.3 Results and Discussions

4.3.1 Reductive Degradation of TCS by Semiquinone

When TCS was mixed with H₂Q in the molar ratio of 1:1 (3 and 3 μM) at pH 3, 5, and 7, no TCS degradation was observed under either oxic or anoxic conditions (**Figure 4-4A**). This indicates that H₂Q cannot reduce TCS within the experimental period (up to 288 h), likely because of the relatively high reduction potential of SQ⁻/H₂Q ($E_H^0 = 1091$ mV and 1327 mV for SQ⁻/H₂Q and SQ⁻ (dissociated ion of SQH)/H₂Q) (Garg et al., 2013; Jiang et al., 2015) which will be discussed with more details below. Parallel measurement confirmed that H₂Q remained constant in the presence or absence of O₂ (**Figure 4-5**), as O₂ cannot oxidize H₂Q due to spin restriction (Roginsky & Barsukova, 2000). This result contradicted the assumption made in previous studies that HQs could participate in the reductive dehalogenation as electron donors or shuttle, i.e., QNs can be reduced microbially or abiotically to HQs, which can consequently donate electrons to organohalogen compounds (Luijten et al., 2004; Zhang et al., 2020).

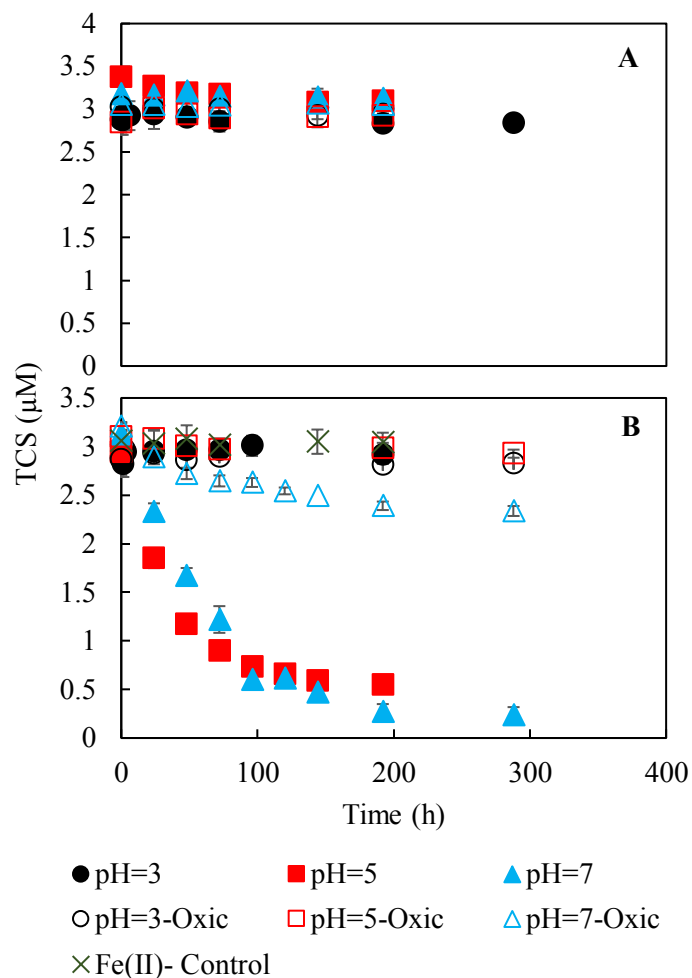


Figure 4-4: Kinetics for triclosan (TCS) degradation in the reactions between hydrobenzoquinone (H_2Q) ($3 \mu\text{M}$) and TCS ($3 \mu\text{M}$) in the absence (**A**) and presence (**B**) of FeCl_3 ($3 \mu\text{M}$). All reactions were conducted at pH 3, 5, and 7; and in anoxic (with dissolved $\text{O}_2 < 10 \mu\text{M}$) (filled symbols) and oxic condition (dissolved $\text{O}_2 = 200 \mu\text{M}$) (open symbols). Error bars represent the standard deviation collected from triplicate measurements. Some error bars were too small to visualize.

With a remarkable difference, in the presence of FeCl_3 , TCS was degraded relatively quickly at pH 5 and 7 (**Figure 4-4B**). To get an overall assessment of the reaction rate, the

TCS degradation was fitted with pseudo-first-order kinetics with a rate constant of 0.0086 and 0.0097 h^{-1} and a half-life of 71.4 – 80.6 h ($p < 0.05$). The reaction rate constant is comparable to the degradation of organohalogen by NOM or BC, with the reported values of 0.00108 – 0.0105 h^{-1} (Lokesh et al., 2020). Such degradation of TCS was shut down at pH 3 or in the presence of saturated dissolved O_2 .

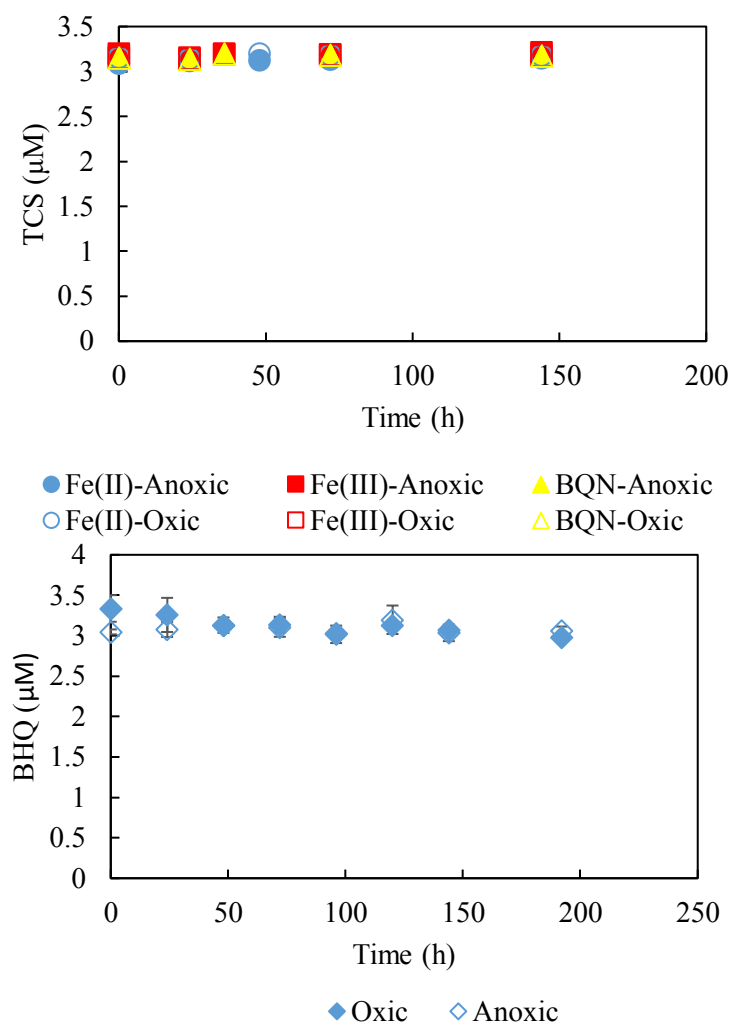


Figure 4-5: (A) Time-dependent concentrations of triclosan (TCS) in the controlled experiments at pH 5 with a) Fe(II) (3 μM FeCl_2); b) Fe(III) (3 μM FeCl_3); c) benzoquinone (Q) (3 μM) under anoxic conditions. To verify the possibility of the degradation of TCS

by the radicals generated through the oxidation of Fe(II), data for TCS in the presence of Fe(II) under oxic condition was also shown. **(B)** Time-dependent concentrations of hydrobenzoquinone (HBQ) in reactions with TCS under oxic and anoxic conditions.

Additional control experiments eliminated the possibility of reactions between Fe(III) or Fe(II) and TCS in the absence or presence of O₂ (**Figure 4-5**). Therefore, degradation of TCS in the presence of Fe(III) was attributed to the products generated by its reaction with H₂Q, predominately as SQ⁻ and possibly with Q as minor components at pH 5, based on recent studies (Garg et al., 2013; Jiang et al., 2015). Direct reactions confirmed that under anoxic conditions, Q did not react with TCS (**Figure 4-4**). Control experiments also determined that FeCl₃ or FeCl₂ did not degrade TCS under this condition. As a result, the generation of SQ⁻ in the presence of H₂Q and FeCl₃ was the critical reagent for the reductive degradation of TCS.

The impact of initial reactant concentration was examined: relatively low concentrations of TCS (0.15, 0.2, 0.3 μM) were reacted with H₂Q (20 μM) and Fe(III) (20 μM) (**Figure 4-6**). Under all the different concentration sets, TCS was degraded substantially. TCS degradation kinetics can be fitted well with pseudo-first-order kinetics with the rate constant of 0.0475 – 0.0154 h⁻¹ and half-life reduced from 45 to 14 h ($p < 0.05$) when the initial concentration of TCS was reduced from 0.3 to 0.15 μM. The system started with 20 μM FeCl₃ and 0.3 μM TCS, when the initial H₂Q concentration was further increased to 200 μM, the reaction was expedited substantially with the pseudo-first-order half-life of 2.8 h. In the system, within the reaction period (6 h), Fe(II) increased to 5.2 μM, and H₂Q reduced to 18.7 μM (Q was increased to 1.1 μM). The minor reduction of Fe(III) was

consistent with the previous report for the system of only FeCl_3 and H_2Q (Jiang et al., 2015).

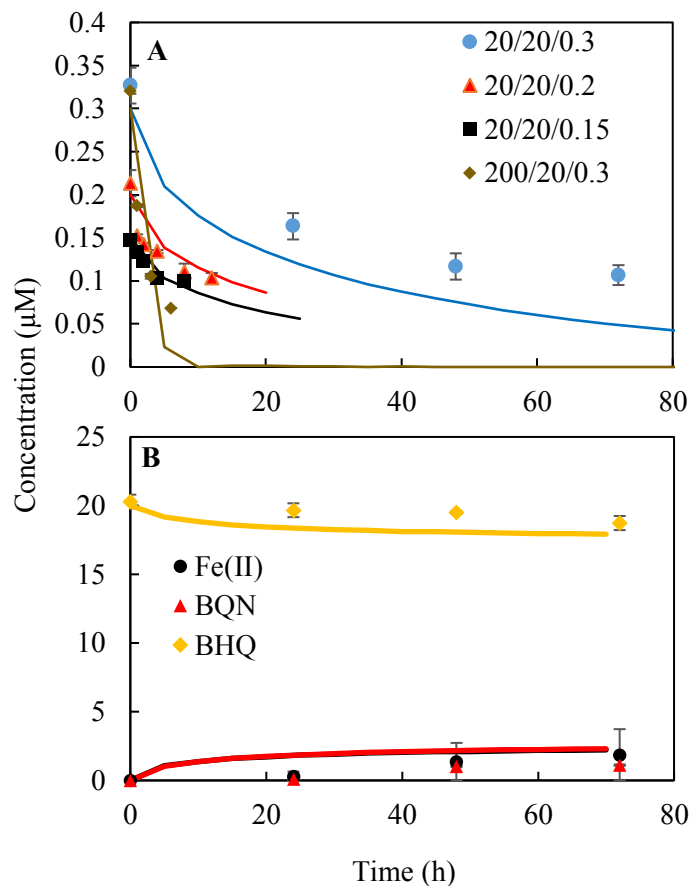


Figure 4-6: (A) Kinetics for the degradation of triclosan (TCS) reacted with hydrobenzoquinone (H_2Q) and FeCl_3 in the absence of O_2 at pH 5, together with the simulation. Four initial concentrations of $\text{H}_2\text{Q}/\text{FeCl}_3/\text{TCS}$ were used, including 20/20/0.3, 20/20/0.2, 20/20/0.15, and 200/20/0.15 μM , marked in the figure legends. Dots represent the measured results, while the lines represent the simulation. (B) Measured time-dependent concentrations of Fe(II), benzoquinone (Q), and H_2Q in the system with an initial concentration of 20/20/0.3 μM $\text{H}_2\text{Q}/\text{FeCl}_3/\text{TCS}$ with the simulation. Error bars

represent the standard deviation collected from triplicate measurements. Some error bars were too small to visualize.

4.3.2 By-product analysis

Furthermore, for the system containing 0.15 μM TCS, 20 μM H_2Q , and 20 μM Fe(III) , dechlorination by-products were analyzed based on the LC-TOFMS analysis. Two major by-products were detected: a dechlorinated phenoxyphenol (m/z of 252.9823, $\text{C}_{12}\text{H}_8\text{Cl}_2\text{O}_2$) and a monochlorinated phenoxyphenol (m/z of 219.0213, $\text{C}_{12}\text{H}_9\text{ClO}_2$). The results showed that after two days of reaction, dechlorinated and the monochlorinated phenoxyphenol by-products were generated from the initial triclosan in the system on day 0. The monochlorinated phenoxyphenol was the major by-product observed after four days of reaction.). The analysis did not capture the fully dechlorinated phenoxyphenol (m/z of 182.0368, $\text{C}_{12}\text{H}_{10}\text{O}_2$) (**Figure 4-7**). Due to a lack of authentic standards, quantification of the by-products generated and reduced was not possible.

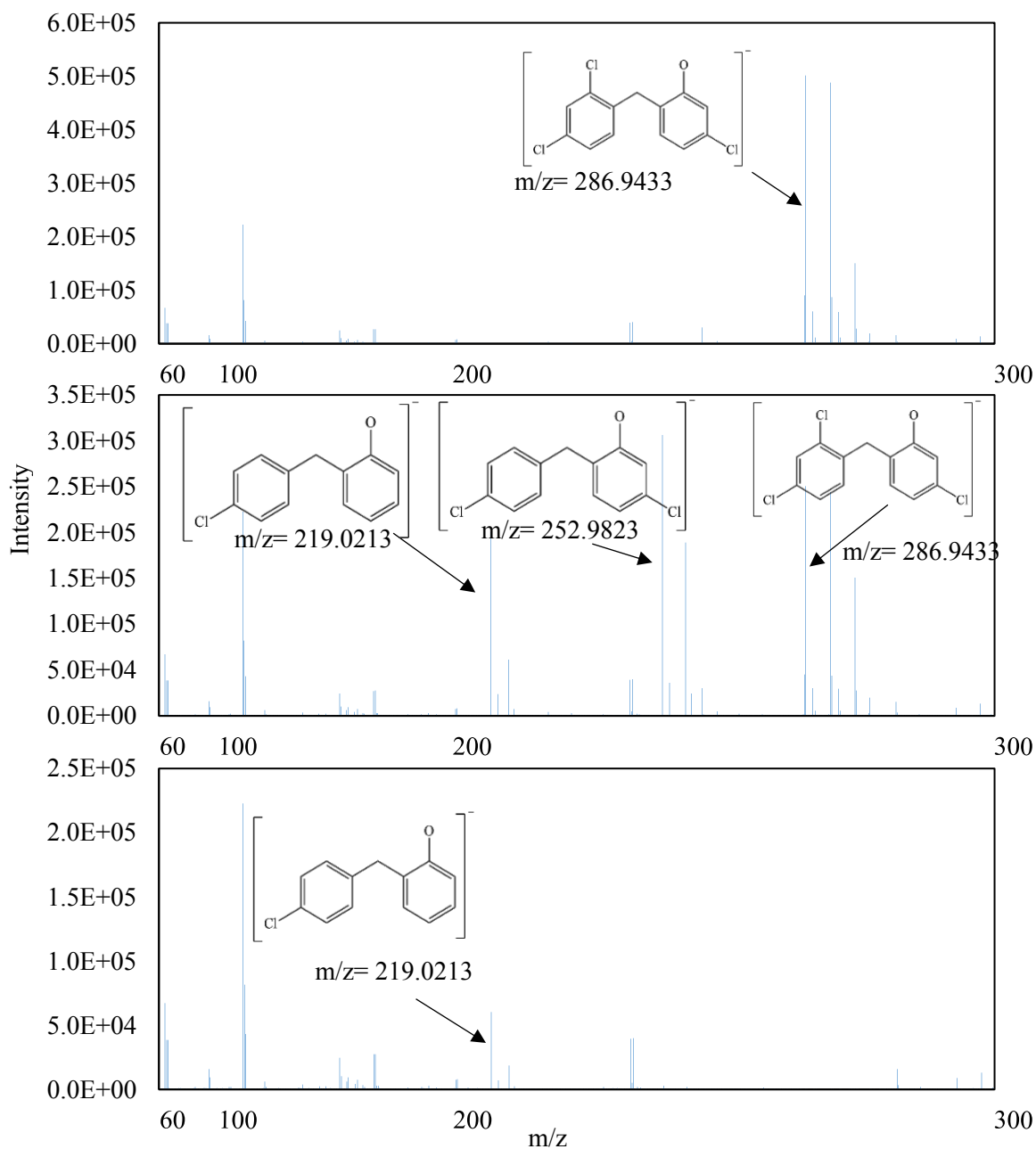


Figure 4-7: By-products analysis of TCS degradation as analyzed by LC-TOFMS: **(A)** Mass spectra of Triclosan at day 0 of reaction; **(B)** Mass spectra of TCS degradation products after 2 days of reaction; **(C)** Mass spectra of TCS degradation by-products after 4 days of reaction.

4.3.3 EPR Analysis

In this study, we report the detection of EPR signals corresponding to semiquinone radicals ($g = 2.006$) in a reaction system containing $300 \mu\text{M}$ H_2Q and $3 \mu\text{M}$ Fe(III) under anoxic conditions. The highest signal intensity was observed at day 0 (intensity = 2050), which decreased over one day (intensity = 262) (**Figure 4-8**). No signals at $g = 2.006$ were detected in control experiments with only H_2Q or Fe(III) . These results provide evidence for the formation of semiquinone radicals in the reaction system containing Fe(III) and H_2Q .

Thermodynamic calculations predict a steady-state concentration of semiquinone at 34.1 nM after 10 hours of reaction. However, the sharp decrease in EPR signals for semiquinone observed over time suggests the formation of a dimer semiquinone molecule. These findings shed light on the redox behavior of H_2Q in the presence of Fe(III) and could have implications for the role of semiquinones in natural and engineered systems.

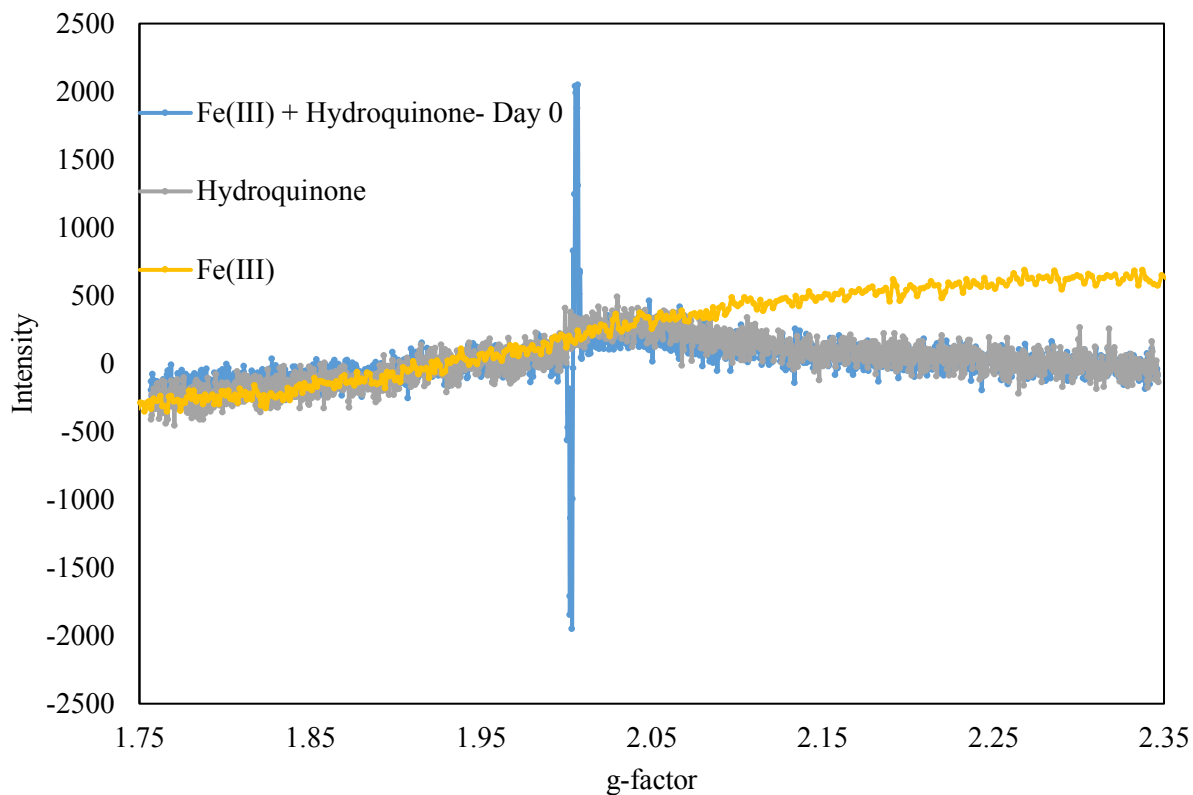


Figure 4-8: Electron paramagnetic resonance (EPR) signals detected for reactions between Fe(III) (3 μM) and H₂Q (300 μM). Control experiments with only Fe(III) or H₂Q were conducted to account for background signals.

4.3.4 Kinetic Simulation and Reaction Rate Constant

The dynamics of H₂Q, SQ⁻, and Q were simulated for the system starting with 20 μM of Fe(III) and H₂Q (**Figure 4-6**). Due to the reversible oxidation of H₂Q by Fe(III), SQ⁻ increased sharply in the first 10 h and approached the steady-state concentration of 34.1 nM. If saturated O₂ was present, SQ⁻ was further oxidized to Q and reduced significantly to less than 10⁻⁴ nM. In the presence of 1 μM O₂, SQ⁻ has fluctuations in the beginning stage of reactions, and the steady-state concentration was around 0.9 nM (**Figure 4-9**). These calculations supported that SQ⁻, much higher under anoxic conditions, was presumably

responsible for the reductive dehalogenation of TCS. pH regulated the reaction between $\text{H}_2\text{Q}/\text{SQ}^-$ and $\text{Fe(III)}/\text{TCS}$ due to the speciation of SQ^- and H_2Q and their pH-dependent reduction potential. Our results showed that the TCS degradation was shut down when pH was reduced to 3 (**Figure 4-4**). The reduction potential (E_h) of Q/SQ^- and $\text{SQ}^-/\text{H}_2\text{Q}$ increased with decreasing pH and potentially disabled TCS reduction at pH 3.

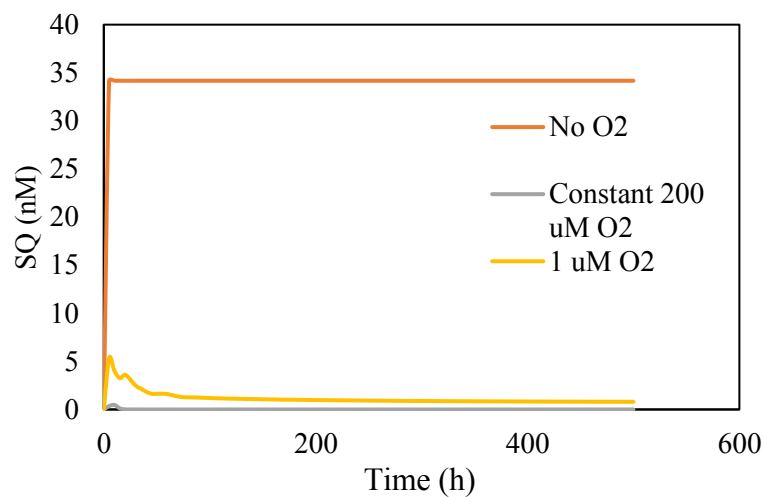


Figure 4-9: Time-dependent concentration of semibenzoquinone (SQ^-) in the reactions between hydrobenzoquinone (H_2Q) ($3\ \mu\text{M}$) and FeCl_3 ($3\ \mu\text{M}$) in the presence of different concentration of dissolved O_2 (0, 1 μM , saturated dissolved O_2 (200 μM)).

Simulation for the kinetics of TCS was conducted for systems with lower TCS concentration, where the consumption of SQ^- by TCS by-products could be neglected. For the system with relatively low concentrations of TCS (0.15, 0.2, 0.3 μM) reacted with H_2Q (20 μM) and Fe(III) (20 μM), the measured results ensured that the influences of TCS degradation on the dynamics of $\text{H}_2\text{Q}/\text{SQ}^-$ and $\text{Fe(III)}/\text{Fe(II)}$ were relatively minor: for the mass balance, the complete dechlorination of TCS would only consume at most 2 μM of H_2Q , accounting for 10% of its mass; from the kinetic perspective, based on the rate

constant, the production and removal flux of SQ^- was around $400 \mu\text{Ms}^{-1}$, when the TCS would only consume at most $2.8 \times 10^{-5} \mu\text{M/s}$ SQ^- , according to the measured half-life of TCS.

A mathematical fitting was conducted by considering all the critical reactions occurring in the system (**Table 4-2**). The kinetics can be fitted well (when the observed value (Y) was related to simulated results (X), $Y=0.98X+0.05$, $r^2 = 0.99$) with the rate constant of $317 \text{ M}^{-2}\text{h}^{-1}$ for the reactions between the SQ^- and TCS at pH 5 (**Figure 4-6A; Table 4-2**). For the system with $200 \mu\text{M}$ H_2Q , $20 \mu\text{M}$ FeCl_2 , and $0.3 \mu\text{M}$ TCS initially, the dynamics of Fe(III)/Fe(II) , $\text{H}_2\text{Q/Q}$ were also fitted well (**Figure 4-6B**).

The rate constant for the reaction between SQ^- and TCS was much higher than those obtained for the reactions between organohalogen and NOM/BC (Aulenta et al., 2010; Collins & Picardal, 1999; Kappler & Haderlein, 2003). The reported pseudo-second-order reaction rate constant between NOM/BC and organohalogen ranged 7.3×10^{-6} – $1.48 \times 10^{-6} \text{ M}^{-1}\text{h}^{-1}$ (Kappler & Haderlein, 2003). As the semiquinone is usually a minor fraction of NOM/BC thermodynamically, our results implied that the real reaction rate constant could also be higher than previously thought for the real reactive components in NOM/BC. These results demonstrated the critical role of semiquinone in reductive dehalogenation, which has not been reported previously. To optimize the application of NOM/BC-mediated dehalogenation reaction, increasing the concentration of semiquinones is crucially important.

4.3.5 Thermodynamics vs. Kinetics and Ubiquitous Importance of SQs in Dehalogenation

Thermodynamically, the concentration of SQs was regulated by the redox conditions in the reaction system. Following the theme of calculation developed by Uchimiya & Stone (2009), pH-dependent concentrations of SQ^- in the system with $20 \mu\text{M H}_2\text{Q}$ and $20 \mu\text{M Q}$ were calculated using a self-built Matlab code. Its equilibrium concentration has a significant response to pH as a result of pH-dependent oxidation-reduction potentials (E_h) of reactions for Q and SQ^- (Figure 4-10).

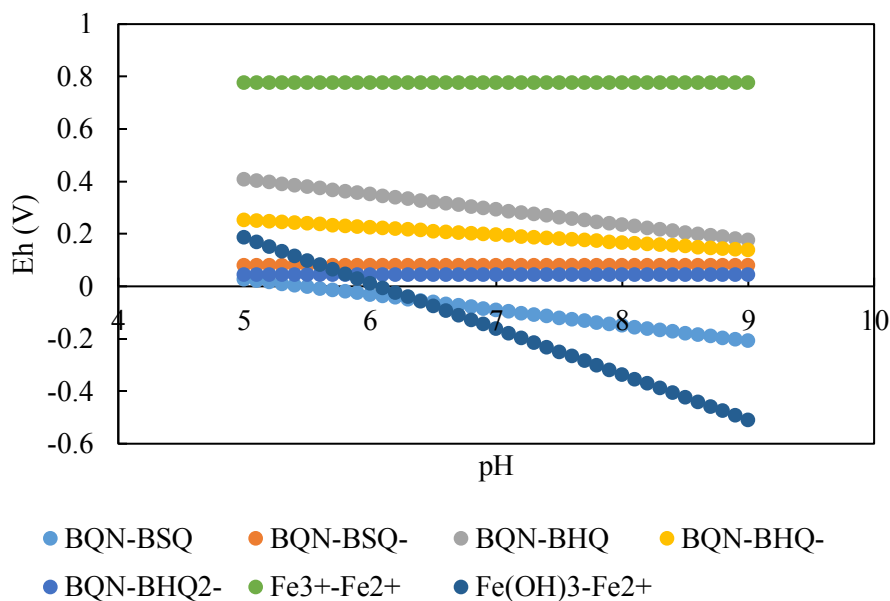


Figure 4-10: pH-dependent E_h for the redox pairs involved in the system.

For the system with FeCl_3 , the reactions were also constrained by the speciation of Fe and solubility of produced minerals (Fe(OH)_3 and Fe(OH)_2). Considering the complexation of Fe(III)/Fe(II) with OH^- and the solubility product of $\text{Fe(OH)}_3/\text{Fe(OH)}_2$, the equilibrium concentrations of SQ^- were also calculated as a pH-dependent range of 3.5×10^{-7} – 3.5×10^{-3}

μM when the $\text{Fe}(\text{OH})_3$ constrained the concentration of $\text{Fe}(\text{III})$ in solution phase for the system above pH of 5.6 (**Figure 4-11**). When the calculation was applied to the system of $20 \mu\text{M}$ H_2Q , and $20 \mu\text{M}$ FeCl_3 , the equilibrium concentration of SQ^- was much lower than that calculated from the kinetic calculation (**Figure 4-12**). Based on redox potentials, oxidation of SQ^- by $\text{Fe}(\text{III})$ was even more favored than oxidation of H_2Q . However, the reactions of SQ^- by $\text{Fe}(\text{III})$ were relatively slower and kinetically limited. So far, there is still no reliable rate constant for the reactions between Q/SQ^- and $\text{Fe}(\text{III})/\text{Fe}(\text{II})$. Such a kinetical limit promoted the production of SQ^- by the reaction between H_2Q and $\text{Fe}(\text{III})$ and the consequent reactions of SQ^- with organohalogen, with TCS as a model compound in this study.

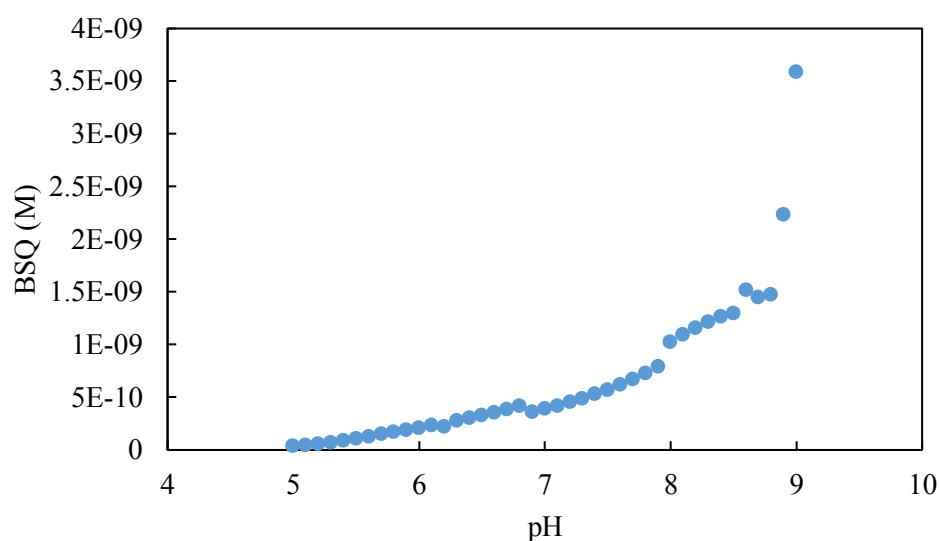


Figure 4-11: pH-dependent equilibrium concentrations of SQ^- in the system with an initial concentration of $20/20 \mu\text{M}$ $\text{FeCl}_3/\text{H}_2\text{Q}$, considering the complexation of $\text{Fe}^{3+}/\text{Fe}^{2+}$ with OH^- and the solubility restriction for $\text{Fe}(\text{OH})_3$ and $\text{Fe}(\text{OH})_2$.

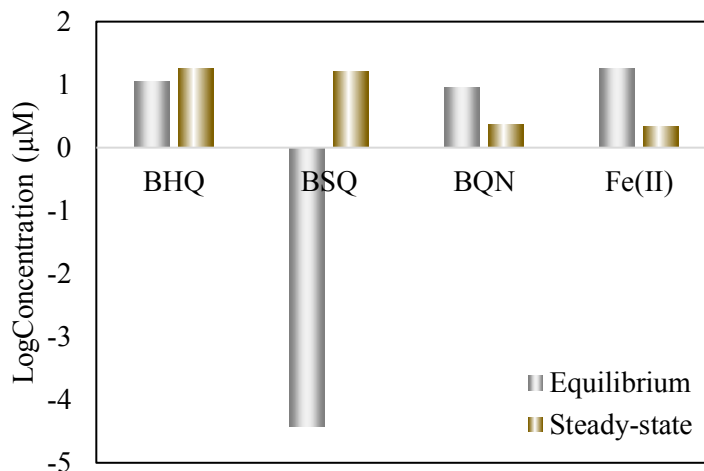


Figure 4-12: Comparison between the thermodynamic equilibrium and steady-state concentration (based on the kinetic simulation) of SQ, HQ, Q, and Fe(II) and thermodynamic equilibrium concentration for the system with 20/20 μM $\text{H}_2\text{Q}/\text{FeCl}_3$ under anoxic condition.

The critical role of SQ $^-$ in the reductive degradation of TCS was partially driven by the relatively higher reduction potential of SQ $^-$ / H_2Q than Q/ SQ $^-$. The relatively higher reduction potential of semiquinone/hydroquinone than quinone/semiquinone was ubiquitous. Based on the compiled data in the review by Song & Buettner (2010), the difference between the semiquinone/hydroquinone and quinone/semiquinone ranged from 300–500 mV for most of the quinone compounds. There are only a few exceptions, such as 2,6-methoxyl-3-methyl-1,4-benzoquinone, for which the reduction potential of semiquinone/hydroquinone is -290 mV when the value for quinone/semiquinone is -110 mV (Roginsky & Barsukova, 2000). Therefore, for most of the quinone system, thermodynamically, semiquinone would serve better as the reducing agent for reductive dehalogenation. Even when both semiquinone and hydroquinone can thermodynamically reduce organohalogen, the rate constant would be higher for semiquinone than

hydroquinone, as the reduction potential difference between the reductant and oxidant has been widely used as an indicator for the rate of redox reactions (Huynh et al., 2016; Kristensen et al., 2020). It has been varied with substituted hydrobenzoquinone and naphthoquinone, which did not degrade TCS under anoxic conditions (20 μM H₂Q and 20 μM TCS, pH = 5). However, when 20 μM FeCl₃ was added to the system, TCS was degraded with a pseudo-first-order half-life of 23.0 – 47.8 h (**Figure 4-13A**). Rate constants for these hydroquinones with FeCl₃ were not available for kinetic simulation when thermodynamically equilibrium concentrations of SQs in these systems were determined to range from 8.5×10^{-9} – 6.7×10^{-7} μM (**Figure 4-13B**). We speculated that the kinetic limit for the reaction between these SQs and Fe(III) also occurred and enhanced the concentration of SQs.

Furthermore, similar reactions occurred for other more widely used and naturally abundant HQs (Mitoxantrone and epigallocatechin, respectively): in the absence of Fe(III), TCS cannot be degraded, while the presence of Fe(III) enabled the substantial degradation of TCS within 12 days (**Figure 4-14**). However, more detailed kinetics studies were unavailable for these compounds due to the lack of data on the thermodynamics of multiple quinone groups present in these compounds. Nevertheless, the results confirmed the critical role of SQ in the reductive dehalogenation for broader groups of QNs.

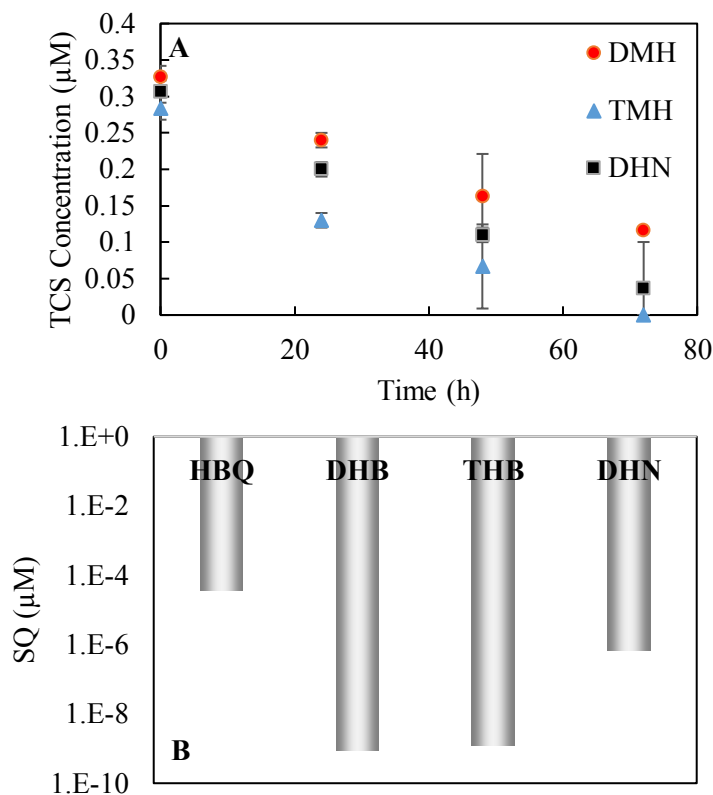


Figure 4-13: Time-dependent TCS concentration in anoxic reactions with substituted hydroquinones (HQs) (dimethyl hydroquinone (DMH), trimethyl hydroquinone (TMH), 1,2-dihydroxynaphthlene (DHN)) with initial concentrations of 20/20/0.3 μM HQ/FeCl₃/TCS (A) and (B) calculated equilibrium semiquinone (SQ) concentrations in the system with different HQs in the system of 20/20/0.3 μM HQ/FeCl₃. The result for HBQ was shown as a comparison.

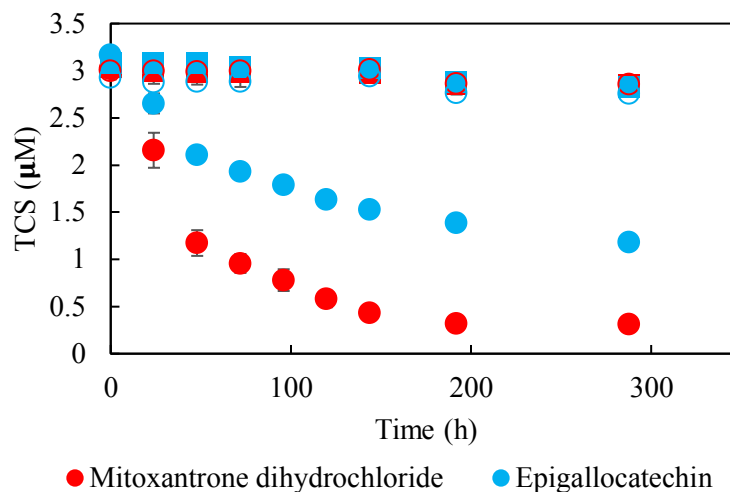


Figure 4-14: Reactions between mitoxantrone (red) and epigallocatechin (blue) and TCS in the presence (circles) and absence (squares) of FeCl_3 under anoxic (filled symbols) and oxic conditions (open symbols).

4.4 Environmental Implications

This study has demonstrated the critical role of SQs in reductive dehalogenation through experimental studies, kinetic fitting, and thermodynamics analysis. Although TCS and H_2Q were used as model compounds, the observed importance can apply to an extensive range of quinone groups. As QNs have been assigned as the key groups in the NOM or BC to promote the reductive degradation of organohalogen and other redox-sensitive organic compounds, this finding has important implications for understanding the NOM/BC-mediated reactions and optimization of their application in the water treatment and groundwater remediation. Our results showed that thermodynamically or kinetically, semiquinone would serve much better as an electron donor for reductive degradation, but it is a relatively minor fraction of the natural QN system. Therefore, the addition of oxidants

(such as Fe(III) or QNs themselves) together with HQ will be crucial for triggering the reductive degradation of organohalogen and other toxic organic compounds.

Chapter 5: Analysis of Reactive Components of Aqueous Biochars

Status: To be submitted.

Abstract

Quinones are believed to play a crucial role in redox reactions in natural organic matter, but identifying quinones in complex environmental media has been a challenge. In this study, we developed a method for tagging quinones using Michael addition reactions between quinones and cysteine. The reactions were monitored using mass spectrometry (MS) and UV spectra, and rapid reactions between model quinones (benzoquinone, naphthoquinone, anthraquinone) and cysteine were observed. Based on these results, cysteine was used to tag quinones in complex environmental samples, namely water extractions of biochar. We identified candidate quinones based on the MS features of the reaction products with cysteine. Our experiments demonstrated that this chemical tagging was efficient for quinones with β -carbon from the same benzene ring available for Michael addition and that the tagging efficiency was not affected by co-occurring compounds such as caffeic acid, cinnamic acid, coumaric acid, and hydrobenzoquinone. This study successfully demonstrated that Michael-addition reactions could be used to tag quinones in complex environmental media and potentially identify their structures. This method could provide insights into the redox chemistry of natural organic matter and their critical chemical compositions and structures.

5.1 Introduction

Understanding the reactive components of aqueous a-BCs can be challenging due to their complex composition. However, characterizing the nano-sized components of a-BCs, known as nano-BCs (n-BCs), can aid in optimizing their applications. Recent studies have examined n-BCs produced by pyrolysis of rice hull and red oak wood at the temperature of 300–900°C and demonstrated their hydrodynamic diameter to range 59–190 nm with a surface conductivity of 0–1.4 S.mm⁻¹ (Pignatello et al., 2017; Yue et al., 2019). In our samples of a-BCs, we have shown through preliminary analysis that 13.1–79.4% of the sample was between 3000 Da–450 nm, while the dissolved a-BCs (<3000 Da) can consist of up to thousands of different individual compounds (**Figure 5-1**). For dissolved natural organic matter (NOM) samples, which serve as an excellent analog to a-BCs, high-resolution electrospray ionization mass spectrometry (HR-ESI-MS) analysis, such as Fourier–transform ion cyclotron resonance MS (FT-ICR-MS), have identified over 2000 small compounds (Qi et al., 2019). To accurately determine the chemical structure of target compounds, extensive analysis, including possible (synthesis and) analysis of authentic standards and additional methods, such as nuclear magnetic resonance (NMR) analysis, is required (Schymanski et al., 2014).

Quinones have been claimed to be one of the most critical components in BCs for their redox reactivity; however, identifying the chemical nature of quinones can be challenging. Electron paramagnetic resonance spectroscopy (EPR) analysis can distinguish semiquinone radicals from other carbon-centered radicals in environmental samples (Dasgupta et al., 2021). Nuclear magnetic resonance (NMR) spectra have been used to analyze model compounds when low-concentration quinones are challenging to detect in

complex environmental samples (Dunkel & Wu, 2007). High-resolution mass spectrometry (HRMS) has been used to assign molecular formulas for compositions in NOM (Simon et al., 2022), but it can be challenging to identify quinones among the diverse components (typically with >2000 HRMS features) if they cannot be separated or screened out from other species.

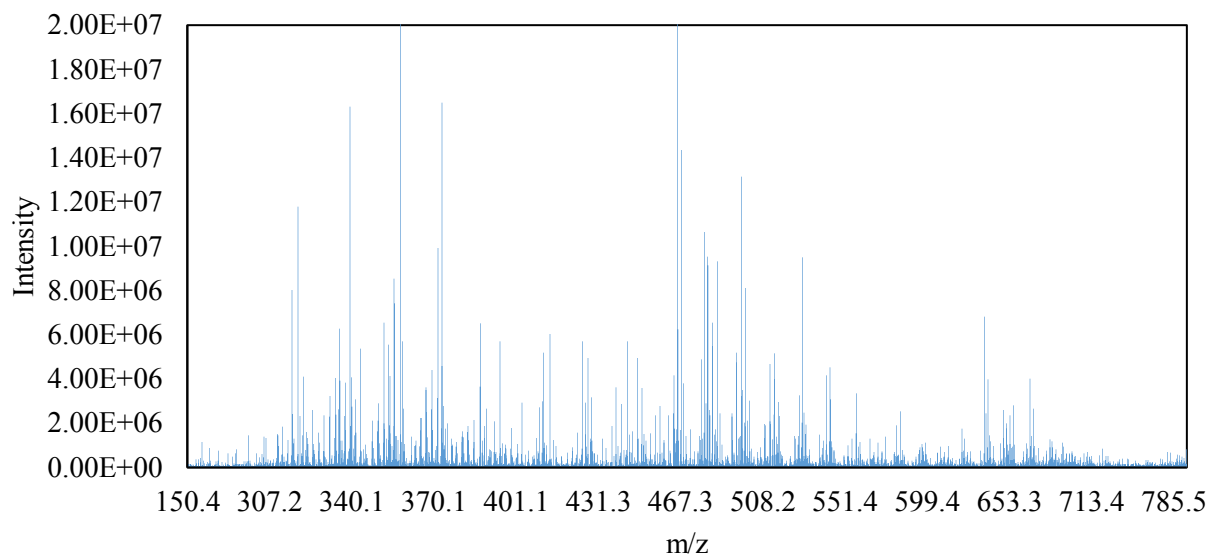


Figure 5-1: Mass spectrometry analysis by Orbitrap mass spectrometry of a-SW.

To address this critical challenge, it would be beneficial to have a chemical tag designed explicitly for identifying quinones through high-resolution mass spectrometry (HRMS). Previous research has demonstrated Michael addition reactions between cysteine and quinones, which can be a potential tagging method for quinones in complex environmental samples for HRMS analysis (Crescenzi et al., 1988; Dayon et al., 2004). While biochemists have used benzoquinone to tag cysteine-containing peptides and proteins, the application of using cysteine to tag quinones in complex environmental samples, such as a-BC (biochar water extract), has yet to be thoroughly examined (Crescenzi et al., 1988; Dayon et al., 2006; Ma et al., 2014).

Therefore, this study aims to: 1) develop a precise and accurate method of chemical tagging for quinones using the Michael addition reaction with cysteine; 2) demonstrate the reliability of this tagging technique by evaluating its efficacy in tagging quinones in the presence of other co-occurring compounds; and 3) identify possible quinone candidates present in a-BC.

5.2 Materials and Methods

5.2.1 Materials

High-performance liquid chromatography (HPLC)-grade methanol and acetonitrile were bought from Fisher Scientific (Ward Hill, MA, USA). Model quinones: 1,4-Benzoquinone (Q), 1,4-Naphthoquinone (NQ), and 1,4-Anthraquinone (AQ) were obtained from Alfa Aesar (Shore Road, Heysham, England), Sigma-Aldrich (St Louis, MO, USA), and Fisher Scientific (Ward Hill, MA, USA). Additional model compounds for co-occurring chemicals, including coumaric acid (CoA) and caffeic acid (CaA), was obtained from TCI (Kita-Ku, Tokyo, Japan); and cinnamic acid (CnA) was obtained from Fisher Scientific (Ward Hill, MA, USA). All model compounds had purity >97%.

5.2.2 Reaction Selectivity and Tagging of Quinone-Spiked Biochar

We prepared stock solutions of benzoquinone (BQ) at a concentration of 10 mM in milliQ water ($\geq 18.2 \text{ M}\Omega \cdot \text{cm}$). In addition, we prepared stock solutions of naphthoquinone (NQ) and anthraquinone (AQ) at concentrations of 10 mM in a mixture of acetonitrile and milliQ water (50/50). These stock solutions were diluted with a 50/50 mixture of acetonitrile and water to prepare a working solution with a concentration of 1 mM. To prepare the reaction mixture, we prepared a stock solution of cysteine at a concentration of 1 mM in milliQ water ($\geq 18.2 \text{ M}\Omega \cdot \text{cm}$). A working solution with a concentration of 100 μM was obtained

by diluting this stock solution with a 50/50 mixture of acetonitrile and water. For the Michael addition reaction between the model quinones and cysteine, we mixed equal volumes of the model quinones and the cysteine solutions. The mixture was allowed to react in the dark at room temperature. The final concentration of the model quinones in the reaction mixture was 500 μM , and that of cysteine was 50 μM . No mechanical agitation was employed during the reaction process.

The reaction was monitored by both UV scanning and mass spectrometry (MS) analysis. The detection limit was determined per the environmental protection agency (EPA) Method 538 document.

5.2.3 Solid-Phase Extraction of Biochar and Chemical Tagging

Solid phase extraction (SPE) to concentrate a-BC was done using Oasis hydrophilic-lipophilic balanced (HLB, 6 cc cartridge with 500 mg column bed and 60 μm pore size) cartridges on AutoTrace 280 automated SPE (Thermo Fisher, Sunnyvale, CA). To prepare the sample for SPE, aqueous phase SW was first acidified to pH 3 using HCl (0.1 M). SPE cartridges were washed with 10 mL methanol and conditioned with 10 mL pH 3 milliQ water at 15 mL/min flow rate. Following conditioning, 500 mL of the acidified samples were loaded onto the cartridge at 1 mL/min flow rate and eluted with 20 mL acetonitrile/methanol (90%/10%). The eluted extracts were evaporated under ultra-high pure N_2 gas (>99.9%) and re-equilibrated in 2.5 mL milliQ water. The final 2.5 mL concentrate was filtered with 0.22 μm sterilized polyvinylidene fluoride (PVDF) filters. Then, 45 μL of concentrate was diluted with 45 μL of methanol.

5.2.4 UV-vis Analysis

UV-vis analysis was performed on the UV-vis spectrophotometer (HACH, DR 6000) using 3 mL quartz cuvettes at various time intervals (5, 10, 20, 30 min), up to 30 min as it was reported to be completed within half an hour.⁴⁷ Wavelength scans from 190 nm to 600 nm were recorded for each sample before and after (30 min) the reaction, and were plotted to confirm the rapid reaction between the cysteine and model quinones.

5.2.5 Time of Flight Mass Spectrometry Analysis (TOF-MS)

The reaction samples were analyzed with direct injection electrospray ionization-time of flight mass spectrometry (ESI-TOF-MS) (G6230A, Agilent Technologies, Folsom, CA, USA). The mobile phase consisted of MS-grade acetonitrile (80%) and water (20%). Both mobile phases contained 0.1% formic acid. The flow rate was fixed at 0.5 mL/min with an injection volume of 20 μ L. For the MS analysis, positive electrospray ionization (ESI) at a fragmentation voltage of 150 V with a mass scan range of 50–3000 m/z and a scan rate of 1 spectra/s was used. The drying gas temperature was set to 325°C at a flow rate of 5 L/min. The nebulizer pressure was set at 20 psi, and the capillary voltage was maintained at 3500 V. Data acquisition and data processing were conducted with mass accuracy of ± 10 ppm and isotope pattern deviation of less than 5%. MestReNova (14.2.0) (Santiago De Compostela, Spain) was used to process the TOF-MS data.

5.2.6 Data Analysis

The analysis was conducted using an in-house developed Python code in the Spyder environment (v5.4.2) to filter out the unique MS spectra with a minimum signal-to-noise ratio of 3 and a background noise cutoff of 1000. The Python code was also used to screen the unique features in positive mode containing parent ions $[M+H]^+$ and $[M+2H]^{2+}$. The

mass difference of the unique peaks with tagged cysteine was calculated to determine the mass of parent quinones, and the results were presented visually using either Python or MS Excel.

5.3 Results and Discussions

5.3.1 Influences of Quinones Structures on the Tagging Reaction

UV analysis was used to study the reactions between model quinones and CY. The absorption peaks of BQ, MBQ, CBQ, and NQ were observed at 245 nm, 250 nm, 255 nm, and 251 nm, respectively. After 30 minutes of reaction with CY, the original quinones peaks were significantly reduced to almost dissipated, while new peaks emerged at 301 nm for the samples of BQ, MBQ, and CBQ, which was consistent with literature reports. However, NQ, AQA, and AQ did not show a new peak at 301 nm after reacting with CY. UV spectra of the AQA and CY reaction samples showed no significant change, indicating minimal reaction. The decrease in the original peak of quinones was attributed to the formation of new compounds with similar or different UV spectra after reacting with CY. The UV results indicated that Q and its substitutes (MBQ and CBQ) were converted into the hydroquinone (H₂Q) form, consistent with literature reports. However, NQ, AQA, and AQ did not show a new peak resembling the H₂Q form after reacting with CY. This difference in UV spectra of model compounds reacted with CY represents stable hydroquinone adducts, including hydrobenzoquinone-CY, methohydroquinone-CY, and chlorohydroquinone-CY, as well as stable quinone adducts, such as NQ-CY and AQ-CY. In contrast, the reaction of CY with NQ, AQA, and AQ did not substantially reduce the original UV spectra, indicating the minimal transformation of these quinones.

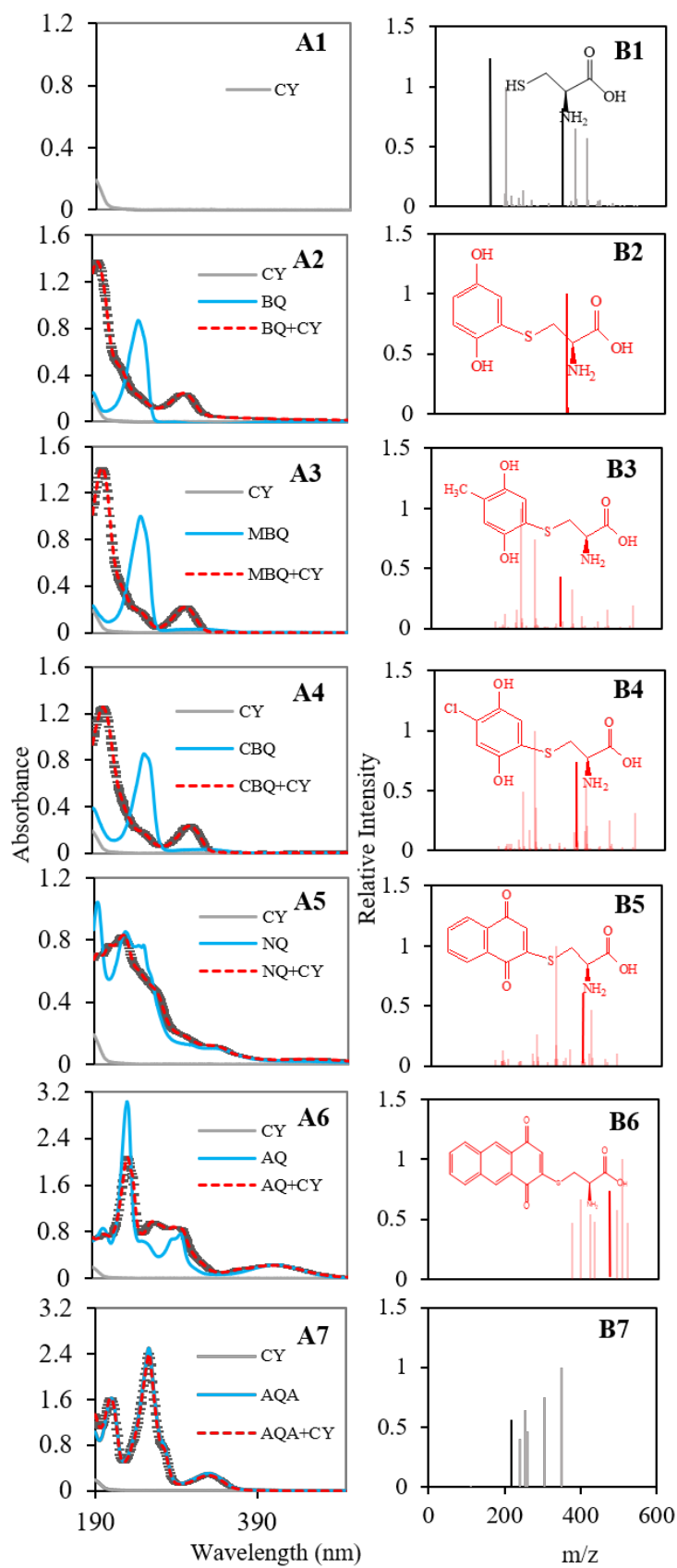


Figure 5-2: UV-spectra and time of flight mass spectrometry (TOF-MS) analysis of quinone and cysteine (CY) reactions. **(A1)** and **(B1)**: UV and MS spectra of 50 μM CY, **(A2)** and **(B2)**: UV and MS spectra of 50 μM 1,4-benzoquinone (BQ) and 50 μM CY reaction, **(A3)** and **(B3)**: UV and MS spectra of 50 μM 2-methyl-1,4-benzoquinone (MBQ) and 50 μM CY reaction, **(A4)** and **(B4)**: UV and MS spectra of 50 μM 2-chloro-1,4-benzoquinone (CBQ) and 50 μM CY reaction, **(A5)** and **(B5)**: UV and MS spectra of 50 μM 1,4-naphthoquinone (NQ) and 50 μM CY reaction, **(A6)** and **(B6)**: UV and MS spectra of 50 μM 1,4-anthraquinone (AQ) and 50 μM CY reaction, **(A7)** and **(B7)**: UV and MS spectra of 50 μM 9,10-anthraquinone-2-carboxylic acid (AQA) and 50 μM CY reaction.

The polar side chains of amino acids such as CY are ideal for studying reaction progress using electrospray ionization mass spectrometry (ESI-MS). In this study, we used CY to label model quinones and time-of-flight mass spectrometry (+ESI) to ionize CY. The mass peaks obtained from the reactions between CY and quinones matched the exact mass of $[\text{M}+\text{H}]^+$ of the respective adduct. New mass peaks for BQ-CY, MBQ-CY, CBQ-CY, NQ-CY, and AQ-CY adducts were found. The results showed that BQ and CY had the highest adduct ionization efficiency. In contrast, the adduct ion intensity decreased as other functional groups or benzene rings were added to the model compound. The efficiency also depended on the type of substitutes added to benzoquinone. These findings demonstrate the effectiveness of ESI-MS in analyzing the reaction progress of CY with model quinones. The elemental composition and structure of the molecules involved strongly influence the reaction rate and the final conversion yield due to polarity or electron density and steric hindrance. Additional fragment and structural differences can affect the polarity at the beta

carbon, thereby influencing the Michael addition rate. As reported in previous literature, the detection of molecules in various ionized forms can affect quantitative detection in mass spectrometry. In this study, we observed that quinones-CY adducts had a significant mass peak for the parent ion as $[M+H]^+$.

Analysis of AQA and CY reaction samples showed no adduct peaks, indicating that quinone structures can only form quinone-CY adducts when the beta carbon from the same benzene ring is available for Michael addition. The detectable structures of quinone adducts can be affected by the original quinone structures, where the presence of reduced and oxidized forms of quinones could play a substantial role through their self-reversible redox cycle or cross-reaction with other quinone structures in the pool. Additionally, the presence of additional benzene rings can lower the pKa due to resonance effects and result in more stable quinone adducts in a multi-component system, which can be controlled by regulating pH. Results also showed that the quinone form predominated the quinone-CY adducts, and the benzoquinones with no additional benzene ring resulted in adducts dominated by the hydroquinone form. These quinone adducts could also be prone to another attack by CY when another beta carbon is available for Michael addition.

5.3.2 TOF Calibration Curves for 1,4-benzoquinone

Using a mass tolerance of 10 ppm, calibration curves were established by plotting BQ concentrations against new adduct intensity. A calibration curve ($r^2 = 0.99$) was developed for quantifying benzoquinone based on the intensity of adduct $[M+H]^+$ with m/z equal to 230.048 for reactions with cysteine. (**Figure 5-3**).

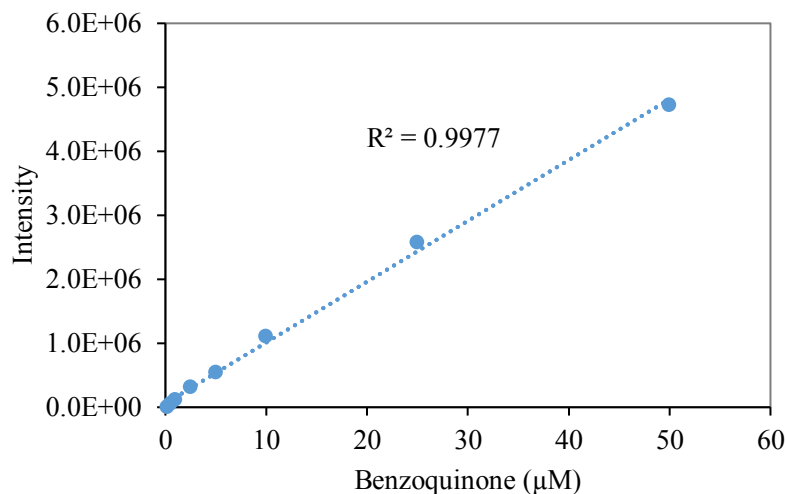


Figure 5-3: Calibration curve for benzoquinone based on the TOF-MS intensity for the selected peaks ($m/z = 230.048$) resulting from the Michael addition reactions between benzoquinone and cysteine.

5.3.3 Reaction Selectivity Study with Quinone-like Compounds

Caffeic acid (CA) displayed an absorption peak at 323 nm, whereas coumaric acid (CoA) and cinnamic acid (CnA) displayed peaks at 308 nm and 271 nm, respectively. After thirty minutes, the UV analysis of the reaction between CY and quinone-like compounds (QLMC) revealed minimal decay in the original peak, with only CoA exhibiting a shift to a new peak at 288 nm. These results indicate a slower reaction rate than quinone and CY reactions and a low rate of original absorbance decay. In addition, the reaction complex exhibited UV decay in the BQ region, indicating that BQ was consumed more rapidly than in other quinone-like model compounds (**Figure 5-4**).

Despite a slight decrease in the original absorbance pattern, indicating a potential slow reaction between QLMCs and CY, TOF-MS analysis did not detect any ionized QLMC-CY adducts. Peaks for CY ($m/z=122.028$) and CY-CY dimers ($m/z=241.032$) were present

in all distinct reactions involving CY and quinone-like model compounds. As the concentration of BQ increased from 5 μM to 50 μM , the intensity of the CY and CY-CY peaks decreased when the concentrations of all other reagents in the complex remained constant (50 μM), indicating that benzoquinones consumed CY primarily. The formation of BQ-CY adducts during reactions involving all quinone-like model compounds and BQ in complex with CY was also observed. At up to a 1:10 molar ratio of BQ and QLMC concentrations, the presence of other quinone-like model compounds did not influence the conversion of BQ to BQ-CY adducts.

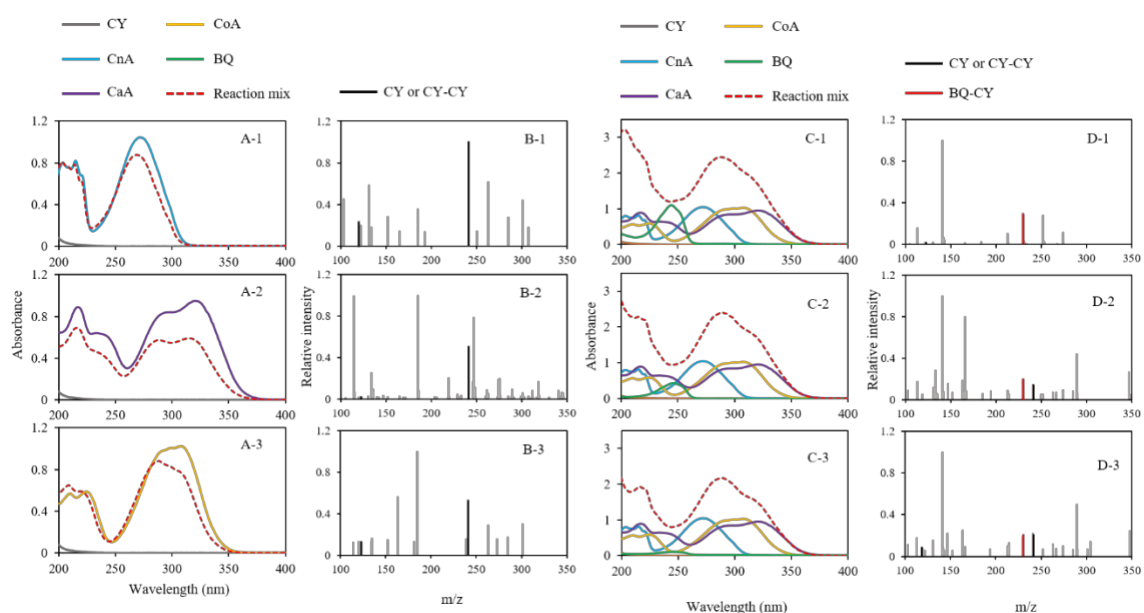


Figure 5-4: UV-spectra and TOF-MS analysis for tagging selectivity. **(A-1)** and **(B-1)**: UV and MS spectra of 50 μM cinnamic acid (CnA) and 50 μM CY reaction, **(A-2)** and **(B-2)**: UV and MS spectra of 50 μM coumaric acid (CoA) and 50 μM CY reaction, **(A-3)** and **(B-3)**: UV and MS spectra of 50 μM caffeic acid (CaA) and 50 μM CY reaction. **(C-1)** and **(D-1)**: UV and MS spectra of 50 μM BQ and μM 50 CY (1:1) reaction in the presence of 50 μM CnA, 50 μM CoA, and 50 μM CaA. **(C-2)** and **(D-2)**: UV and MS spectra of 25 μM

BQ and μM 50 CY (0.5:1) reaction in the presence of 50 μM CnA, 50 μM CoA, and 50 μM CaA. **(C-3)** and **(D-3)**: UV and MS spectra of 10 μM BQ and μM 50 CY (0.1:1) reaction in the presence of 50 μM CnA, 50 μM CoA, and 50 μM CaA.

5.3.4 Tagging Model Quinones in Complex Biochar Media

The successful tagging of benzoquinone and naphthoquinone in complex aqueous media using cysteine has been achieved (**Figure 5-5**). The selectivity and reactivity of CY influence adduct formation efficiency in the presence of various chemicals in a multi-component or complex medium. CY can be consumed substantially within a short period; consequently, the formation of CY-quinone adducts and their subsequent transformation due to further reactions in complex media can result in low CY-quinone adduct intensity.

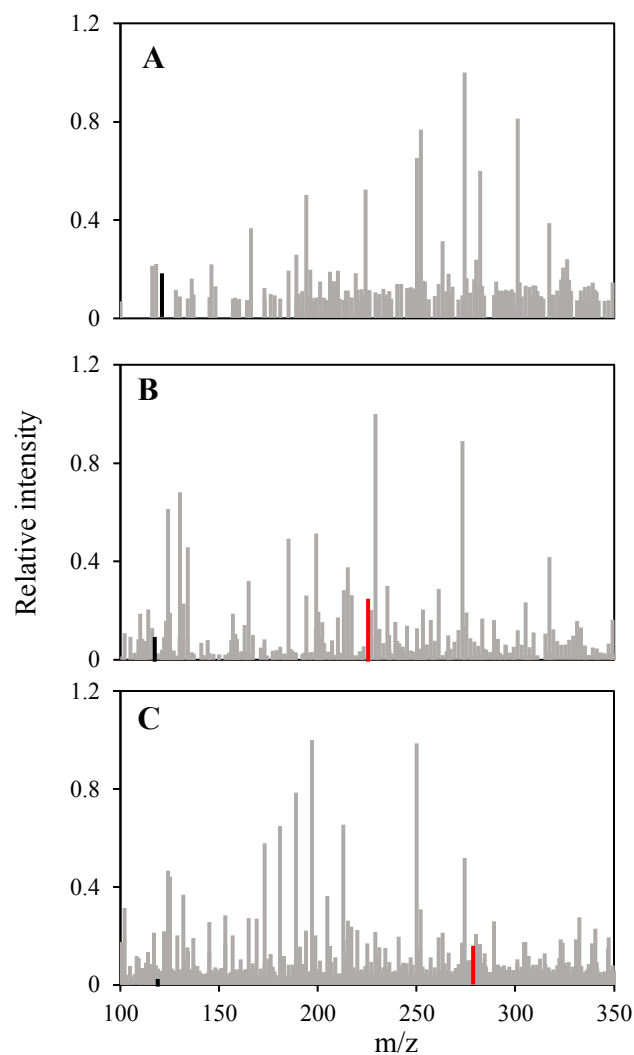


Figure 5-5: Time of flight mass spectrometry (TOF-MS) analysis of **(A)** Swiss biochar extract (SW) and 10 μ M Cysteine (CY) reaction, **(B)** SW, 10 μ M 1,4-benzoquinone (BQ), and 10 μ M CY reaction, **(C)** SW, 10 μ M 1,4-naphthoquinone (NQ), and 10 μ M CY reaction.

5.3.5 SPE Concentrated Swiss Biochar Tagging and Quinone Candidate Screening

The CY molecules possess an amine and acidic group, resulting in singly charged ($[M+H]^+$ & $[M-H]^-$) ions for CY and its quinone adducts when analyzed by ESI+ and ESI-. Upon reaction with concentrated SW, the quinone compounds in the CY solution transformed

into either CY-hydroquinone or CY-quinone adduct forms, producing unique mass-to-charge (m/z) features. Although nonionic quinone compounds may exist in the solution, they may not ionize with ESI+ and ESI-. Screening of quinone compounds before (apo compounds) and after the reaction (quinone-cysteine adducts) revealed 81–150 potential m/z suspects with different reactions and ionization modes (**Figure 5-6**). In ESI+ mode, there were 1343 and 1375 features for CY-hydroquinone adducts, and CY-quinone adducts with mass differences of CY and CY-2H, respectively. Out of the 602 unique features formed after the SW-CY reaction in ESI+ mode, 108 corresponded to ionized quinone compounds transformed to CY-hydroquinone adducts, and 130 corresponded to ionized quinone compounds transformed to CY-quinone adducts. Similarly, in ESI- mode, there were 752 and 850 features for CY-hydroquinone adducts, and CY-quinone adducts with mass differences of CY and CY-2H, respectively. Out of the 456 unique features formed after the SW-CY reaction in ESI- mode, 81 corresponded to quinone compounds transformed to CY-hydroquinone adducts, and 86 corresponded to quinone compounds transformed to CY-quinone adducts.

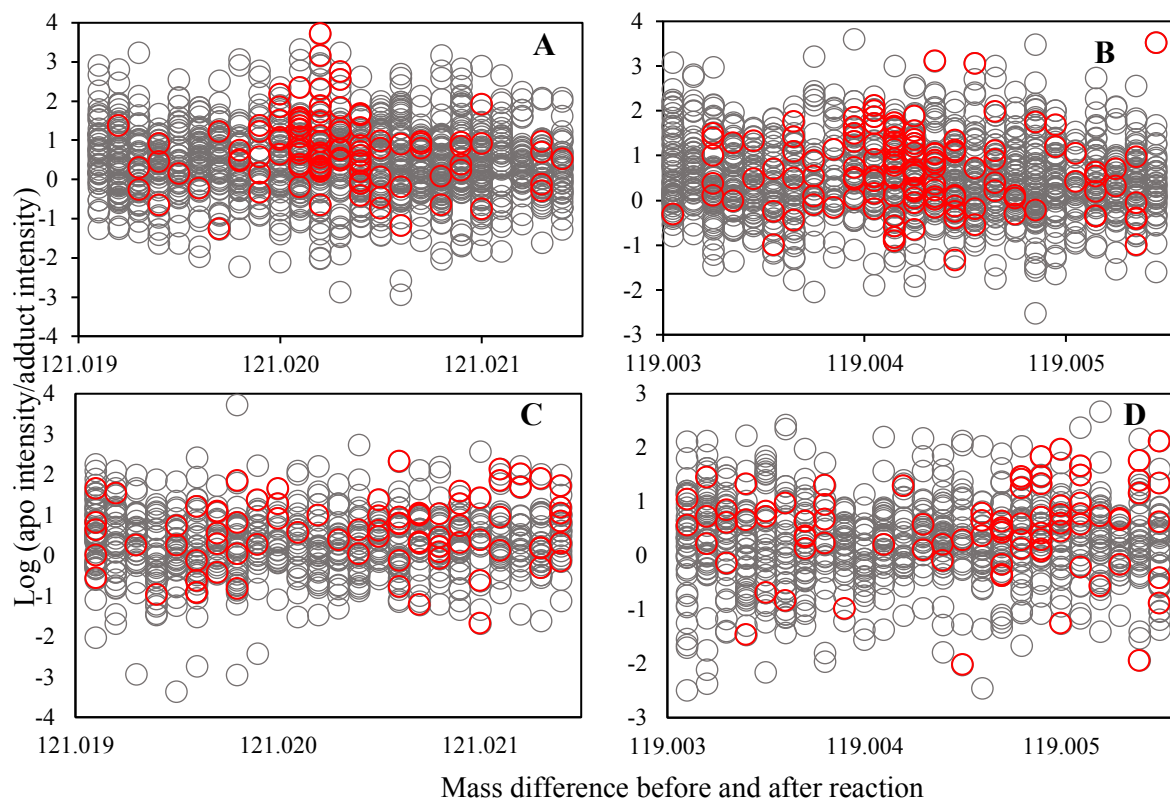


Figure 5-6: Orbitrap mass spectrometry (MS) analysis of solid phase extracted (SPE) concentrated Swiss biochar extracts reacted with cysteine. Mass difference on X-axis is the difference between the m/z value of the candidate compound after the reaction and the m/z value of the candidate compound before the reaction. The scale on the Y-axis is the log transformed ratio of the candidate compound's intensity before the reaction to the candidate compound's intensity after the reaction. The gray circle represents the candidates with a mass difference of cysteine, and the red circle highlights the unique candidates formed after the reaction. Panels **A** and **B** are the results of positive mode, and **C** and **D** are the results of negative mode.

5.3.6 Environmental Implications

The natural occurrence of quinone compounds in organic matter, specifically biochar, can be effectively analyzed using the methods detailed in this study. Quinones and their functional groups play an essential role in nutrient cycles as electron transporters for crucial elements such as carbon, nitrogen, phosphorus, and iron. The identification of quinone structures and chemical compositions can provide insight into the environmental implications of natural organic matter and pyrogenic carbon, including the potential redox reaction mechanisms in which they participate. This study's findings offer valuable information on the distinguishable structures of quinones, which can be applied to identify their chemical structures in complex systems. Due to the significant changes in molecule size and hydrophilic properties resulting from the reaction, the quinone-CY adduct can be readily detected as a novel feature using size-, ion-, and hydrophilicity-hydrophobicity-based separation processes in mass spectrometry coupled with liquid chromatography. This method enables a comprehensive understanding of quinone chemistry, facilitating the identification of these compounds in environmental samples and providing insight into their roles in redox processes.

Chapter 6: Conclusion

The goals of this dissertation were to 1) study the degradation of organohalogen (with triclosan as a model compound) by aqueous biochars, 2) investigate the impact of the chemical nature of quinones on their reactivity for organohalogen degradation, and 3) analyze the reactive chemical compositions of aqueous biochars.

Our study demonstrated the potential of reduced aqueous biochars to reductively degrade organohalogens, as evidenced by the anaerobic degradation of triclosan with a pseudo first-order degradation rate constant. The degradation was found to be correlated with the amount of a-BC-bound electrons available for donation, and the recovery of chlorine based on residual triclosan and generated Cl^- indicated a major fraction of triclosan was fully dechlorinated. The study suggests that reduced a-BCs have potential applications in wastewater treatment and groundwater remediation for a range of redox-sensitive trace organic compounds.

To understand the critical components of a-BCs for reductive dehalogenation, we investigated the role of quinones and their products in the reductive degradation of organohalogens mediated by natural and pyrogenic organic matter. We used a model organohalogen, triclosan (TCS), and 1,4-benzohydroquinone (H_2Q) or corresponding 1,4-benzosemiquinone (SQ^-) to determine the degradation of TCS. The study found that degradation of TCS occurred in the presence of H_2Q and FeCl_3 under anoxic conditions at pH 5 and 7. The study also revealed that SQ^- was responsible for the reductive degradation of TCS and that SQ^- s play a critical role in reductive dehalogenation reactions. These findings could have significant implications for quinone-mediated redox reactions in natural and engineering systems.

To identify the chemical nature of quinones in a-BCs, chemical tagging of quinones using Michael addition reaction with cysteine was developed. The reaction products of Michael addition reactions between model quinones and cysteine were analyzed using mass spectrometry and UV spectra. Minimal interferences of a range of possible co-occurring compounds were demonstrated. For a-BCs, after tagging with cysteine, the possible quinones compounds were identified based on the new features generated for the reaction products or the expected m/z difference between the original MS feature and adducts. The study demonstrated that Michael addition reactions could efficiently tag quinones and potentially provide insights into the redox chemistry of natural organic matter and their critical chemical compositions and structures.

References:

- Adrian, L., & Löffler, F. E. (2016). Organohalide-Respiring Bacteria—An Introduction. In L. Adrian & F. E. Löffler (Eds.), *Organohalide-Respiring Bacteria* (pp. 3–6). Springer.
- Agarry, S. E., Owabor, C. N., & Ajani, A. O. (2013). Modified plantain peel as cellulose-based low-cost adsorbent for the removal of 2, 6-dichlorophenol from aqueous solution: Adsorption isotherms, kinetic modeling, and thermodynamic studies. *Chemical Engineering Communications*, 200(8), 1121–1147.
- Agegnehu, G., Srivastava, A. K., & Bird, M. I. (2017). The role of biochar and biochar-compost in improving soil quality and crop performance: A review. *Applied Soil Ecology*, 119, 156–170.
- Almatroodi, S. A., Almatroudi, A., Khan, A. A., Alhumaydhi, F. A., Alsahli, M. A., & Rahmani, A. H. (2020). Potential Therapeutic Targets of Epigallocatechin Gallate (EGCG), the Most Abundant Catechin in Green Tea, and Its Role in the Therapy of Various Types of Cancer. *Molecules (Basel, Switzerland)*, 25(14), E3146.
- Arnold, W. A., & Roberts, A. L. (2000). Pathways and Kinetics of Chlorinated Ethylene and Chlorinated Acetylene Reaction with Fe(0) Particles. *Environmental Science & Technology*, 34(9), 1794–1805.
- Arun Gavaskar, Lauren Tatar, & Wendy Condit. (2005). *Nanoscale zero-valent iron technologies for source remediation* [Cost and performance report]. Naval Facilities Engineering Command.

- Atashgahi, S., Liebensteiner, M. G., Janssen, D. B., Smidt, H., Stams, A. J. M., & Sipkema, D. (2018). Microbial Synthesis and Transformation of Inorganic and Organic Chlorine Compounds. *Frontiers in Microbiology*, 9.
- Aulenta, F., Maio, V. D., Ferri, T., & Majone, M. (2010). The humic acid analogue anthraquinone-2,6-disulfonate (AQDS) serves as an electron shuttle in the electricity-driven microbial dechlorination of trichloroethene to cis-dichloroethene. *Bioresource Technology*, 101(24), 9728–9733.
- Barkovskii, L. A.; Adriaens, P. (2009). Impact of humic constituents on microbial dechlorination of polychlorinated dioxins. *Environmental Toxicology and Chemistry*. 17(6), 1013–1020
- Bellar, T. A., Lichtenberg, J. J., & Kroner, R. C. (1974). The Occurrence of Organohalides in Chlorinated Drinking Waters. *Journal (American Water Works Association)*, 66(12), 703–706. JSTOR.
- Berggren, D. R. V., Marshall, I. P. G., Azizian, M. F., Spormann, A. M., & Semprini, L. (2013). Effects of Sulfate Reduction on the Bacterial Community and Kinetic Parameters of a Dechlorinating Culture under Chemostat Growth Conditions. *Environmental Science & Technology*. 47(4), 1879–1886.
- Bhatt, P., Kumar, M. S., Mudliar, S., & Chakrabarti, T. (2007). Biodegradation of Chlorinated Compounds—A Review. *Critical Reviews in Environmental Science and Technology*, 37(2), 165–198.
- Bielski, B., Cabelli, D., Arudi, R. L., & Ross, A. (1985). *Reactivity of HO₂/O₂-2 Radicals in Aqueous Solution*.

- Boiteau, R. M., Mende, D. R., Hawco, N. J., McIlvin, M. R., Fitzsimmons, J. N., Saito, M. A., Sedwick, P. N., DeLong, E. F., & Repeta, D. J. (2016). Siderophore-based microbial adaptations to iron scarcity across the eastern Pacific Ocean. *Proceedings of the National Academy of Sciences*, *113*(50), 14237–14242.
- Bokare, A. D., & Choi, W. (2010). Chromate-Induced Activation of Hydrogen Peroxide for Oxidative Degradation of Aqueous Organic Pollutants. *Environmental Science & Technology*. *44*(19), 7232–7237.
- Butler, E. C., & Hayes, K. F. (1999). Kinetics of the Transformation of Trichloroethylene and Tetrachloroethylene by Iron Sulfide. *Environmental Science & Technology*, *33*(12), 2021–2027.
- Chacon, F. J., Sanchez-Monedero, M. A., Lezama, L., & Cayuela, M. L. (2020). Enhancing biochar redox properties through feedstock selection, metal preloading and post-pyrolysis treatments. *Chemical Engineering Journal*, *395*, 125100.
- Chan, K., Xu, L., & Fang, H. (2002). Anaerobic electrochemical corrosion rug of mild steel in the presence of extracellular polymeric substances produced by a culture enriched in sulfate-reducing bacteria. *Environmental Science & Technology*. *36*(8), 1720–1727.
- Chen, S., Rotaru, A.-E., Shrestha, P. M., Malvankar, N. S., Liu, F., Fan, W., Nevin, K. P., & Lovley, D. R. (2014). Promoting Interspecies Electron Transfer with Biochar. *Scientific Reports*, *4*(1), Article 1.
- Chen, Z., Chen, B., & Chiou, C. T. (2012). Fast and Slow Rates of Naphthalene Sorption to Biochars Produced at Different Temperatures. *Environmental Science & Technology*, *46*(20), 11104–11111.

- Collins, R., & Picardal, F. (1999). Enhanced anaerobic transformations of carbon tetrachloride by soil organic matter. *Environmental Toxicology and Chemistry*, *18*(12), 2703–2710.
- Cornelissen, G., Gustafsson, O., Bucheli, T., Jonker, M., Koelmans, A., & Van Noort, P. (2005). Extensive sorption of organic compounds to black carbon, coal, and kerogen in sediments and soils: Mechanisms and consequences for distribution, bioaccumulation, and biodegradation. *Environmental Science & Technology*, *39*(18), 6881–6895.
- Crescenzi, O., Prota, G., Schultz, T., & Wolfram, L. J. (1988). The reaction of cysteine with 1, 4-benzoquinone: A revision. *Tetrahedron*, *44*(20), 6447–6450.
- Curtis, G., & Reinhard, M. (1992). Reductive dehalogenation of hexachlorethane, carbon-tetrachloride and bromoform by anthrahydroquinone disulfonate and humic-acid. *Environmental Science & Technology*, *28*(13), 2393–2401.
- Dai, Y., Zhang, N., Xing, C., Cui, Q., & Sun, Q. (2019). The adsorption, regeneration and engineering applications of biochar for removal organic pollutants: A review. *Chemosphere*, *223*, 12–27.
- Dasgupta, A., Richards, E., & Melen, R. L. (2021). Frustrated Radical Pairs: Insights from EPR Spectroscopy. *Angewandte Chemie International Edition*, *60*(1), 53–65.
- Dayon, L., Roussel, C., & Girault, H. H. (2006). Probing cysteine reactivity in proteins by mass spectrometric EC-tagging. *Journal of Proteome Research*, *5*(4), 793–800.
- D. Lin, R., & F. Steinmetz, N. (2018). Tobacco mosaic virus delivery of mitoxantrone for cancer therapy. *Nanoscale*, *10*(34), 16307–16313.

- Dunkel, R., & Wu, X. (2007). Identification of organic molecules from a structure database using proton and carbon NMR analysis results. *Journal of Magnetic Resonance (San Diego, Calif. : 1997)*, 188(1), 97–110.
- Exner, M., & Färber, H. (2006). Perfluorinated Surfactants in Surface and Drinking Waters (9 pp). *Environmental Science and Pollution Research - International*, 13(5), 299–307.
- Field, J. A., & Sierra-Alvarez, R. (2008). Microbial transformation and degradation of polychlorinated biphenyls. *Environmental Pollution*, 155(1), 1–12.
- Fu, H., Guo, Y., Chen, W., Gu, C., & Zhu, D. (2014). Reductive dechlorination of hexachloroethane by sulfide in aqueous solutions mediated by graphene oxide and carbon nanotubes. *Carbon*, 72, 74–81.
- Garg, S., Ito, H., Rose, A. L., & Waite, T. D. (2013). Mechanism and Kinetics of Dark Iron Redox Transformations in Previously Photolyzed Acidic Natural Organic Matter Solutions. *Environmental Science & Technology*, 47(4), 1861–1869.
- Garg, S., Jiang, C., & David Waite, T. (2015). Mechanistic insights into iron redox transformations in the presence of natural organic matter: Impact of pH and light. *Geochimica et Cosmochimica Acta*, 165, 14–34.
- Hägglom, M., & Bossert, I. (2004). *Halogenated Organic Compounds—A Global Perspective* (pp. 3–29).
- Hamilton, R. H. (1966). A Direct Photometric Method for Chloride in Biological Fluids, Employing Mercuric Thiocyanate and Perchloric Acid. *Clinical Chemistry*, 12(1), 1–17.

- Hasan, Ö. (2018). A new approach to soil solarization: Addition of biochar to the effect of soil temperature and quality and yield parameters of lettuce (*Lactuca sativa* L. Duna). *Scientia Horticulturae*, 228, 153–161.
- Heymann, K., Lehmann, J., Solomon, D., Schmidt, M. W. I., & Regier, T. (2011). C 1s K-edge near edge X-ray absorption fine structure (NEXAFS) spectroscopy for characterizing functional group chemistry of black carbon. *Organic Geochemistry*, 42(9), 1055–1064.
- Huang, B., Gu, L., He, H., Xu, Z., & Pan, X. (2016). Enhanced biotic and abiotic transformation of Cr (VI) by quinone-reducing bacteria/dissolved organic matter/Fe (III) in anaerobic environment. *Environmental Science: Processes & Impacts*, 18(9), 1185-1192.
- Huynh, M. T., Anson, C. W., Cavell, A. C., Stahl, S. S., & Hammes-Schiffer, S. (2016). Quinone 1 e⁻ and 2 e⁻/2 H⁺ Reduction Potentials: Identification and Analysis of Deviations from Systematic Scaling Relationships. *Journal of the American Chemical Society*, 138(49),
- Ilan, Y. A., Czapski, G., & Meisel, D. (1976). The one-electron transfer redox potentials of free radicals. I. The oxygen/superoxide system. *Biochimica et Biophysica Acta (BBA) - Bioenergetics*, 430(2), 209–224.
- Jiang, C., Garg, S., & Waite, T. D. (2015). Hydroquinone-mediated redox cycling of iron and concomitant oxidation of hydroquinone in oxic waters under acidic conditions: Comparison with iron–natural organic matter interactions. *Environmental Science & Technology*, 49(24), 14076–14084.

- Jiang, J., & Kappler, A. (2008). Kinetics of Microbial and Chemical Reduction of Humic Substances: Implications for Electron Shuttling. *Environmental Science & Technology*, 42(10), 3563–3569.
- Jiang, S., Nguyen, T. A. H., Rudolph, V., Yang, H., Zhang, D., Ok, Y. S., & Huang, L. (2017). Characterization of hard- and softwood biochars pyrolyzed at high temperature. *Environmental geochemistry and Health*. 39(2, SI), 403–415.
- Jirka, S., & Tomlinson, T. (2015). State of the biochar industry 2014. *International biochar initiative rep.*
- Jovanovic, S. V., Hara, Y., Steenken, S., & Simic, M. G. (1995). Antioxidant potential of galliccatechins. A pulse radiolysis and laser photolysis study. *Journal of the American Chemical Society*, 117(39), 9881–9888.
- Kappler, A., & Haderlein, S. B. (2003). Natural Organic Matter as Reductant for Chlorinated Aliphatic Pollutants. *Environmental Science & Technology*, 37(12), 2714–2719.
- Kappler, A., Wuestner, M. L., Ruecker, A., Harter, J., Halama, M., & Behrens, S. (2014). Biochar as an electron shuttle between bacteria and Fe (III) minerals. *Environmental Science & Technology Letters*, 1(8), 339–344.
- Keiluweit, M., Nico, P. S., Johnson, M. G., & Kleber, M. (2010). Dynamic Molecular Structure of Plant Biomass-Derived Black Carbon (Biochar). *Environmental Science & Technology*, 44(4), 1247–1253.
- Keum, Y.-S., & Li, Q. X. (2005). Reductive Debromination of Polybrominated Diphenyl Ethers by Zerovalent Iron. *Environmental Science & Technology*, 39(7), 2280–2286.

- Khan, K. N. M., Hard, G. C., & Alden, C. L. (2013). Chapter 47—Kidney. In W. M. Haschek, C. G. Rousseaux, & M. A. Wallig (Eds.), *Haschek and Rousseaux's Handbook of Toxicologic Pathology (Third Edition)* (pp. 1667–1773). Academic Press.
- Khan, N., Afaq, F., Saleem, M., Ahmad, N., & Mukhtar, H. (2006). Targeting Multiple Signaling Pathways by Green Tea Polyphenol (–)-Epigallocatechin-3-Gallate. *Cancer Research*, *66*(5), 2500–2505.
- Kim, J.-H., Tratnyek, P. G., & Chang, Y.-S. (2008). Rapid Dechlorination of Polychlorinated Dibenzo-p-dioxins by Bimetallic and Nanosized Zerovalent Iron. *Environmental Science & Technology*, *42*(11).
- Kjellerup, B. V., Naff, C., Edwards, S. J., Ghosh, U., Baker, J. E., & Sowers, K. R. (2014). Effects of activated carbon on reductive dechlorination of PCBs by organohalide respiring bacteria indigenous to sediments. *Water Research*, *52*, 1–10.
- Kliegman, S., Eustis, S. N., Arnold, W. A., & McNeill, K. (2013). Experimental and Theoretical Insights into the Involvement of Radicals in Triclosan Phototransformation. *Environmental Science & Technology*, *47*(13), 6756–6763.
- Kluepfel, L., Keiluweit, M., Kleber, M., & Sander, M. (2014). Redox Properties of Plant Biomass-Derived Black Carbon (Biochar). *Environmental Science & Technology*, *48*(10), 5601–5611.
- Kodavanti, P. R. S., & Loganathan, B. (2016). Organohalogen Pollutants and Human Health. In *International Encyclopedia of Public Health*.

- Koelmans, A., Jonker, M., Cornelissen, G., Bucheli, T., Van Noort, P., & Gustafsson, O. (2006). Black carbon: The reverse of its dark side. *Chemosphere*, *63*(3), pp. 365–377).
- Kookana, R. S., Sarmah, A. K., Van Zwieten, L., Krull, E., & Singh, B. (2011). Biochar application to soil: Agronomic and Environmental benefits and unintended consequences. *Advances in Agronomy*, *112*, 103–143.
- Kristensen, S. B., van Mourik, T., Pedersen, T. B., Sørensen, J. L., & Muff, J. (2020). Simulation of electrochemical properties of naturally occurring quinones. *Scientific Reports*, *10*(1), Article 1.
- Lefevre, E., Bossa, N., Gardner, C. M., Gehrke, G. E., Cooper, E. M., Stapleton, H. M., Hsu-Kim, H., & Gunsch, C. K. (2018). Biochar and activated carbon act as promising amendments for promoting the microbial debromination of tetrabromobisphenol A. *Water Research*, *128*, 102–110
- Leglize, P., Alain, S., Jacques, B., & Corinne, L. (2008). Adsorption of phenanthrene on activated carbon increases mineralization rate by specific bacteria. *Journal of Hazardous Materials*, *151*(2–3), 339–347.
- Lehmann, J. (2007). Bio-Energy in the Black. *Frontiers in Ecology and the Environment*, *5*(7), 381–387.
- Lehmann, J., & Joseph, S. (Eds.). (2009). *Biochar for environmental management: Science and technology*. Earthscan.
- Lehmann, J., & Joseph, S. (2015). *Biochar for environmental management: Science, technology and implementation*. Routledge.

- Letcher, R. J., Gebbink, W. A., Sonne, C., Born, E. W., McKinney, M. A., & Dietz, R. (2009). Bioaccumulation and biotransformation of brominated and chlorinated contaminants and their metabolites in ringed seals (*Pusa hispida*) and polar bears (*Ursus maritimus*) from East Greenland. *Environment International*, 35(8), 1118–1124).
- Liu, C., Zachara, J. M., Foster, N. S., & Strickland, J. (2007). Kinetics of Reductive Dissolution of Hematite by Bioreduced Anthraquinone-2,6-disulfonate. *Environmental Science & Technology*, 41(22), 7730–7735.
- Liu, G., Zheng, H., Jiang, Z., Zhao, J., Wang, Z., Pan, B., & Xing, B. (2018). Formation and Physicochemical Characteristics of Nano Biochar: Insight into Chemical and Colloidal Stability. *Environmental Science & Technology*, 52(18), 10369–10379.
- Liu, J., & Mejia Avendaño, S. (2013). Microbial degradation of polyfluoroalkyl chemicals in the environment: A review. *Environment International*, 61, 98–114.
- L,Kux. (n.d.). *Federal Register Vol. 81 No. 126*. <https://www.gpo.gov/fdsys/pkg/FR-2016-06-30/pdf/2016-15410.pdf>.
- Lokesh, S., Kim, J., Zhou, Y., Wu, D., Pan, B., Wang, X., Behrens, S., Huang, C.-H., & Yang, Y. (2020). Anaerobic Dehalogenation by Reduced Aqueous Biochars. *Environmental Science & Technology*.
- Nikel, P. I., Pérez-Pantoja, D., & de Lorenzo, V. (2013). Why are chlorinated pollutants so difficult to degrade aerobically? Redox stress limits 1, 3-dichloroprop-1-ene metabolism by *Pseudomonas pavonaceae*. *Philosophical Transactions of the Royal Society B: Biological Sciences*, 368(1616), 20120377.

- Lovley, D. R., Coates, J. D., Blunt-Harris, E. L., Phillips, E. J., & Woodward, J. C. (1996). Humic substances as electron acceptors for microbial respiration. *Nature*, *382*(6590), 445–448.
- Lowry, G. V., & Johnson, K. M. (2004). Congener-Specific Dechlorination of Dissolved PCBs by Microscale and Nanoscale Zerovalent Iron in a Water/Methanol Solution. *Environmental Science & Technology*, *38*(19), 5208–5216.
- Lu, L., Yu, W., Wang, Y., Zhang, K., Zhu, X., Zhang, Y., Wu, Y., Ullah, H., Xiao, X., & Chen, B. (2020). Application of biochar-based materials in environmental remediation: From multi-level structures to specific devices. *Biochar*, *2*(1), 1–31.
- Luijten, M. L. G. C., Weelink, S. A. B., Godschalk, B., Langenhoff, A. A. M., van Eekert, M. H. A., Schraa, G., & Stams, A. J. M. (2004). Anaerobic reduction and oxidation of quinone moieties and the reduction of oxidized metals by halorespiring and related organisms. *FEMS Microbiology Ecology*, *49*(1), 145–150.
- Ma, R., Hu, J., Cai, Z., & Ju, H. (2014). Dual quinone tagging for MALDI-TOF mass spectrometric quantitation of cysteine-containing peptide. *Analytical Chemistry*, *86*(16), 8275–8280.
- Marchal, G., Smith, K. E., Rein, A., Winding, A., de Jonge, L. W., Trapp, S., & Karlson, U. G. (2013). Impact of activated carbon, biochar and compost on the desorption and mineralization of phenanthrene in soil. *Environmental pollution*, *181*, 200–210.

- Martínez, C. M., Alvarez, L. H., & Cervantes, F. J. (2012). Simultaneous biodegradation of phenol and carbon tetrachloride mediated by humic acids. *Biodegradation*, *23*, 635-644.
- Mei, K.-C., Liao, Y.-P., Jiang, J., Chiang, M., Khazaieli, M., Liu, X., Wang, X., Liu, Q., Chang, C. H., Zhang, X., Li, J., Ji, Y., Melano, B., Telesca, D., Xia, T., Meng, H., & Nel, A. E. (2020). Liposomal Delivery of Mitoxantrone and a Cholesteryl Indoximod Prodrug Provides Effective Chemo-immunotherapy in Multiple Solid Tumors. *ACS Nano*, *14*(10),
- Meisel, D. (1975). Free energy correlation of rate constants for electron transfer between organic systems in aqueous solutions. *Chemical Physics Letters*, *34*(2), 263–266.
- Miller, D. M., Buettner, G. R., & Aust, S. D. (1990). Transition metals as catalysts of “autoxidation” reactions. *Free Radical Biology and Medicine*, *8*(1), 95-108.
- Mohn, W., & Tiedje, J. (1992). Mohn WW, Tiedje JM. Microbial reductive dehalogenation. *Microbiol Rev* 56: 482-507. *Microbiological Reviews*, *56*, 482–507.
- Nagle, D. G., Ferreira, D., & Zhou, Y.-D. (2006). Epigallocatechin-3-gallate (EGCG): Chemical and biomedical perspectives. *Phytochemistry*, *67*(17), 1849–1855.
- Oh, S.-Y., Son, J.-G., & Chiu, P. C. (2013). Biochar-mediated reductive transformation of nitro herbicides and explosives. *Environmental Toxicology and Chemistry*, *32*(3), 501–508.
- O’Loughlin, E. J. (2008). Effects of Electron Transfer Mediators on the Bioreduction of Lepidocrocite (γ -FeOOH) by *Shewanella putrefaciens* CN32. *Environmental Science & Technology*, *42*(18), 6876–6882.

- Orsetti, S., Laskov, C., & Haderlein, S. B. (2013). Electron Transfer between Iron Minerals and Quinones: Estimating the Reduction Potential of the Fe(II)-Goethite Surface from AQDS Speciation. *Environmental Science & Technology*, *47*(24), 14161–14168.
- Pariyar, P., Kumari, K., Jain, M. K., & Jadhao, P. S. (2020). Evaluation of change in biochar properties derived from different feedstock and pyrolysis temperature for environmental and agricultural application. *Science of the Total Environment*, *713*, 136433.
- Perlinger, J. A., Angst, W., & Schwarzenbach, R. P. (1996). Kinetics of the Reduction of Hexachloroethane by Juglone in Solutions Containing Hydrogen Sulfide. *Environmental Science & Technology*, *30*(12), 3408–3417.
- Pessah, I. N., Lein, P. J., Seegal, R. F., & Sagiv, S. K. (2019). Neurotoxicity of polychlorinated biphenyls and related organohalogenes. *Acta neuropathologica*, *138*(3), 363-387.
- Pignatello, J. J., Mitch, W. A., & Xu, W. (2017). Activity and Reactivity of Pyrogenic Carbonaceous Matter toward Organic Compounds. *Environmental Science & Technology*, *51*(16), 8893–8908.
- Pracht, J., Boenigk, J., Isenbeck-Schröter, M., Keppler, F., & Schöler, H. F. (2001). Abiotic Fe(III) induced mineralization of phenolic substances. *Chemosphere*, *44*(4), 613–619.
- Qi, Y., Fu, P., & Volmer, D. A. (2019). Analysis of natural organic matter via fourier transform ion cyclotron resonance mass spectrometry: An overview of recent non-petroleum applications. *Mass Spectrometry Reviews*.

- Redon, P. O., Abdelouas, A., Bastviken, D., Cecchini, S., Nicolas, M., & Thiry, Y. (2011). Chloride and organic chlorine in forest soils: storage, residence times, and influence of ecological conditions. *Environmental Science & Technology*, 45(17), 7202-7208.
- Richardson, S. D. (2003). Disinfection by-products and other emerging contaminants in drinking water. *TrAC Trends in Analytical Chemistry*, 22(10), 666–684.
- Richardson, S. D., & Ternes, T. A. (2018). Water Analysis: Emerging Contaminants and Current Issues. *Analytical Chemistry*, 90(1), 398–428.
- Roden, E. E., Kappler, A., Bauer, I., Jiang, J., Paul, A., Stoesser, R., Konishi, H., & Xu, H. (2010). Extracellular electron transfer through microbial reduction of solid-phase humic substances. *Nature Geoscience*, 3(6), Article 6.
- Roginsky, V., & Barsukova, T. (2000). Kinetics of oxidation of hydroquinones by molecular oxygen. Effect of superoxide dismutase. *Journal of the Chemical Society, Perkin Transactions 2*, 7, 1575–1582.
- Rush, J. D., & Bielski, B. H. (1985). Pulse radiolytic studies of the reaction of perhydroxyl/superoxide O₂-with iron (II)/iron (III) ions. The reactivity of HO₂/O₂-with ferric ions and its implication on the occurrence of the Haber-Weiss reaction. *The Journal of Physical Chemistry*, 89(23), 5062–5066.
- Sanroman, M. A., Lee, D. J., Khanal, S., & Ok, Y. S. (2017). Special Issue on Biochar: Production, Characterization and Applications - Beyond Soil Applications. *Bioresource Technology*, 246, 1.

- Saquin, J. M., Yu, Y.-H., & Chiu, P. C. (2016). Wood-derived black carbon (biochar) as a microbial electron donor and acceptor. *Environmental Science & Technology Letters*, 3(2), 62–66.
- Scherer, M. M., Balko, B. A., Gallagher, D. A., & Tratnyek, P. G. (1998). Correlation Analysis of Rate Constants for Dechlorination by Zero-Valent Iron. *Environmental Science & Technology*, 32(19), 3026–3033.
- Schymanski, E. L., Jeon, J., Gulde, R., Fenner, K., Ruff, M., Singer, H. P., & Hollender, J. (2014). Identifying Small Molecules via High Resolution Mass Spectrometry: Communicating Confidence. *Environmental Science & Technology*, 48(4), 2097–2098.
- Scott, D. T., McKnight, D. M., Blunt-Harris, E. L., Kolesar, S. E., & Lovley, D. R. (1998). Quinone moieties act as electron acceptors in the reduction of humic substances by humics-reducing microorganisms. *Environmental Science & Technology*, 32(19), 2984–2989.
- Simon, C., Dührkop, K., Petras, D., Roth, V. N., Böcker, S., Dorrestein, P. C., & Gleixner, G. (2022). Mass difference matching unfolds hidden molecular structures of dissolved organic matter. *Environmental Science & Technology*, 56(15), 11027-11040.
- Singer, H., Müller, S., Tixier, C., & Pillonel, L. (2002). Triclosan: occurrence and fate of a widely used biocide in the aquatic environment: field measurements in wastewater treatment plants, surface waters, and lake sediments. *Environmental science & technology*, 36(23), 4998-5004.

- Sinkkonen, S., & Paasivirta, J. (2000). Degradation half-life times of PCDDs, PCDFs and PCBs for environmental fate modeling. *Chemosphere*, *40*(9), 943–949.
- Sleighter, R. L., & Hatcher, P. G. (2007). The application of electrospray ionization coupled to ultrahigh resolution mass spectrometry for the molecular characterization of natural organic matter. *Journal of Mass Spectrometry*, *42*(5), 559–574.
- Song, B., Chen, M., Zhao, L., Qiu, H., & Cao, X. (2019). Physicochemical property and colloidal stability of micron- and nano-particle biochar derived from a variety of feedstock sources. *Science of The Total Environment*, *661*, 685–695.
- Song, Y., & Buettner, G. R. (2010). Thermodynamic and kinetic considerations for the reaction of semiquinone radicals to form superoxide and hydrogen peroxide. *Free Radical Biology & Medicine*, *49*(6), 919–962.
- Stack, A. G., Eggleston, C. M., & Engelhard, M. H. (2004). Reaction of hydroquinone with hematite. *Journal of Colloid and Interface Science*, *274*(2), 433–441.
- Sun, T., Levin, B. D., Guzman, J. J., Enders, A., Muller, D. A., Angenent, L. T., & Lehmann, J. (2017). Rapid electron transfer by the carbon matrix in natural pyrogenic carbon. *Nature Communications*, *8*(1), 14873.
- Svingen, B. A., & Powis, G. (1981). Pulse radiolysis studies of antitumor quinones: Radical lifetimes, reactivity with oxygen, and one-electron reduction potentials. *Archives of Biochemistry and Biophysics*, *209*(1), 119–126.
- Swallow, A. J. (1982). 3—Physical Chemistry of Semiquinones. In B. L. Trumpower (Ed.), *Function of Quinones in Energy Conserving Systems* (pp. 59–72). Academic Press.

- Tan, W., Wang, L., Yu, H., Zhang, H., Zhang, X., Jia, Y., Li, T., Dang, Q., Cui, D., & Xi, B. (2019). Accelerated microbial reduction of azo dye by using biochar from iron-rich-biomass pyrolysis. *Materials*, *12*(7), 1079.
- Thompson, K. A., Shimabuku, K. K., Kearns, J. P., Knappe, D. R. U., Summers, R. S., & Cook, S. M. (2016). Environmental Comparison of Biochar and Activated Carbon for Tertiary Wastewater Treatment. *Environmental Science & Technology*, *50*(20), 11253–11262.
- Tian, Z., Zhao, H., Peter, K. T., Gonzalez, M., Wetzel, J., Wu, C., Hu, X., Prat, J., Mudrock, E., Hettinger, R., Cortina, A. E., Biswas, R. G., Kock, F. V. C., Soong, R., Jenne, A., Du, B., Hou, F., He, H., Lundeen, R., ... Kolodziej, E. P. (2021). A ubiquitous tire rubber-derived chemical induces acute mortality in coho salmon. *Science*, *371*(6525), 185–189.
- Tomczyk, A., Sokołowska, Z., & Boguta, P. (2020). Biochar physicochemical properties: pyrolysis temperature and feedstock kind effects. *Reviews in Environmental Science and Bio/Technology*, *19*, 191-215.
- Tong, H., Hu, M., Li, F. B., Liu, C. S., & Chen, M. J. (2014). Biochar enhances the microbial and chemical transformation of pentachlorophenol in paddy soil. *Soil Biology and Biochemistry*, *70*, 142–150.
- Toral-Sánchez, E., Rangel-Mendez, J. R., Hurt, R. H., Valdés, J. A. A., Aguilar, C. N., & Cervantes, F. J. (2018). Novel application of magnetic nano-carbon composite as redox mediator in the reductive biodegradation of iopromide in anaerobic continuous systems. *Applied Microbiology and Biotechnology*, *102*(20), 8951–8961.

- Trainer, E. L., Ginder-Vogel, M., & Remucal, C. K. (2020). Organic structure and solid characteristics determine reactivity of phenolic compounds with synthetic and reclaimed manganese oxides. *Environmental Science: Water Research & Technology*, 6(3), 540-553.
- Uchimiya, M., & Stone, A. T. (2009). Reversible redox chemistry of quinones: Impact on biogeochemical cycles. *Chemosphere*, 77(4), 451–458.
- Van der Zee, F. P., Bisschops, I. A., Lettinga, G., & Field, J. A. (2003). Activated carbon as an electron acceptor and redox mediator during the anaerobic biotransformation of azo dyes. *Environmental Science & Technology*, 37(2), 402-408.
- Vreugdenhil, H. J. I., Slijper, F. M. E., Mulder, P. G. H., & Weisglas-Kuperus, N. (2002). Effects of perinatal exposure to PCBs and dioxins on play behavior in dutch children at school age. *Environmental Health Perspectives*, 110(10), A593–A598.
- Vriens, A., Nawrot, T. S., Janssen, B. G., Baeyens, W., Bruckers, L., Covaci, A., ... & Plusquin, M. (2019). Exposure to environmental pollutants and their association with biomarkers of aging: a multipollutant approach. *Environmental Science & Technology*, 53(10), 5966-5976.
- Wang, C.-B., & Zhang, W. (1997). Synthesizing Nanoscale Iron Particles for Rapid and Complete Dechlorination of TCE and PCBs. *Environmental Science & Technology*, 31(7), 2154–2156.
- Wang, S., Gao, B., Zimmerman, A. R., Li, Y., Ma, L., Harris, W. G., & Migliaccio, K. W. (2015). Removal of arsenic by magnetic biochar prepared from pinewood and natural hematite. *Bioresource Technology*, 175, 391–395.

- Wang, Y., Wang, L., Fang, G., Herath, H. M. S. K., Wang, Y., Cang, L., Xie, Z., & Zhou, D. (2013). Enhanced PCBs sorption on biochars as affected by environmental factors: Humic acid and metal cations. *Environmental Pollution*, *172*, 86–93.
- Wang, Y., Wu, C., Wang, X., & Zhou, S. (2009). The role of humic substances in the anaerobic reductive dechlorination of 2, 4-dichlorophenoxyacetic acid by *Comamonas koreensis* strain CY01. *Journal of hazardous materials*, *164*(2-3), 941-947.
- Wardman, P. (1989). Reduction potentials of one-electron couples involving free radicals in aqueous solution. *Journal of Physical and Chemical Reference Data*, *18*(4), 1637–1755.
- Weatherill, J. J., Atashgahi, S., Schneidewind, U., Krause, S., Ullah, S., Cassidy, N., & Rivett, M. O. (2018). Natural attenuation of chlorinated ethenes in hyporheic zones: A review of key biogeochemical processes and in-situ transformation potential. *Water Research*, *128*, 362–382.
- Weatherly, L. M., & Gosse, J. A. (2017). Triclosan Exposure, Transformation, and Human Health Effects. *Journal of Toxicology and Environmental Health. Part B, Critical Reviews*, *20*(8), 447–469.
- Wiegel, J., & Wu, Q. (2000). Microbial reductive dehalogenation of polychlorinated biphenyls. *FEMS Microbiology Ecology*, *32*(1), 1–15.
- Windeatt, J. H., Ross, A. B., Williams, P. T., Forster, P. M., Nahil, M. A., & Singh, S. (2014). Characteristics of biochars from crop residues: Potential for carbon sequestration and soil amendment. *Journal of Environmental Management*, *146*, 189–197.

- Wiseman, L. R., & Spencer, C. M. (1997). Mitoxantrone. *Drugs & Aging*, *10*(6), 473–485.
- Xu, S., Adhikari, D., Huang, R., Zhang, H., Tang, Y., Roden, E., & Yang, Y. (2016). Biochar-Facilitated Microbial Reduction of Hematite. *Environmental Science & Technology*, *50*(5), 2389–2395.
- Xu, W., Pignatello, J. J., & Mitch, W. A. (2013). Role of Black Carbon Electrical Conductivity in Mediating Hexahydro-1,3,5-trinitro-1,3,5-triazine (RDX) Transformation on Carbon Surfaces by Sulfides. *Environmental Science & Technology*, *47*(13), 7129–7136.
- Yamazaki, I., & Ohnishi, T. (1966). One-electron-transfer reactions in biochemical systems I. Kinetic analysis of the oxidation-reduction equilibrium between quinol-quinone and ferro-ferricytochrome c. *Biochimica et Biophysica Acta (BBA) - Biophysics Including Photosynthesis*, *112*(3), 469–481.
- Yang, Y., Hunter, W., Tao, S., Crowley, D., & Gan, J. (2009). Effect of activated carbon on microbial bioavailability of phenanthrene in soils. *Environmental Toxicology and Chemistry: An International Journal*, *28*(11), 2283-2288.
- Ying, G.-G., Yu, X.-Y., & Kookana, R. S. (2007). Biological degradation of triclocarban and triclosan in a soil under aerobic and anaerobic conditions and comparison with environmental fate modelling. *Environmental Pollution*, *150*(3), 300–305.
- Yu, H., Zou, W., Chen, J., Chen, H., Yu, Z., Huang, J., Tang, H., Wei, X., & Gao, B. (2019). Biochar amendment improves crop production in problem soils: A review. *Journal of Environmental Management*, *232*, 8–21.

- Yu, L., Yuan, Y., Tang, J., Wang, Y., & Zhou, S. (2015). Biochar as an electron shuttle for reductive dechlorination of pentachlorophenol by *Geobacter sulfurreducens*. *Scientific Reports*, 5(1), 16221.
- Yuan, X., Pham, A. N., Miller, C. J., & Waite, T. D. (2013). Copper-catalyzed hydroquinone oxidation and associated redox cycling of copper under conditions typical of natural saline waters. *Environmental Science & Technology*, 47(15), 8355–8364.
- Yuan, Y., Bolan, N., Prévosteau, A., Vithanage, M., Biswas, J. K., Ok, Y. S., & Wang, H. (2017). Applications of biochar in redox-mediated reactions. *Bioresource Technology*, 246, 271-281.
- Yue, L., Lian, F., Han, Y., Bao, Q., Wang, Z., & Xing, B. (2019). The effect of biochar nanoparticles on rice plant growth and the uptake of heavy metals: Implications for agronomic benefits and potential risk. *Science of The Total Environment*, 656, 9–18.
- Zall, D. M., Fisher, Donald., & Garner, M. Q. (1956). Photometric Determination of Chlorides in Water. *Analytical Chemistry*, 28(11), 1665–1668.
- Zhang, C., & Katayama, A. (2012). Humic as an electron mediator for microbial reductive dehalogenation. *Environmental Science & Technology*, 46(12), 6575–6583.
- Zhang, Y., Xu, X., Zhang, P., Ling Zhao, Qiu, H., & Cao, X. (2019). Pyrolysis-temperature depended quinone and carbonyl groups as the electron accepting sites in barley grass derived biochar. *Chemosphere*, 232, 273–280.

- Zhang, Y., Zhang, Z., Liu, W., & Chen, Y. (2020). New applications of quinone redox mediators: Modifying nature-derived materials for anaerobic biotransformation process. *Science of The Total Environment*, 744, 140652.
- Zhao, S., Rogers, M. J., Ding, C., & He, J. (2018). Reductive Debromination of Polybrominated Diphenyl Ethers—Microbes, Processes and Dehalogenases. *Frontiers in Microbiology*, 9.
- Zhuang, Y., Ahn, S., & Luthy, R. G. (2010). Debromination of Polybrominated Diphenyl Ethers by Nanoscale Zerovalent Iron: Pathways, Kinetics, and Reactivity. *Environmental Science & Technology*, 44(21), 8236–8242.